Universidade do Minho
Escola de Engenharia

Rui Daniel Vilaça Fernandes

Development of structural colors, assisted by plasma technology and biopolymer coating, for high visibility technical fabrics

Julho 2026

Development of structural colors, assisted by plasma technology and biopolymer coating, for high visibility technical fabrics

Rui Fernandes

UMinho | 2026

Universidade do Minho
Escola de Engenharia

Rui Daniel Vilaça Fernandes

Development of structural colors, assisted by plasma technology and biopolymer coating, for high visibility technical fabrics

Tese de Doutoramento
Doutoramento em Engenharia Têxtil

Trabalho efetuado sob a orientação do
Professor Doutor Andrea Zille
Professor Doutor António Pedro Garcia de Valadares Souto

Julho 2026

Direitos de autor e condições de utilização do trabalho por terceiros

Este é um trabalho académico que pode ser utilizado por terceiros desde que respeitadas as regras e boas práticas internacionalmente aceites, no que concerne aos direitos de autor e direitos conexos.

Assim, o presente trabalho pode ser utilizado nos termos previstos na licença abaixo indicada.

Caso o utilizador necessite de permissão para poder fazer um uso do trabalho em condições não previstas no licenciamento indicado, deverá contactar o autor, através do RepositóriUM da Universidade do Minho.



Atribuição-NãoComercial-SemDerivações
CC BY-NC-ND

https://creativecommons.org/licenses/by-nc-nd/4.0/

Acknowledgments

The execution of this work would not be possible without the financial support from Fundação para a Ciência e Tecnologia (SFRH/BD/145269/2019), and all the facilities, equipments and resources provided by the Centre for Textile Science and Technology (2C2T). I am truly grateful for all who contributed in one way or another in the execution of this research.

First, I would like to thank the late Professor António Pedro Souto, who was the one to bring me to 2C2T and the initiator of this project, without him this research would never happen.

To my supervisor Professor Andrea Zille, for being available every time I needed, providing his knowledge, support and guidance. I have acquired an immense amount of knowledge and experience through the participation on different projects and challenges over the years. In the end of this thesis, I consider him not only my academic guru, but also a friend since our sense of humor is practically the same!

A very special thanks to Linköping University (LiU), the Department of Physics, Chemistry and Biology, in particular to the Thin Film Physics group, led by Professor Kenneth Järrendahl, and to his research group, Hans, Roger, Sergiy, Ivan and Alina, for receiving and helping me with open arms during my stay in Sweden, your contribution was outstanding. Samiran, thank you for being my guide at LiU, I appreciated it so much my friend. To the rest of the Material Optics group, thank you for all the game nights and time spent away from LiU, all of you contributed to fight my homesickness!

To the Swedish Armed Forces (FOI), in special to Hans, Thomas and Cecilia, for their scientific contribution, analysis performed and fellowship.

Thanks to the Centre for Nanotechnology and Advanced Materials (CENTI) for letting me use their facilities to apply plasma treatments in fabrics.

Thanks to Professor Diego Moldes for supplying lignin and to Professor Nuno Dourado for the schematics done in SolidWorks.

To all the people who had work and to those that are still working in the Acabamentos Funcionais II laboratory, namely Marta, Vitor, Ana Isabel, Isabel C., Diana S., Xinyu, Derya, Lu'u, Inês, Sofia, Patricia, Tânia T., Marta S.T., Bárbara, Behnaz, Rui Pedro, Adriana, Fábio C., Manu, Jorge P. and Helena F., thank you very much! Last but not least, thank you Cátia Alves and Liliana Melro for everything in the last 2 years, not only for your help academically but also for all the laughs and patience! For all the 2C2T people I forgot, thanks to you too!

Thanks to all the technicians Ângela, Joaquim Jorge, Avelino and Sónia for the help with the equipment's and tests.

Finally, I want to thank my family, my mother Maria, my father Orlando, my brother Filipe, my in-laws Aurora, Carlos, Patrícia, Pedro and niece Sofia. Thank you Liliane, the love of my life, without your support this would have been impossible, I am blessed for having you in my life, can't wait to see what the next 20 years will bring, LY!!

Sorry it took this long, I'm almost there!!!

Scientific Outputs

Thesis outputs

Part of the work presented herein resulted in scientific communications in the form of two research papers in peer-reviewed Journals, one book chapter, one oral presentation and two poster communications:

(Paper) **Fernandes, Rui D.V.**; Gomes, Pedro; Zille, Andrea; Souto, A. P.. "The influence of chemical reaction conditions upon poly(styrene-methyl methacrylate-acrylic acid) synthesis: Variations in nanoparticle size, colour and deposition methods". *Coloration Technology* (2020) 136, 101-109. doi: 10.1111/cote.12452

(Paper) **Fernandes, Rui D.V.**; Pranovich, Alina; Valyukh, Sergiy; Zille, Andrea; Hallberg, Tomas; Järrendahl, Kenneth. "Iridescence Mimicking in Fabrics: A Ultraviolet/Visible Spectroscopy Study". *Biomimetics* (2024) 9, 71. doi: 10.3390/biomimetics9020071

(Book Chapter) Fernandes, Marta; **Fernandes, Rui D.V.**; Padrão, Jorge; Melro, Liliana; Alves, Cátia; Rodrigues, Rui; Ribeiro, Ana Isabel ; Zille, Andrea. "Plasma in textile wastewater treatment". In *Advances in Plasma Treatment of Textile Surfaces*, 267-322. Elsevier, 2024. doi: 10.1016/B978-0-443-19079-7.00008-7

(Oral Presentation) **Fernandes, Rui D.V.**; Padrão, Jorge; Zille, Andrea. "Structural Color for Enhanced Camouflage Textiles". *AuxDefense 2022 - 3rd World Conference on Advanced Materials for Defense*, Guimarães, 2022.

(Poster) **Fernandes, Rui D.V.**; Padrão, Jorge; Zille, Andrea. "Effect of color substrate in structurally colored PES fabrics". *iTechStyle Summit 2022*, Porto, 2022.

(Poster) **Fernandes, Rui D.V.**; Rodrigues, Rui; Vieira, Bárbara; Padrão, Jorge; Zille, Andrea. "Combining photonic crystals of different sizes and tuning structural colors by color addition". *Seventh International Symposium Frontiers in Polymer Science*, Gothemburg, 2023

This research work was also divulged and presented to the general public and society in NEI (Noite Europeia dos Investigadores – Braga), in the editions of 2021, 2022, 2023, 2024 and 2025.

Outputs not directly related with the thesis

During the course of the PhD, I was invited to participate in several projects which resulted in publications, non-related to the PhD:

Research Papers

(1) Joana M. Domingues; Marta O. Teixeira; Marta A. Teixeira; David Freitas; Samira F. da Silva; Shafagh D. Tohidi; **Rui D.V. Fernandes**; Jorge Padrão; Andrea Zille; Helena P. Felgueiras. "Inhibition of Escherichia Virus MS2, Surrogate of SARS-CoV-2, via Essential Oils-Loaded Electrospun Fibrous Mats: Increasing the Multifunctionality of Antivirus Protection Masks". *Pharmaceutics* (2022), 14 (2), 303. doi: 10.3390/pharmaceutics14020303

(2) Marta Fernandes; Jorge Padrão; Ana I. Ribeiro; **Rui D.V. Fernandes**; Liliana Melro; Talita Nicolau; Behnaz Mehravani; Cátia Alves; Rui Rodrigues; Andrea Zille. "Polysaccharides and Metal Nanoparticles for Functional Textiles: A Review". *Nanomaterials* 12 6 (2022): 1006-1006. doi: 10.3390/nano12061006.

(3) **Rui D.V. Fernandes**; Liliana Melro; Jorge Padrão; Ana Isabel Ribeiro; Behnaz Mehravani; Filipa Monteiro; Eduardo Pereira; Marcos S. Martins; Nuno Dourado; Andrea Zille. "Active Neutralizing Mats for Corrosive Chemical Storage". *Gels* (2022), 8 (8), 489. doi: 10.3390/gels8080489.

(4) Alves, Cátia; Soares-Castro, Pedro; **Fernandes, Rui D.V.**; Pereira, Adriana ; Rodrigues, Rui; Ana Rita Fonseca; Correia dos Santos, Nuno; Zille, Andrea. "Application of Prodigiosin Extracts in Textile Dyeing and Novel Printing Processes for Halochromic and Antimicrobial Wound Dressings". *Biomolecules* (2025)15 (8), 1113. doi: 10.3390/biom15081113

(5) Ana Francisca Ferreira; **Rui D.V. Fernandes**; Bárbara Vieira; Joaquim Peixoto; Helena P. Felgueiras; Andrea Zille; Graça Soares; Isabel Cabral; Jorge Padrão. "Elastic bands antimicrobial functionalization". *Surfaces and Interfaces* (2025) 76, 107858. doi: 10.1016/j.surfin.2025.107858

(6) Beatriz Caseiro, Cátia Alves, **Rui D.V. Fernandes**, Liliana Melro, Behnaz Mehravani, Joaquim Peixoto, Filipa Monteiro, Andrea Zille, Joana C. Antunes and Jorge Padrão. “Reusable multifunctional textile-based

smart packaging for fruit preservation and spoilage monitoring". *Reactive and Functional Polymers* (accepted)

(7) Liliana Melro; Cátia Alves; Marta Fernandes; **Rui D.V. Fernandes**; Adriana Pereira; Diego Moldes; Ana Cristina Rodrigues; Vitor Sencadas; Bogdana Mitu; Veronica Satulu; José Lourenço; Giorgio Pace; Luis A. Martins; José Luis Gómez Ribelles; António J. Salgado; Jorge Padrão; Andrea Zille. "Phenolic-Functionalised Bacterial Nanocellulose Composites with Antimicrobial and Antioxidant Activity for Implantable Biomaterials". *Composites Part A* (submitted)

(8) **Rui D.V. Fernandes,** Cátia Alves, Liliana Melro, Marta Fernandes, Jorge Padrão, Diego Moldes, António J. Salgado, Hélder Puga and Andrea Zille. "Kraft Lignin Tunable-Sized Nanoparticles Production Via Ultrasonication And Surfactant-Assisted Method". *ACS Nano* (submitted)

Book Chapters

(1) Padrão, Jorge; Melro, Liliana; Fernandes, Marta; **Fernandes, Rui D.V.**; Ribeiro, Ana Isabel; Song, Xinyu; Yu, Liangmin; Zille, Andrea. "Bio-compatibility of nanocellulose: Emerging biomedical applications". In *Handbook of Biopolymers*. Springer Nature Singapore, 2022. doi: 10.1007/978-981-16-6603-2_36-1

(2) Fernandes, Marta; Alves, Cátia; Melro, Liliana; **Fernandes, Rui D.V.**; Padrão, Jorge; Salgado, António; Zille, Andrea. "Modification of Nanocellulose". In *Handbook of Biomass*, 1-39. Springer Nature Singapore, 2023. doi: 10.1007/978-981-19-6772-6_35-1

Conference papers

(1) Ribeiro, Ana Isabel; Mehravani, Behnaz; Magalhães, Cátia; Nicolau, Talita; Melro, Liliana; **Fernandes, Rui D.V.**; Shvalya, Vasyl; Cvelbar, Uros; Padrão, Jorge; Zille, Andrea. "Enhancing the antimicrobial efficacy of polyester fabric impregnated with silver nanoparticles using DBD plasma treatment". *AUTEX World Textile Conference 2021*, *Guimarães*, 2021. doi: 10.4028/p-256i32

(2) Padrão, Jorge; Inês Pinheiro; Carla Silva; Alice Ribeiro; Verónica Bouça; Melro, Liliana; **Fernandes, Rui D.V.**; Zille, Andrea. "Distinct antimicrobial analysis to evaluate multi-component wound dressing performance". *20th AUTEX World Textile Conference,* Guimarães, 2021. doi: 10.4028/p-kdad2h

(3) Mehravani, Behnaz; Padrão, Jorge; **Fernandes, Rui D.V.**; Nicolau, Talita; Alves, Cátia; Ribeiro, Ana Isabel; Jorge, Joaquim; Carvalho, Helder; Zille, Andrea. "Sustainable and Multifunctional natural fiber-based electric wire sheaths for smart textiles". *21th AUTEX World Textile Conference*, Lodz, 2022. doi: 10.34658/9788366741751.125

(4) Melro, Liliana; **Fernandes, Rui D.V.**; Pinheiro, Inês; Ribeiro, Alice; Bouça, Verónica; Dourado, Fernando; Gama, Miguel; Padrão, Jorge; Zille, Andrea. "Antiviral properties of flame retardant bacterial nanocellulose modified with mordenite". *21th AUTEX World Textile Conference*, Lodz, 2022. doi: 10.34658/9788366741751.129

Posters

(1) Padrão, Jorge; Pinheiro, Inês; Silva, Carla Joana Santos Marinho; Ribeiro, Alice; Bouça, Verónica; Melro, Liliana; **Fernandes, Rui D.V.**; Ribeiro, Ana Isabel; Felgueiras, Helena P.; Zille, Andrea. "Multicomponent Wound Dressing". *ICNF - International Conference on Natural Fibers* (online), 2021.

(2) Domingues, Joana; Teixeira, Marta O.; Teixeira, Marta A.; Freitas, David; Silva, Samira; Shafagh D.Tohidi; **Fernandes, Rui D.V.**; Padrão, Jorge; Zille, Andrea; Felgueiras, Helena P.. "Essential oils-loaded nanofibrous mats for an enhanced protection against SARS-CoV-2". *3rd International Online-Conference on Nanomaterials*, 2022.

(3) Nicolau, Talita; Alves, Cátia; Melro, Liliana; **Fernandes, Rui D.V.**; Mehravani, Behnaz; Forte, Jorge; Ribeiro, Vitor; Ribeiro, Marinho; Dourado, Fernando; Gama, Miguel; Padrão, Jorge; Zille, Andrea. "A functionalized nanobiopolymer as an alternative for burn wound dressing". *Seventh International Symposium Frontiers in Polymer Science*, Gothemburg, 2023.

(4) Fernandes, Marta; Melro, Liliana; **Fernandes, Rui D.V.**; Ribeiro, Ana Isabel; Felgueiras, Helena P.; Silva, Carla Joana Santos Marinho; Pinheiro, Inês; Bouça, Verónica; Ribeiro, Alice; Padrão, Jorge; Zille,

Andrea. "Physical properties of an antibacterial and antiviral woven cotton functionalized with a multi-nanocomposite". *Seventh International Symposium Frontiers in Polymer Science*, Gothemburg, 2023.

(5) Soares-Castro, Pedro; Fonseca, Ana Rita; Alves, Cátia; Pereira, Adriana; Rodrigues, Rui; **Fernandes, Rui D.V.**; Zille, Andrea; Gonçalves, Sónia; Santos, Nuno C.. "Bacterial prodigiosin as natural biocolorant for sustainable textile applications". *EMBO Young Scientists Forum*, Lisbon, 2023.

(6) **Fernandes, Rui D.V.**; Magalhães, Sofia; Rodrigues, Soraia; Vieira, Bárbara; Alves, Cátia; Moldes, Diego; Padrão, Jorge; Almeida-Aguiar, Cristina; Zille, Andrea. "Cellulosic fabrics bio-finishing with natural products". *Autex2025 - World Textile Conference*, Dresden, 2025.

Patents

(1) Roniê Bezerra da Silva; Jefferson Mendes de Souza; Carla Eiras; **Rui D.V. Fernandes**; Andrea Zille. "Compósito sustentável reforçado com material fibroso em matriz polimérica termofixa aplicado na produção de armações de óculos". Universidade Federal do Piauí, *Instituto Nacional da Propriedade Industrial (Brasil)*, reference BR 10 2026 003464 9 (**submitted**)

Others

(1) Melro, Liliana; Fernandes, Marta; Nicolau, Talita; Tavares, Tânia D.; **Fernandes, Rui D.V.**; Felgueiras, Helena; Padrão, Jorge; Dourado, Fernando; Gama, Miguel; Zille, Andrea. "Produção de nanocelulose bacteriana". *eBook de Comunicação de Ciência em Microbiologia - Sociedade Portuguesa de Microbiologia*, 2022.

Statement of Integrity

I hereby declare having conducted this academic work with integrity. I confirm that I have not used plagiarism or any form of undue use of information or falsification of results along the process leading to its elaboration.

I further declare that I have fully acknowledged the Code of Ethical Conduct of the University of Minho.

Universidade do Minho, 6 de abril de 2026

Full name: Rui Daniel Vilaça Fernandes

Development of structural colors, assisted by plasma technology and biopolymer coating, for high visibility technical fabrics

Abstract

The textile industry is considered one of the most polluting industries in the world. One of the main ecological concerns is the high consumption of water used in textile processing and its effluents, which contain a high load of environmentally toxic chemicals. The application of photonic crystals (PCs) allows the coloring of textile substrates by structural coloration, possibly mitigating this ecological problem, as water consumption is drastically reduced. This research project presents a thorough colorimetric study to evaluate PCs capability of substituting conventional dyes. PCs with different chemical compositions (P(St-MMA-AA), SiO_2 and Kraft lignin (KL)) were synthetized, characterized and applied onto three different textiles substrates, polyamide (PA), polyester (PES) and cotton (CO). The sizes of the synthesized PCs were determined by Dynamic Light Scattering and Scanning Electronic Microscopy techniques. With the obtained PCs several structural colors were produced, namely violet, blue, green, yellow and red. As the native color of KL is brown, it possibly masked the reflectance of the produce structural color, only presenting some iridescent effect (in glass substrate). Among all possible PC/substrate combination, the best colorimetric response was obtained with P(St-MMA-AA) deposited onto PA's surface. As such, these fabrics were characterized in more details in opposition to the other PC type/substrate combinations. Nevertheless, the other PC/substrate combinations were also characterized, to an extent. P(St-MMA-AA)/PA presented remarkable brightness and iridescent effect, being exhaustively studied by SEM and UV/Vis spectroscopy techniques, confirming the PC self-assembly (hexagonal packed structure) and iridescence effect through UV/Vis band shifting. Regarding color fastness, P(St-MMA-AA)/PA presented excellent light fastness without any finishing coating applied. As for washing fastness, several biopolymers and commercial finishing agents were tested, where most failed to retain the coating and color properties. The exception was Sylgard™ 184, a commercial silicone-based coating agent, which could maintain color, brightness and iridescence after washing fastness tests. Pristine PC mixture and the influence of color substrate when combined with pristine/dyed PCs were also studied. Both studies showed that PCs follow the principle of color addition, however the dye color overwhelms structural color when its concentration is greater than 1 wt%.

With this research project, an alternative and more sustainable coloration method was developed, aiming its application in technical fabrics with high visibility for segments of workwear and/or sportswear.

Keywords: structural color; photonic crystals; iridescence; biopolymer; sensor; plasma radiation.

Desenvolvimento de cores estruturais, auxiliado pela tecnologia de plasma e revestimento de biopolímeros, para têxteis técnicos de alta visibilidade

Resumo

A indústria têxtil é considerada uma das mais poluentes do mundo. Uma das principais preocupações ecológicas é o elevado consumo de água utilizado, onde os seus efluentes contêm uma elevada carga de substâncias químicas tóxicas. A aplicação de cristais fotónicos (PCs) permite a coloração de substratos têxteis através da cor estrutural, possivelmente mitigando este problema ecológico, uma vez que o consumo de água é drasticamente reduzido. Este projeto de investigação apresenta um estudo colorimétrico detalhado para avaliar a capacidade dos PCs em substituir corantes convencionais. PCs com diferentes composições químicas (P(St-MMA-AA), SiO_2 e Lignina Kraft (KL)) foram sintetizados, caracterizados e aplicados em três diferentes substratos têxteis, poliamida (PA), poliéster (PES) e algodão (CO). O tamanho dos PCs sintetizados foi determinado por técnicas de Espalhamento Dinâmico de Luz e Microscopia Eletrónica de Varrimento. Os PCs obtidos permitiram produzir várias cores estruturais, nomeadamente violeta, azul, verde, amarelo e vermelho. Como a cor nativa da KL é castanha, esta possivelmente mascarou a cor estrutural produzida, apresentando apenas efeito iridescente (em substrato de vidro). De entre todas as combinações possíveis de PC/substrato, a melhor resposta colorimétrica foi obtida com o P(St-MMA-AA) depositado na superfície do PA. Assim, estes tecidos foram caracterizados com mais detalhe de que as outras combinações de PC/substrato. O P(St-MMA-AA)/PA apresentou brilho e um efeito iridescente notáveis, sendo exaustivamente estudado por técnicas de MEV e espectroscopia UV/Vis, confirmando a auto-organização dos PCs (estrutura hexagonal compacta) e o efeito de iridescência através do deslocamento das bandas de refletância. Em relação à solidez da cor, o P(St-MMA-AA)/PA apresentou uma excelente resistência à luz sem a aplicação de qualquer acabamento. Quanto à solidez à lavagem, foram testados vários biopolímeros e agentes de acabamento comerciais, sendo que a maioria não conseguiu reter as propriedades de revestimento e de cor. A exceção foi o Sylgard™ 184, um agente comercial à base de silicone, que conseguiu manter a cor, o brilho e a iridescência após testes de lavagem. A mistura de PCs e a influência da cor do substrato quando combinada com PCs não tingidos/tingidos também foram estudadas. Ambos os estudos mostraram que os PCs seguem o princípio da adição de cor, onde a cor do corante se sobrepõe à cor estrutural quando a sua concentração é superior a 1% em peso.

Com este projeto de investigação foi desenvolvido um método de coloração alternativo e mais sustentável, visando a sua aplicação em têxteis técnicos de alta visibilidade para segmentos de vestuário de trabalho e/ou desportivo.

Palavras-chave: cor estrutural; cristais fotónicos; iridescência; biopolímero; sensor; radiação plasmática.

Table of Content

Acknowledgments iii

Scientific Outputs v

Statement of Integrity x

Abstract xi

Resumo xii

List of Abbreviations xvi

Figure Index xx

Table Index xxiv

1 Introduction 1

1.1. Framework 2

1.2. Research Questions 3

1.3. Objectives 3

1.4. Thesis Outline 4

2 Literature Overview 6

2.1. State of the art 7

2.1.1. Environmental context 7

2.1.2. Photonic Crystals 11

2.1.3. Light/substrate interaction 14

2.1.4. Photonic crystals' structures 16

2.1.5. Structural color production techniques 19

2.1.6. Plasma radiation technology 23

2.1.7. Biopolymers applied to textiles 24

3 Materials and Methods 27

3.1. Materials and Chemicals 28

3.2. Fabrics Characterization 29

3.3. Photonic crystal synthesis 29
3.3.1. P(St-MMA-AA) 29
3.3.2. SiO_2 30
3.3.3. Kraft Lignin 30
3.4. Dyeing Processes 30
3.4.1. Cotton dyeing 30
3.4.2. Polyester and P(St-MMA-AA) dyeing 31
3.5. Photonic crystal deposition on fabrics 32
3.5.1. P(St-MMA-AA) deposition by dip-drawing method 32
3.5.2. SiO_2 and KL deposition by gravitational sedimentation method 32
3.6. P(St-MMA-AA) PCs mixture 32
3.7. Adhesive synthesis 32
3.8. Plasma discharge for textile surface activation 32
3.9. Application of adhesives and finishing agents 33
3.10. Reflectance measurements 33
3.10.1. Spectrophotometry with integrating sphere 33
3.10.2. Scatterometry 33
3.10.3. Conversion of data to 3D color coordinates and IP-BRDF imaging 34
3.11. Scanning electron microscopy and scanning transmission electron microscopy 34
3.12. Fourier-transform infrared spectroscopy with attenuated total reflectance 35
3.13. Surface Roughness analysis 35
3.14. Differential scanning calorimetry 35
3.15. Simultaneous thermogravimetric analysis 36
3.16. Dynamic light scattering and Zeta potencial 36
3.17. Digital photographs 36
3.18. Angular support design 37

3.19. Standard Methods for color fastness 37

4 Photonic crystal synthesis and characterization 38

4.1. Synthesis of poly(styrene-methylmetacrylate-acrylic acid) (P(St-MMA-AA)) PCs 39

4.2. Synthesis of SiO_2 PCs 44

4.3. Synthesis of KL PCs 48

5 PC deposition onto textile substrates 52

5.1. P(St-MMA-AA) deposition onto polyamide, polyester and cotton fabrics 53

5.1.1. PCs as water/humidity sensors 70

5.1.2. Color fastness assays 71

5.2. Polymeric application in PES and CO fabrics for structural color improvement 75

5.2.1. SiO_2 PCs deposition onto polyester and cotton fabrics 75

5.2.2. KL PCs deposition onto polyester and cotton fabrics 76

6 Color substrate and PC dyeing influence in structural coloration 78

6.1. Deposition of pristine P(St-MMA-AA) PCs on PES fabrics with different colors 79

6.2. Deposition of dyed P(St-MMA-AA) PCs on PES fabrics with different colors 81

7 Mixture of pristine P(St-MMA-AA) PCs 86

7.1. Deposition of mixtures of pristine P(St-MMA-AA) PCs in PA fabrics 87

8 Conclusions and Future Perspectives 91

8.1. Conclusions 92

8.1.1. Photonic crystals synthesis 92

8.1.2. P(St-MMA-AA) PCs deposition on fabrics 92

8.1.3. Main conclusions 93

8.2. Future Perspectives 95

Bibliography 96

Annexes 115

List of Abbreviations

#	
1D	One-dimensional
2D	Two-dimensional
3D	Three-dimensional
A	
a*	CIEL*a*b* color coordinate in the red-green axis
AA	Acrylic acid
AOP	Advanced oxidation processes
AOX	Adsorbable organically bound halogen
ASTM	American Society for Testing Materials
ATR	Attenuated Total Reflection
B	
b*	CIEL*a*b* color coordinate in the yellow-blue axis
BA	Butyl acrylate
BCC	Body centered cubic
BI	Biodegradability index
BMA	Butyl methacrylate
BOD	Biological oxygen demand
C	
CB	Coralene Black MD dye
CIELab	International Commission on Illumination L* a* b*
CO	Cotton
COD	Chemical oxygen demand
D	
D_{50}	Daylight illuminant
DBV-R	Dianix Brilliant Violet R dye
DHR	Directional Hemispheric Reflectance
DLS	Dynamic Light Scattering
DMSO	Dimethyl sulfoxide
DSC	Differential scanning calorimetry
DTG	Derivative Thermogravimetry

E

ECE	European Colourfastness Establishment
EP	Electrophoresis

F

FCC	Face centered cubic
FTIR	Fourier Transformed Infrared Spectroscopy

G

GD11	Green disperse dye
GS-HWF	Green Seriline HWF dye

H

hcp	Hexagonal closed packing

I

IA	Illuminant A
IP-BRDF	In-Plane Bidirectional Reflectance Distribution Function
IOPC	Inverse opal photonic crystal
ISO	International Organization of Standardization

K

KL	Kraft Lignin
kHz	Kilohertz
kV	Kilovolt

L

L*	Lightness in CIEL*a*b* color space

M

MMA	Methylmetacrylate
MPN	Most probable number

N

O

ofw	over fiber weight
OS-ADS	Orange Seriline ADS dye

P

PA	Polyamide
PAA	Poly(acrylic acid)

PBG	Photonic Band Gap
PC	Photonic Crystal
PCB	Photonic crystal bead
PdI	Polydispersity index
PDMS	Polydimethylsiloxane
PE	Polyethylene
PES	Polyester
PMMA	Polymethylmetacrylate
P(MMA-BA)	Poly(methylmetacrylate- butyl acrylate)
P(MMA-BMA)	Poly(methylmetacrylate- butyl metacrylate)
PP	Polypropylene
PSt	Polystyrene
P(St-MMA-AA)	Poly(styrene- methylmetacrylate- acrylic acid)
PTFE	Polytetrafluorethylene
PVA	Polyvinyl alcohol
Q	
QUV	UV Accelerated Weathering Tester
R	
Ra	Roughness average
RD-K3G	Red Dianix K-3G dye
rpm	Revolutions per minute
RS-ADS	Red Seriline ADS dye
S	
SDS	Sodium dodecylsulphate
SEM	Scanning electron microscopy
SRB-ADS	Seriline Royal Blue ADS dye
St	Styrene
STA	Simultaneous thermogravimetric analysis
STEM	Scanning transmission electron microscopy
T	
TDS	Total dissolved solids
TEOS	Tetraethyl orthosilicate

TN	Total nitrogen
TOC	Total organic carbon
TP	Total phosphorous
TSS	Total suspended solids

U

UV	Ultraviolet
UV/Vis	Ultraviolet/visible

V

vv%	Percentage in volume

W

wt%	Percentage in weight

Y

YS-ADS	Yellow Seriline ADS dye

Z

ZDHC	Zero Discharge of Hazardous Chemicals

Symbol

α_i	Light incidence angle
α_o	Observation angle
Δa_{avg}	averages of the modular difference for all α_i and α_o between a* under D_{50} and IA light sources
Δb_{avg}	averages of the modular difference for all α_i and α_o between b* under D_{50} and IA light sources
ΔE	Color difference
μm	Micrometer

Figure Index

Figure 1 Examples of photonic crystals found in nature. a) mallard duck, b) *Morpho* butterfly, c) rainbow leaf beetle and d) opal stones. 2

Figure 2 Proposed methodology for the production of technical fabrics. 4

Figure 3 a) Schematic representation of 1D, 2D and 3D photonic crystals and b) schematic outline of the incorporation process of smart polymers into photonic structure. [7] Copyright with permission from Royal Society of Chemistry. 11

Figure 4 Phenolic precursors of hardwood Kraft lignin. 13

Figure 5 Examples of some light reflectance processes, a) conventional reflectance of a dyed substrate, b) thin film interference; c) multilayer interference and d) diffraction in 3D structures. Adapted from [51, 66, 68] 14

Figure 6 a) Schematic drawing of the conventional method for preparing IOPCs with an open cell structure, b) Schematic design to prepare IOPCs with a closed cell structure. [87] Copyright with permission from Royal Society of Chemistry. 17

Figure 7 Schematic illustration of packing modes formed by colloidal crystals. a) hexagonal closed packing (hcp), b) face-centered cubic (FCC) packing, and c) body-centered cubic (BCC) packing, where the hexagonal array can form either a hcp (Figure 7a) or a FCC (Figure 7b) crystal, while the square array can form either a FCC (Figure 7b) or a BCC (Figure 7c) crystal. (This image was generated by GeminiPro) 18

Figure 8 Schematic illustration of the periodic structure change of PC film before (close-packed) and after (non-close packed) hydratation. (This image was generated by GeminiPro) 18

Figure 9 Schematic illustration of gravitational sedimentation of PCs. (This image was generated by GeminiPro) 20

Figure 10 Schematic outline for PC self-assembly through physical confinement. (This image was generated by GeminiPro) 21

Figure 11 Schematic diagram of vertical deposition method. (This image was generated by GeminiPro) 21

Figure 12 Scheme of dip-drawing method. (This image was generated by GeminiPro) 22

Figure 13 A schematic of the processing steps involved in electrophoresis (EP) to fabricate colloidal crystals. [116] Copyright with permission from Elsevier. 22

Figure 14 Classification of biopolymers and their origins. (Adapted from [146]) 25

Figure 15 Dyeing process used for CO at 60°C. 31
Figure 16 Dyeing process used for PES and P(St-MMA-AA) PCs at 130°C. 31
Figure 17 Schematic of IP-BRDF setup. 34
Figure 18 Sample holder with 30, 45 and 70° angles, used for structural color photographic documentation, a) front view and b) side view. 37
Figure 19 Reaction setup for P(St-MMA-AA) PC synthesis. 39
Figure 20 STEM micrographs (200.000 × magnification) of a) ~170, b) ~190, c) ~210, d) ~230 and e) ~250 nm P(St-MMA-AA) spheres. 41
Figure 21 ATR-FTIR spectra from styrene (St), methylmethacrylate (MMA), acrylic acid (AA) and poly(styrene-methylmethacrylate-acrylic acid) (P(St-MMA-AA)). 42
Figure 22 DSC thermogram of P(St-MMA-AA) PCs. 43
Figure 23 STA curve of P(St-MMA-AA) PCs. 44
Figure 24 Reaction setup for SiO_2 PC synthesis. 45
Figure 25 SEM micrographs (40000× magnification) of the obtained SiO_2 particles with different ratios of TEOS:NH_3.H_2O:EtOH, a) 1:2:20 (SiO_2-1), b) 2:1:20 (SiO_2-2) and c) 1:4:40 (SiO_2-3). 45
Figure 26 ATR-FTIR of SiO_2 PCs. 46
Figure 27 DSC thermogram of SiO_2 PCs. 47
Figure 28 STA curve of SiO_2 PCs. 47
Figure 29 Reaction setup for KL PC synthesis. 48
Figure 30 ATR-FTIR of KL PCs. 49
Figure 31 SEM micrograph (magnification of 10000×) of KL PCs. 50
Figure 32 DSC thermogram of KL PCs. 50
Figure 33 STA curve of KL PCs. 51
Figure 34 Digital photographs of uncoated polyamide (PA, L* = 21.11, a* = 0.52, b* = −1.13), polyester (PES, L* = 20.36, a* = −0.34, b* = −3.13) and cotton (CO, L* = 21.19, a* = 0.80, b* = −3.97) fabrics, and PA, PES and CO fabrics coated with 170, 190, 210, 230 and 250 nm PCs. **Note:** the uncoated PA and CO appear grey in photographs but are black. 54
Figure 35 SEM micrographs of polyamide (row a), polyester (row b) and cotton (row c) uncoated fabrics at 150x (a1, b1, c1), 1000× (a2, b2, c2) and 10,000× (a3, b3, c3) magnifications. 55
Figure 36 SEM micrographs of polyamide (row a), polyester (row b) and cotton (row c) coated fabrics with 190 nm PCs at 150× (a1, b1, c1), 1000× (a2, b2, c2), 10,000× (a3, b3, c3) and 100,000× (a4, b4, c4) magnifications. 56

Figure 37 Fixed angle of incidence (8°) UV/Vis reflectance (DHR) spectra for (a) 170, (b) 190, (c) 210, (d) 230 and (e) 250 nm P(St-MMA-AA) PCs in polyamide, polyester and cotton fabrics. 58
Figure 38– Photographs of a) PA uncoated fabric, PA coated with P(St-MMA-AA) photonic crystals with different sizes, b) 170 nm, c) 190 nm, d) 210 nm, e) 230 nm and f) 250 nm, and the observed iridescent effect in each sample. 59
Figure 39 UV/Vis reflectance (s-polarized light) spectra analysis of PA coated with 190 nm PCs, with αi ranging from 12° to 80°. 60
Figure 40. (top) IP-BRDF measurements of PA coated with 190 nm PCs, αi = 30° to 70° and αo = 0° to 70°; (bottom) 2D representation of color coordinates movement in CIEL*a*b* space, where the arrows represent the direction from low to high αo (0° to 70°) for each αi (30° to 70°). 61
Figure 41 UV/Visible reflectance (s-polarized light) analysis of PA coated with 230 nm PCs, with αi ranging from 12° to 80°. 62
Figure 42 (top) IP-BRDF measurements of PA coated with 230 nm PCs, αi = 30° to 70° and αo = 0° to 70°; (bottom) 2D representation of color coordinates movement in CIEL*a*b* space, where the arrows represent the direction from low to high αo (0° to 70°) for each αi (30° to 70°). 63
Figure 43 (top) IP-BRDF measurements of PA coated with 170 nm PCs, αi = 30° to 70° and αo = 0° to 70°; (bottom) 2D representation of color coordinates movement in CIEL*a*b* space, where the arrows represent the direction from low to high αo (0° to 70°) for each αi (30° to 70°). 64
Figure 44 (top) IP-BRDF measurements of PA coated with 210 nm PCs, αi = 30° to 70° and αo = 0° to 70°; (bottom) 2D representation of color coordinates movement in CIEL*a*b* space, where the arrows represent the direction from low to high αo (0° to 70°) for each αi (30° to 70°). 65
Figure 45 (top) IP-BRDF measurements of PA coated with 250 nm PCs, αi = 30° to 70° and αo = 0° to 70°; (bottom) 2D representation of color coordinates movement in CIEL*a*b* space, where the arrows represent the direction from low to high αo (0° to 70°) for each αi (30° to 70°). 66
Figure 46 IP-BRDF measurements of PES coated samples. 67
Figure 47 IP-BRDF measurements of CO coated samples. 68
Figure 48 Structural color changes when P(St-MMA-AA) PCs are in dry/wet state on PA substrates. ... 70
Figure 49 Water marks left on the P(St-MMA-AA) structure upon drying after being partially wetted. 71
Figure 50 Evolution of color change at 0, 24, 48, 76 and 168 h, for a) blue and b) green P(St-MMA-AA) structural colors. An overall view of the substrate is presented below the times of each sample. 72
Figure 51 PA samples covered with a) 190 nm, b) 210 nm and c) 250 nm P(St-MMA-AA) PCs after being coated with Sylgard™ 184, before washing fastness test. 73

Figure 52 PA samples covered with a) 190 nm, b) 210 nm and c) 250 nm P(St-MMA-AA) PCs after being coated with Sylgard™ 184, after washing fastness test. 74
Figure 53 SEM micrographs (500× magnification) of a) uncoated PA and PA samples covered with 250 nm P(St-MMA-AA) PCs b) without Sylgard™ 184, c) coated with Sylgard™ 184, d) coated with Sylgard™ 184 in the peeled off area before washing fastness test and e) Sylgard™ 184 in the peeled off area after washing. 74
Figure 54 Blue, green and red SiO_2 PCs applied onto precoated P(MMA-BA) PES and CO fabrics. 76
Figure 55 KL PCs deposited on a) glass substrate, b) PES fabric and c) CO fabric with P(MMA-BA) precoating. 77
Figure 56 Photonic crystals (170 (violet) to 250 nm (red)) applied onto different colored PES fabrics, with one and two dippings. 80
Figure 57 Effect of PC color on substrates with an opposite CIEL*a*b* axis color, with one, three and five dippings. 81
Figure 58 210 nm P(St-MMA-AA) PCs dyed with disperse dyes DBV-R, SRB-ADS, GD11, YS-ADS and RD-K3G at 2% concentration. 82
Figure 59 210 nm PCs@DBV-R (2 wt%) applied onto dyed polyester samples with one and five dippings. 82
Figure 60 210 nm PCs@SRB-ADS (2 wt%) applied onto dyed polyester samples with one and five dippings. 83
Figure 61 210 nm PCs@GD11 (2 wt%) applied onto dyed polyester samples with one and five dippings. 83
Figure 62 210 nm PCs@YS-ADS (2 wt%) applied onto dyed polyester samples with one and five dippings. 83
Figure 63 210 nm PCs@RD-K3G (2 wt%) applied onto dyed polyester samples with one and five dippings. 84
Figure 64 210 nm PCs@ RD-K3G (0.5 and 1 wt%) applied onto dyed polyester samples with five dippings. 84
Figure 65 Photographs of mixed photonic crystals in different proportions onto PA fabric with the respective CIEL*a*b* color coordinates. 87
Figure 66 SEM cross-sectional micrographs of pre-mixed violet and red PCs (1:1) on PA at different magnifications, a) 4000x, b) 15000x, c) 20000x and d) 50000x. 89

Figure 67 Particle size distribution in the cross-section (left) and on the bottom of the fabric (right). (cross section n=1271; bottom n=926) 89

Figure A 1 The design of a sample holder for structurally colored fabrics. Schematics in a) side view, b) overall view, c) back view and d) front view..... 116

Figure A 2 Size optimization of 250 nm P(St-MMA-AA) PCs. Red structural color on PA fabric, a) synthetized at 60°C and 300 rpm reactional conditions and b) synthetized varying monomers proportions, at 70°C and 300 rpm reactional conditions..... 116

Table Index

Table 1 Water quality parameters with threshold values listed at a safe level [17] and real textile wastewater values [14, 18]. 8

Table 2 Disperse dyes utilized for polyester and photonic crystal dyeing processes..... 28

Table 3 P(St-MMA-AA) PCs size analysis comparison between DLS and STEM of the tested reactional conditions..... 40

Table 4 Fabrics characterization according to the ISO standards. 53

Table 5 Surface roughness (Ra) measurements values of uncoated and PC coated fabrics (n = 3). 56

Table 6 UV/Vis reflectance peaks of PA coated samples with 170, 210 and 250 nm PCs according to changes in the angle of incident light (αi). 64

Table 7 Differences in CIEL*a*b* color coordinates of PA coated samples under D_{50} and IA light sources illuminations. Δa_{avg} and Δb_{avg} are the overall averages of the modular difference for all αi and αo between a* and b* under D_{50} and IA for each PA coated sample. $\Delta a_{avg} = |a_{D50} - a_{IA}|$; $\Delta b_{avg} = |b_{D50} - b_{IA}|$ 69

Table 8 Effect of PC coating in CIEL*a*b* color coordinates L*, a* and b* when compared to the uncoated PES fabric. (+) increased, (-) decreased and (=) maintained. 80

Table A 1 CIEL*a*b* color coordinates of violet, blue, green and red photonic crystals applied onto black polyester substrate, with 1 and 2 dippings. 117

Table A 2 CIEL*a*b* color coordinates of violet, blue, green and red photonic crystals applied onto different colored PES substrates (1 dippping). 117

Table A 3 CIEL*a*b* color coordinates of violet, blue, green and red photonic crystals applied onto different colored PES substrates (2 dipppings)..... 118

Table A 4 CIEL*a*b* color coordinates of 210 nm PCs@DBV-R (2 wt%) applied onto dyed polyester samples with one and five dippings. 118
Table A 5 CIEL*a*b* color coordinates of 210 nm PCs@ SRB-ADS (2 wt%) applied onto dyed polyester samples with one and five dippings. 119
Table A 6 CIEL*a*b* color coordinates of 210 nm PCs@GD11 (2 wt%) applied onto dyed polyester samples with one and five dippings. 119
Table A 7 CIEL*a*b* color coordinates of 210 nm PCs@ YS-ADS (2 wt%) applied onto dyed polyester samples with one and five dippings. 120
Table A 8 CIEL*a*b* color coordinates of 210 nm PCs@ RD-K3G (2 wt%) applied onto dyed polyester samples with one and five dippings. 120
Table A 9 CIEL*a*b* color coordinates of 210 nm PCs@ RD-K3G (0.5 wt%) applied onto dyed polyester samples with 1, 3 and 5 dippings. 121
Table A 10 CIEL*a*b* color coordinates of 210 nm PCs@ RD-K3G (1 wt%) applied onto dyed polyester samples with 1, 3 and 5 dippings. 122

In memorium

To Professor António Pedro Souto

"A great soul never dies. It brings us together again and again."

Maya Angelou

1

Introduction

1.1. Framework

Every year, 6 million tons of 8,000 different chemicals are used in textile processing units [1]. To mention some in textile processing, cleaning involves alkali, bleaching requires aggressive chemicals, crosslinking agents involve formaldehyde-derived auxiliaries, dyeing is carried out using non-biodegradable synthetic dyes containing azo groups or heavy metals and finally, the finishing step involves the use of chemicals that may contain antimony and bromine. These hazardous chemicals pose serious threats to the health of workers at processing plants. [2] In addition, the remains of these chemicals in wastewater cause environmental pollution. Since the last few decades, the use of non-toxic, ecological and less dangerous chemicals has been emphasized to reduce health risks for workers operating in processing units and to avoid environmental risks. In recent years, the use of biodegradable and less toxic chemicals is increasing in wet textile processing, using "green" chemicals as an alternative, having been adapted for better biodegradability and to reduce the toxicity of effluents discharged from processing units. As part of a greener approach, it is better to avoid producing waste than to plan and adopt treatment strategies to dispose of it, [3] hence the research presented herein.

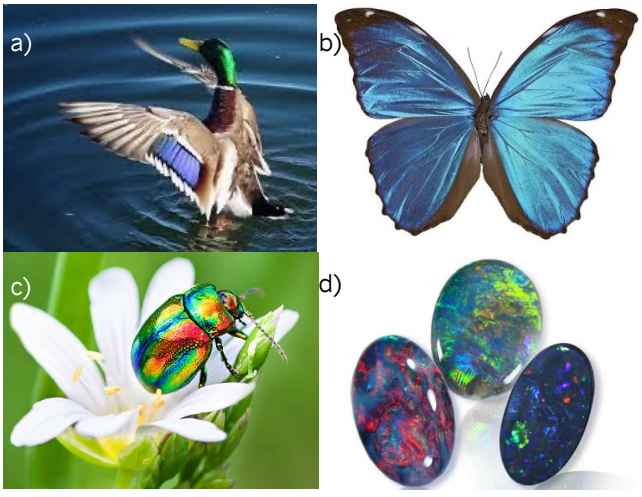


Figure 1 Examples of photonic crystals found in nature. a) mallard duck, b) *Morpho* butterfly, c) rainbow leaf beetle and d) opal stones.

Unlike traditional color, which comes from dyes or pigments that absorb light, structural color is produced by physical interactions of light with biomaterials which have nanostructural variation in the refractive index on the order of the visible wavelength [4]. These nanostructured materials can be found in nature in animals (Figure 1a-c), insects and fruits, being used for signaling and communication [5]. They also can be found as natural opal stones (Figure 1d). It mostly arises from selectively reflected light

by a physical periodically textured structure interacting with incident light, such as dispersion, scattering, interference and diffraction [3, 4]. Most of structural colors found in nature are originated from five fundamental optical processes and their combinations: thin-film interference, multilayer interference, diffraction grating effect, photonic crystals and light scattering [6]. Structural color has a variety of potential applications, because of its long-term resistance to discoloration; furthermore, iridescence obtained by structural colors cannot be reproduced by pigments, and pigment-free coloration is preferable from ecological viewpoint, where water is essentially needed for the synthesis of photonic crystals from which color is achieved [7]. There is a need to progress studies in this field, not only to further understand structural color behavior but also to implement a more sustainable future.

1.2. Research Questions

The aims of this innovative research project need to be divided in six fundamental questions:

1. Is it possible to obtain a broad spectrum of colors from photonic crystal (PC) synthesis?
2. Will the usage of plasma radiation influence the uniformity of PCs deposition or the coating adhesion?
3. How will the color of the textile substrate influence the structural color produced by PCs?
4. What will be the effect on the original structural when the PCs themselves are dyed with conventional dyes?
5. Is it possible to increase the fastness of PC deposited textile substrate without interfering on the obtained colors?
6. Is it possible to apply a biopolymer coating after photonic crystal deposition, maintaining all PC properties (color, brightness and iridescence), with improved fastness properties?

1.3. Objectives

The main objective of this thesis is to promote sustainability in the Textile Industry by replacing the usage of dyes or pigments with colors originating from their structural arrangement, structural coloration, avoiding the production of effluents. As such, the methodology adopted in this research was divided into six specific objectives in order to achieve the final prototype, technical fabrics with high visibility for segments of workwear or sportswear with optimized iridescence. The proposed methodology to execute these objectives is presented in Figure 2.

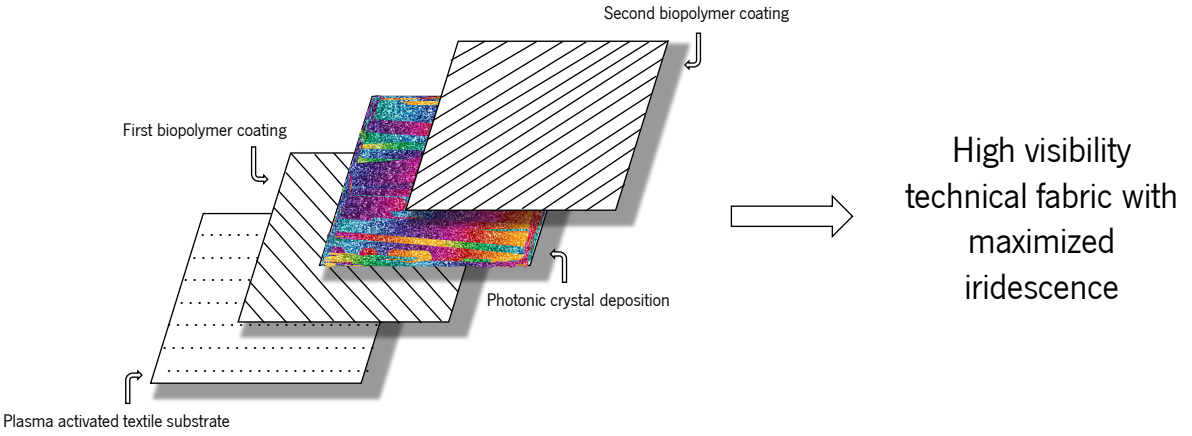


Figure 2 Proposed methodology for the production of technical fabrics.

Thus, the specific objectives are:

- Synthesis and production of different types of photonic crystals;
- Application of photonic crystals onto several textile substrates;
- Improvement of PCs adhesion, washing and light fastness to textile substrates through biopolymer coating;
- Study the influence of color substrate when combined with structural color;
- Study the influence of color substrate when combined with dyed PCs at different size;
- Study the effect of color addition/subtraction when different sized PCs are mixed.

1.4. Thesis Outline

In alignment with the proposed objectives, this thesis is organized as follows:

Chapter 1 Introduction

In the Introduction section, an overview of the thesis can be found, contextualizing the problem to be solved throughout this thesis, as well as the main objectives and the thesis outline.

Chapter 2 Literature Overview

In this chapter a revision of the fundamental literature was performed and compiled, according to the methodologies used throughout the execution of the thesis. Thus, key topics as an environmental context, photonic crystals (different types and application techniques), substrate properties for PC deposition,

plasma radiation, and biopolymers were discussed in detail in how they can influence the production and stabilization of structural colors.

Chapter 3 Materials and Methods

In this chapter are described all reagents, equipment, assays and methodologies used during the execution of this work.

Chapter 4 Photonic crystal synthesis and characterization

This chapter describes the synthesis and optimizations performed to obtain different sizes of photonic crystals composed by P(St-MMA-AA), SiO_2 or KL, and their respective characterization through FTIR, SEM, DLS, DSC and STA.

Chapter 5 PC deposition onto textile substrates

This chapter describes how P(St-MMA-AA), SiO_2 and KL PCs are applied onto different textile substrates. Different colors and effects were obtained, depending on PC composition and size, and type of fiber of the substrate. The most promising samples, P(St-MMA-AA) onto PA fabric, were characterized, mainly through SEM and UV/Vis spectroscopy. The application of adhesives (pre-PC deposition), finishing agents (post PC deposition) and color fastness tests can also be found in this section.

Chapter 6 Color substrate and PC dyeing influence on structural coloration

In this chapter, substrate color influence is studied on how it affects the produced structural color. Photonic crystals were dyed with different disperse dyes, applied onto the different colored substrates, evaluating the effects of both substrate and PC dyeing color at the same time.

Chapter 7 Mixture of pristine P(St-MMA-AA) PCs

This chapter studies the self-assembly of PCs with different sizes, in polyamide fabrics, to verify if PCs follow the principles of color addition. Furthermore, the cross-section of the PC layer deposited onto the fabric surface was analyzed via SEM, analyzing the percentage of PC sizes and sphere arrangement.

Chapter 8 Conclusion and future perspectives

This final chapter present the major conclusions of the thesis and some future perspectives for this research work, proposing further studies and potential advancements from this work.

2

Literature Overview

Part of this chapter is based on the following publications:

(Book Chapter) Fernandes, Marta; **Fernandes, Rui D.V.**; Padrão, Jorge; Melro, Liliana; Alves, Cátia; Rodrigues, Rui; Ribeiro, Ana Isabel; Zille, Andrea. "Plasma in textile wastewater treatment". In Advances in Plasma Treatment of Textile Surfaces, 267-322. Elsevier, 2024. doi: 10.1016/B978-0-443-19079-7.00008-7

(Paper) **Fernandes, Rui D.V.**; Pranovich, Alina; Valyukh, Sergiy; Zille, Andrea; Hallberg, Tomas; Järrendahl, Kenneth. "Iridescence Mimicking in Fabrics: A Ultraviolet/Visible Spectroscopy Study". *Biomimetics* (2024) 9, 71. doi: 10.3390/biomimetics9020071

2.1. State of the art

2.1.1. Environmental context

Water is an essential resource for all the forms of life on this planet. It is also a critical source of anthropogenic social and economic development [8]. Nevertheless, freshwater scarcity is a real issue that must be dealt worldwide. It is estimated that by the year 2050 around 6 billion people will suffer from potable water scarcity [9]. The depletion of freshwater is a consequence of rapid population growth, climate change, industrial and farming activities, poorly planned urbanization, and economy [10, 11].

The population growth prompts a natural intensification in water consumption, which leads to an increase in the generation of effluents. These effluents, especially those from industrial activities, contain organic contaminants, presenting a serious threat to the environment and the health of all living beings. Annually, 380 billion m^3 of wastewater are generated, with an estimated increase of 24% by the year 2030 and 51% by 2050 [12].

Textile industry is among the top industries which contribute to water shortage and pollution, as it consumes enormous amounts of water (150 L of freshwater per 1 kg of the product) and consequently generates large volumes of effluents contaminated with organic pollutants (about 200 to 350 m^3/ton of final product) [13, 14]. More than 8000 chemical substances were already found in textile wastewater [15, 16]. Therefore, several countries established legal thresholds for several wastewater parameters, including the Zero Discharge of Hazardous Chemicals (ZDHC) program, which launched the ZDHC wastewater guidelines. These guidelines set out limits for different wastewater parameters (e.g., pH, temperature, biological oxygen demand (BOD), chemical oxygen demand (COD), etc.), heavy metals, and other chemicals such as harmful dyes [17]. Table 1 indicates some threshold parameters for wastewater to be qualified as safe according to the ZDHC wastewater guidelines, as well as an example of textile wastewater values. It is perceivable that the composition of textile wastewater is highly variable. It is characterized by a dark color, a wide range of pH, elevated temperature, high electrical conductivity, alkalinity, total dissolved solids (TDS), total suspended solids (TSS), total organic carbon (TOC), COD, BOD, oils, grease, total nitrogen (TN), total phosphorous (TP), and heavy metals.

Table 1 Water quality parameters with threshold values listed at a safe level [17] and real textile wastewater values [14, 18].

Stage process	Threshold value (ZDHC guidelines)	Observed textile wastewater parameters
pH	6-9	5.5-12
Temperature (°C)	Δ+15	20-45 °C
Escherichia coli (MPN/100 mL)	126	-
Electrical conductivity (μS/cm)	-	<1000
Alkalinity (mg/L)	-	200-800
Color (Pt-Co)	-	50-2,500
TDS (mg/L)	-	1500-12,000
TSS (mg/L)	50	80-10,000
TOC (mg/L)	150	100-350
COD (mg/L)	150	100-30,000
BOD (mg/L)	30	80-6,000
Oil and grease (mg/L)	10	5-30
TN (mg/L)	20	10-50
TP (mg/L)	3	5-30
AOX (mg/L)	3	0.11-1.05
Heavy metals:		
Antimony (mg/L)	0.1	-
Arsenic (mg/L)	0.05	<10
Cadmium (mg/L)	0.1	0.07-2
Chromium (VI) (mg/L)	0.05	-
Chromium, total (mg/L)	0.2	2-5
Cobalt (mg/L)	0.05	<10
Copper (mg/L)	1	2-10
Lead (mg/L)	0.1	3-6
Nickel (mg/L)	0.2	0.5-3
Mercury (mg/L)	0.01	<10
Silver (mg/L)	0.1	-

Zinc (mg/L)	5	<10
Anions:		
Chloride (mg/L)	-	200-6,000
Cyanide (mg/L)	0.2	-
Sulfate (mg/L)	-	500-1,000
Sulfide (mg/L)	0.5	5-20
Sulfite (mg/L)	2	-
Dyes:		
Carcinogenic or equivalent concern (μg/L)	500	-
Disperse (allergenic) (μg/L)	50	-
Navy blue colorant (μg/L)	500	-

MPN - most probable number, AOX - adsorbable organically bound halogen.

Among the contaminants, dyes have the greatest impact on water degradation. The textile industry is responsible for half of the dye effluents generated worldwide. Annually, this sector produces over 700,000 tons of synthetic dyes, from which nearly 40% end up being released in the effluents. [11, 19, 20] Azo dyes are the most commonly used dyes in the textile industry (60-70%). However, they can be cleaved into aromatic amines and present cytotoxic, carcinogenic, and recalcitrant properties. They can accumulate in the food chain and disrupt the photosynthesis mechanisms of aquatic organisms, as they prevent the absorption of light, and increase the BOD and COD. [16] Light deprivation drastically endangers the survival of photosynthetic organisms, which further potentiates the eutrophication of an already high load of BOD and COD. Several wastewater treatments are performed to mitigate the negative impacts of textile effluents. Nonetheless, the conventional methodologies are grievously ineffective in degrading recalcitrant compounds such as azo dyes. [21]

In the dyeing process, based on the fibrous material, different classes of dyes are used (e.g., direct, reactive, disperse, acid, basic, vat, sulfur, and azoic dyes). Dyes are soluble organic compounds, and the color is provided by chromophore groups, such as: azo (-N=N-), nitro (-N=O), carbonyl (-C=O), quinoid groups, and by auxochrome groups (e.g., amine, carboxyl, sulphonate, and hydroxyl). The auxochrome groups are responsible for electron withdrawing or donation, as well as for the amplification of color. [22, 23] Azo dyes are chemically stable compounds, being the most ubiquitously used. [16] These dyes have high recalcitrance and polarization properties, which together with the high solubility in water, make their removal very difficult. [24, 25]. Nearly 50% of the dyes used in textile dyeing are not fixed on the

substrates, being released in the wastewater. [26] In addition to the dyes, other products (e.g., organic auxiliaries, formaldehyde, heavy metals, surfactants, salts, and sulfides) are added during the dyeing process to enhance dye adsorption onto the fibers, which are also important sources of effluent contamination.[23] All these chemicals contribute to a strongly toxic colored wastewater, which contains high BOD, COD, and TSS. [22] In the printing process, the color is added by applying dyes and pigments in the form of a thick paste to fix the dyes on the textile surface and prevent their diffusion. [22] About 25% of the world's total print production is carried out using reactive printing whose pastes contain 10-20 wt% of urea. The wastewater from this process contains a high concentration of ammonia-nitrogen, due to the degradation of urea, and other pollutants such as thickeners and unfixed dyes. [27] Lastly, finishing processes are used to confer to the textile product some desired properties (e.g., smoothness, waterproof, antibacterial, and ultraviolet (UV) protection) and the wastewater characteristics from these processes rely on the finishing agents used. [22]

Ingestion or prolonged exposure by humans to contaminated water with a dye concentration above 1 mg/L can lead to skin irritation, respiratory problems, nausea, headaches, cancer, or even teratogenic issues. Potentially carcinogenic compounds are generated when dyes undergo anaerobic degradation, such as aromatic amines due to the azo and nitro groups present in organic dyes. [22, 23, 28] Moreover, during the degradation process of several dyes, dangerous heavy metals, such as copper, zinc, chromium, lead, cobalt, nickel, and manganese, are released. These heavy metals represent a serious threat to human health and the environment, as they easily contaminate both water bodies and soil. [10, 23] Finally, the textile industry wastewater owes its recalcitrant nature towards conventional treatments due to its low biodegradability index (BI<0.4). [15] Thus, persistent primary (pristine dye) and secondary (generated during dye degradation) hazardous compounds will remain and bioaccumulate in the ecosystem, threatening all living organisms. [23] These issues can be overturned using advanced oxidation processes (AOPs), which are able to decompose persistent organic compounds into carbon dioxide (CO_2) gas and H_2O using OH radicals (•OH). [29] AOPs represent an alternative method to conventional treatments, where organic pollutants are completely mineralized into CO_2 and water or are degraded into non-toxic or less toxic by-products, with minimal sludge production. These processes include ozonation, UV, Fenton process, photocatalysis, electrochemical reactions, ultrasound irradiation, and cold plasma technology. Cold plasma technology is a sustainable and emergent AOP for the treatment of textile wastewater where the high-energy active particles with superior oxidation potential are produced at low temperature, atmospheric pressure, and without using any hazardous chemical products. [8, 29, 30] When AOPs are not possible to be applied in textile effluents, as some processes can have a high

cost, the alternative is to not produce them; the use of photonic crystals for textile coloration dramatically reduces waste generation.

2.1.2. Photonic Crystals

Human beings have been trying to imitate Nature characteristics in laboratory since the early stages of modern science. Some optical characteristics can be achieved through structural coloration and photonic crystals (PCs), in opposition to other principles of color production, such as optical absorption (dye/pigment), emission (for example light emitting diode), interference (soap bubble or rainbow coloring on a compact disc) or dispersion (for example blue sky or red sunset). [31]

PCs are innovative materials inspired by Nature, particularly the iridescent colors of butterfly bird feathers, and beetle exoskeletons having color generating structures in one, two, or three dimensions (Figure 3). [7, 32-34] Is generally used as a signal to alert enemies through mimicry or to deceive them through camouflage, to convey information or choosing partners. [35-37]

These artificial structures mimic the intricate patterns found in biological organisms to manipulate and control light. By emulating nature's designs, photonic crystals exhibit unique optical properties that can bend, reflect, or trap light of specific wavelengths.

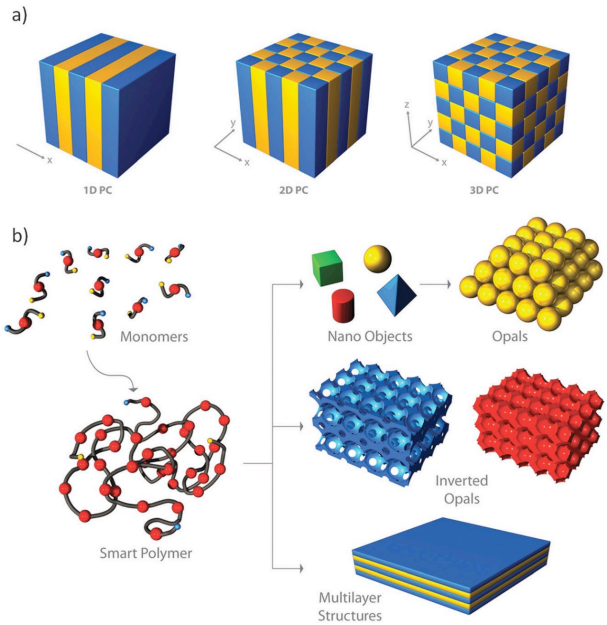


Figure 3 a) Schematic representation of 1D, 2D and 3D photonic crystals and b) schematic outline of the incorporation process of smart polymers into photonic structure. [7] Copyright with permission from Royal Society of Chemistry.

PCs are periodic structures that exhibit a bandgap for certain wavelengths of the electromagnetic radiation, similar to how semiconductors have electronic bandgaps for electron energy levels. [38, 39] The photonic bandgap (PBG) arises from the periodic variation in refractive index within the structure, where light is forbidden to propagate within the PCs, thus being determined by the crystal lattice and periodicity. Depending on material choices for the PCs synthesis (polystyrene (PSt) or silica (SiO_2) particles) and the substrate (glass, metallic, or fabric), structural colors with iridescent effects can occur due to angular resolved Bragg diffraction from the lattice planes. [40] Structural colors are generally iridescent, very bright, deeply saturated, free from solar fading and resistant to long-term discoloration. PCs can be applied in ink-jet printing, [41, 42] 3D printing, [43, 44] lithography [45, 46] and sensors, [47, 48] among others, [49, 50] to produce structural colors. They can also be applied in textiles, an area of research that had demonstrated great interest in the last decade. [40, 51-53] Being one of the most pollutant industries in the world, there is a constant demand that the textile industry searches for more ecological methods of coloration, using less chemicals and water. One promising approach to a more ecological production of colored fabrics is the application of structurally coloring PCs where, compared to traditional dyeing processes, the consumption of water is dramatically reduced. The reason is that there is no need for water to rinse the fabrics after coloring, thus effluents can be severely reduced. However, a fabric surface is very irregular when compared to glass or metallic surfaces, so applying PCs on fabrics can be challenging since, the fiber (natural or synthetic, shape, cross-section area), yarn properties (number of cables, torsion, linear density) and fabric construction (number of yarns at warp and weft, type of structure) will influence its surface roughness. [54] Li *et al* studied the influence of weave, yarn diameter and yarn density of polyester and silk fabrics on obtaining SiO_2-based structural colors. It was observed that both physical and chemical properties of the fabric influence structural color. Li *et al* observed that, physically, more compact and flat substrates would promote better PC self-assembly, meaning that plain fabrics were better substrates than twill fabrics due to the small gaps between fibers, for both polyester and silk. Chemically, fabrics that possess less polar and water-soluble groups in their composition will be preferred to achieve better structural colors, which in this study were exemplified with polyester fabrics. [54] Zhou *et al* also performed structural coloration studies on polyester fabrics, with variations on the PC's mass fraction utilized for the coating, humidity percentage and temperature. It was noted that using a mass fraction of 1.5% of SiO_2 PCs led to better arranged structures versus mass fractions of 0.5, 1.0 and 2.5%. Furthermore, higher relative humidity percentages (60%) and lower temperatures (25°C) also led to better organized structures meaning the evaporation rate of the PCs

colloidal solution, liquid retention and stability of the fabrics (shrinkage) are determinant factors to obtain good structural colors. [55]

A more sustainable alternative to polystyrene-based or SiO_2 PCs, is to obtain structural color through natural compounds, one of them being lignin. Lignin is a natural polymer with a structure that comprises a large number of unsaturated and conjugated groups. Lignin properties are influenced by a sort of factors such as plant source, pulping method, and solvent system. The chemical pulping usually yields heterogeneous polymers via in situ polymerization of p-coumaryl, coniferyl, and sinapyl alcohols (Figure 4). Kraft lignin presents diverse inter-unit linkages, with hardwood lignin (guaiacyl (G) and syringyl (S) units) being less condensed, lower in molecular weight, and more reactive than softwood lignin (G-units prevalent). [56]

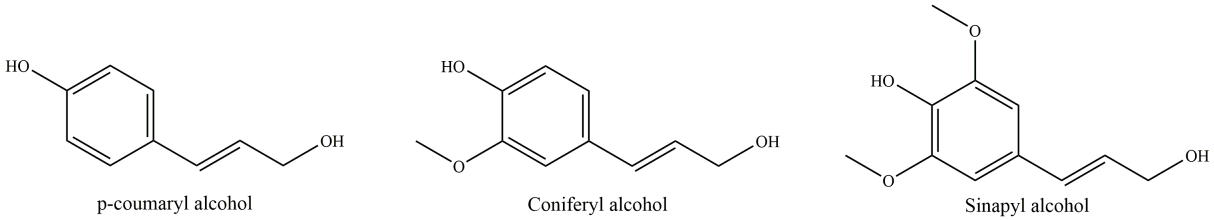


Figure 4 Phenolic precursors of hardwood Kraft lignin.

The synthesis of Kraft lignin nanoparticles predominantly relies on bottom-up techniques—such as nanoprecipitation, antisolvent precipitation, solvent shifting, and self-assembly—wherein water typically serves as the primary nonsolvent. [57] Solvation of Kraft lignin in organic or alkaline media yields an elongated, ellipsoidal conformation that is highly prone to aggregation. Consequently, the introduction of water drives intermolecular chain association, facilitating the precipitation and formation of nanoparticles. [58] Upon self-assembly, these nanoparticles organize into specific microstructures that exhibit structural color. Liu *et al* fabricated colloidal lignin particles achieving stable structural colors and photothermal conversion, with spherical nanoparticles sizes comprising between 200-300 nm. [59] Wang *et al* synthetized tunable lignin particles (181 to 279 nm) able to produce water-responsive structural colors (purple, blue, green, yellow and red), applied onto a variety of substrates (glass, metal, plastic, wood and skin). [60] Dghoughi *et al* obtained lignin nanotriangles after a long period of dialysis to remove DMSO. Although these particles presented high PdI values, they were applied onto glass substrates to produce iridescent colors. [61] Other authors were able to produce lignin structural colors through photonic glasses, a disarranged structure of particles, densely packed, where color arises from short-range order

(unlike photonic crystals, which rely on a long-range). Photonic glasses are usually angle-independent, producing solid colors with reduced brightness. [62, 63]

Thus, colloidal self-assembly is proposed as the most reliable method due to the low production costs of PCs over large areas.

2.1.3. Light/substrate interaction

Unlike the color obtained by selective absorption of wavelengths of incident light, usually obtained with the use with dyes or pigments, the structural color is produced by physical interactions of light with biomaterials that have a nanostructural variation in the refractive index in the order the visible wavelength. [4] The structural color arises mainly from the light reflected selectively by a structure periodically textured physics interacting with incident light, such as dispersion, scattering, interference and diffraction. [31, 64] Most structural colors found in nature originate from five fundamental optical processes and their combinations: thin film interference, multilayer interference, diffraction grid effect, photonic crystals and light scattering (Figure 5). [65-67]

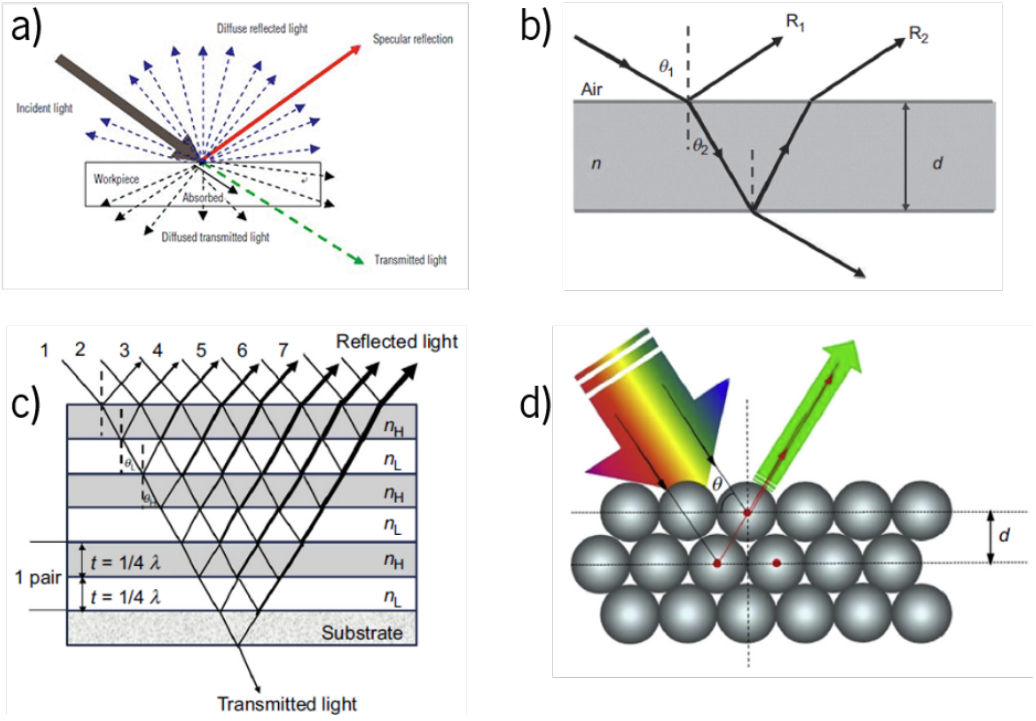


Figure 5 Examples of some light reflectance processes, a) conventional reflectance of a dyed substrate, b) thin film interference; c) multilayer interference and d) diffraction in 3D structures. Adapted from [51, 66, 68]

In light scattering processes, light strikes randomly arranged particles or irregularities that are smaller than the light's wavelength. The particles deflect shorter wavelengths much more aggressively in all directions than longer wavelengths. In thin films, light reflects off both the top and bottom boundaries of a single, microscopic thin layer. The overlapping light waves combine, reinforcing specific colors while canceling out others depending on the viewing angle. As for the multilayer interference, multiple thin films are stacked on top of each other, where light will reflect off numerous alternating sub-layers, which greatly intensifies the brightness and purity of the resulting color. In the case of photonic crystals, the length scale on which the variation occurs is a few hundred nanometers, which corresponds to the wavelength of light in the UV-visible and infrared regions. Like ordinary crystals, where there is a periodic variation in the crystal potential, in materials with PBG the refractive index or the dielectric constant of the medium varies periodically. The greater the difference in refractive indices between the two photonic crystal materials, the greater the effect on light behavior. [66]

Another important aspect in terms of coloring textile substrates with photonic crystals, and in which there are few scientific studies, is the color of the textile substrate. [69] Most of published papers about photonic crystals in textiles use a black colored substrate, [40, 70-73] usually of synthetic fiber due to their smooth fiber appearance, low moisture property, high dimensional stability, good resistance to heat, and relatively flat and compact surface compared with natural fibers substrates. [54, 55] Black colored substrates are important because the transmitted light and scattered light outside the photonic band gap are absorbed by the black substrate, thus enhancing the chroma produced by structural color. On the other hand the structural colors of photonic crystals constructed on white substrates are usually inconspicuous and barely noticeable. [74]

Some studies have been made with dyed PCs in order to enhance structural colors, where PC brightness, iridescent effect and reflectance of the coated fabric was enhanced by dyeing PCs with disperse dyes, which also increased saturation and brightness of color. When white substrates were used the structural colors of dyed photonic crystals were more vivid and monochromatic. [6, 75]

Zhou *et al* deposited photonic crystals onto polyester fabrics, were they studied the correlation between structural colors and base color, specifically opponent colors in b axis (yellow and blue) of the CIEL*a*b* (International Commission on Illumination L* a* b*) system, were they observed that the final color of the assembled fabrics display a blurry and milky color. [51]

Given the limited existence of scientific publications on this crucial aspect in the deposition of photonic crystals on textile substrates, part of this research will be dedicated to the study of the influence of the color of the substrate on PC deposition, either with dyed or pristine photonic crystals.

2.1.4. Photonic crystals' structures

Colloidal photonic crystal beads (PCBs) can be arranged with different structures, such as inverse opals, non-closed-packed or closed-packed. [76-80]

Inverse opal photonic crystal (IOPCs) spheres can be manufactured by mold replication or co-assembly. In the replication process, the materials that the final inverse opal sample must consist of are filled in the empty spaces free from the molds. These filled materials for making reverse opal films include ultrafine nanoparticles (which are much smaller than the free empty channels), metal oxide precursors, pre-polymeric hydrogel solutions, etc. However, when manufacturing inverse opal spheres with rigid materials, the colloidal crystal ball molds must be fully incorporated into the rigid materials to obtain a complete filling, thus preventing the release of inverse opal spheres in the materials. [76, 81] In contrast, soft hydrogel materials can be shredded without destroying the molds of the colloidal crystal spheres, so the hybrid spheres can be separated from the hydrogel even when they are completely embedded. [82] After removing the nanoparticles, inverse opal hydrogel spheres with perfect spherical geometry could be obtained. So far, metals, semiconductors, polymers, blocks of co-polymers and composites with an opal inversed structure have been reported. [83-86] However, most reported IOPCs have open cell structures (ie, all cavities are interconnected) (Figure 6a). Open cell IOPCs have a serious disadvantage, as their low mechanical properties restrict their applications a lot. Compared to open cell structures, closed cell structures (that is, all wells are isolated and separated by a continuous solid phase) have greater mechanical strength, thus the potential for application in fields such as aerospace, thermal insulation or energy absorption is augmented.

It is, therefore, desirable to prepare closed-cell IOPCs to improve mechanical properties and increase their application field. However, it is quite difficult to prepare IOPCs with closed cell structures by the conventional method.

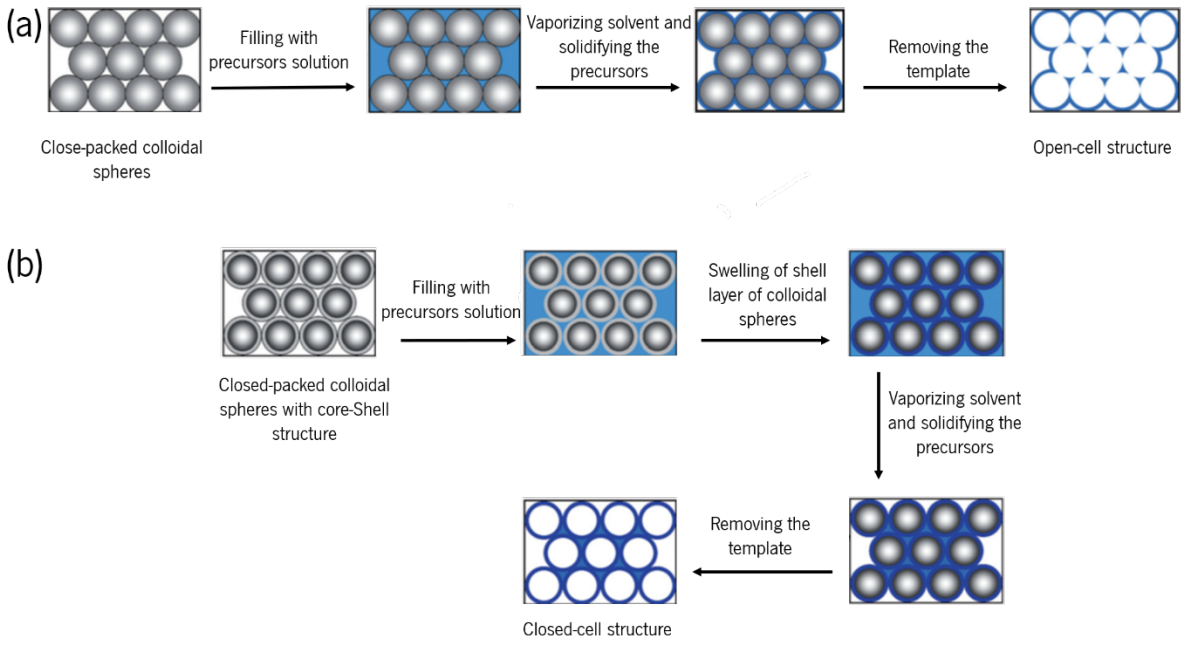


Figure 6 a) Schematic drawing of the conventional method for preparing IOPCs with an open cell structure, b) Schematic design to prepare IOPCs with a closed cell structure. [87] Copyright with permission from Royal Society of Chemistry.

In conventional methods, IOPCs are generally prepared using colloidal spheres of close-packed structure (such as polystyrene or silica spheres) as a model. As shown in Figure 6, the precursors first penetrate the void of the mold; then the precursors are solidified; finally, the mold is removed. It can be concluded that the precursors cannot enter the points of mutual contact of the closed-packed shaped spheres, so that open cell structures can only be formed after removal of the mold. As a result, reports on the manufacture of closed cell IOPCs are scarce.

PCBs with a non-closed-packed crystalline colloidal structure can be manufactured by models of water or oil droplets that contain colloidal nanoparticles. [68, 88] When some electrically charged colloidal nanoparticles are encapsulated in a droplet of pure water with a relatively high concentration, a significant interparticle repulsion occurs in the interparticle spacing, and the minimum energy configuration causes the colloidal nanoparticles to assemble in a non-close-packed FCC (face-centered cubic) or BCC (body-centered cubic) formation (Figure 7). Although the colloidal crystal matrix can be stable for a long time, it can become disordered with the introduction of ionic impurities. [87]

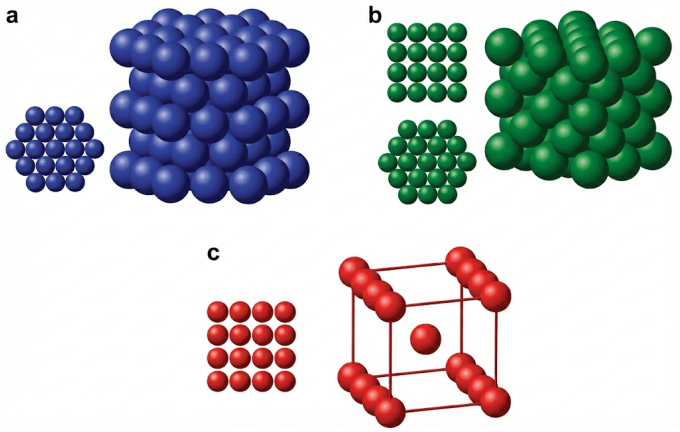


Figure 7 Schematic illustration of packing modes formed by colloidal crystals. a) hexagonal closed packing (hcp), b) face-centered cubic (FCC) packing, and c) body-centered cubic (BCC) packing, where the hexagonal array can form either a hcp (Figure 7a) or a FCC (Figure 7b) crystal, while the square array can form either a FCC (Figure 7b) or a BCC (Figure 7c) crystal. (This image was generated by GeminiPro)

Closed packed configurations can also transition to a non-closed formation by absorbing water (hydrochromism), stretching the distance between spheres, resulting in a volume increase. This can also lead to an increase in thickness, redshift phenomenon of the stopband and color change off-prepared PCs (Figure 8), often observed in humidity sensors. Structural color can also be altered by physical or chemical stimuli, such as mechanochromic, thermochromic, electrochromic, magnetochromic, solvatochromic, gasochromic, vapochromic, among others. [64, 89, 90]

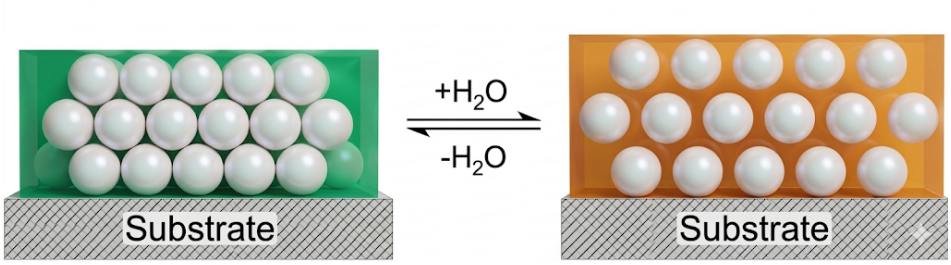


Figure 8 Schematic illustration of the periodic structure change of PC film before (close-packed) and after (non-close packed) hydratation. (This image was generated by GeminiPro)

Close-packed colloidal PCBs are essentially sets of spherical colloidal crystals. Evaporation-induced crystallization of colloidal nanoparticles is the most popular approach to forming PCBs from droplet models. [91, 92] Intrinsically, the colloidal assembly induced by evaporation can be considered as a concentration process, in which the volume fraction increases to a maximum value. [77] In this process, capillary forces provide a compressive force that causes the arrangement of colloidal nanoparticles.

Capillary forces thus "close" the nanoparticles in their final spherical configuration and van der Waals forces later join the nanoparticles.

As such, closed packed structures are easily obtained by dip-drawing, due to the simplicity of solvent evaporation. Zhang *et al* prepared hydrophobic angle-dependent structurally colored fabrics, by dip-coating a white polyester fabric in a solution containing functionalized SiO_2 photonic crystals. Fabrics were immersed for 1 minute and vertically dried at room temperature. These samples demonstrated great color fastness results, as well as bending and stretching fastness. [93] Fu *et al* developed an antifouling fabric, with wash resistance and angle-independent structural color, by dip-coating several different fabrics into a SiO_2/PDMS solution. Fabrics with different weaves, surface densities and chemical compositions were tested and evaluated on their ability to produce the desired properties. [94] Martusciello *et al* dip coated glass substrates with photonic crystals to produce a multilayer dielectric mirror. The multilayer was produced by substrate immersion, at different withdrawal speeds, into the colloidal solution, which was then dried and heated with an infrared lamp, with different irradiation powers. This process was repeated until the number of desired layers was achieved, which in this case was 11. [95]

Closed packed structures production is facilitated by the simplicity of dip-coating (or dip-drawing) methodology, thus these structures will be applied throughout the execution of the thesis.

2.1.5. Structural color production techniques

Several techniques have been developed to produce periodic matrices of dielectric materials that can exhibit a PBG. Some synthesis techniques are quite elaborate, including multilayer lithography, [64] holographic lithography, [96, 97] optical interference methods [98] and production of IOPC structures. [77] IOPCs have been proposed to obtain optimal 3D structures with photonic crystal properties, from SiO_2 or spherical polymers (mainly polystyrene (PSt), poly (methyl methacrylate) (PMMA) or poly (styrene-methyl methacrylate-acrylic acid) (P(St-MMA-AA))), due to the facile control of the polymer colloids size through soap-free emulsion polymerization. [99, 100] Nevertheless, other simpler techniques can be utilized to produce structural colors, based on the principles of colloidal self-assembly. Monodisperse colloidal spheres are observed to spontaneously assemble into periodic matrices under specific conditions. However, the colloidal self-assembly process exhibits inherent limitations; for example, particles preferentially crystallize into a FCC lattice structure, despite the fact that a diamond-type network is theoretically predicted to be more effective at producing a complete or omnidirectional photonic band gap. [101-103] Some examples of colloidal self-assembly techniques are described below:

- **Gravitational sedimentation**. [71, 104, 105] Is a technique used to form 3D crystalline matrices by allowing colloidal spheres suspended in a fluid to settle (Figure 9). This process can produce a polycrystalline matrix reaching several millimeters in thickness. While it is considered the simplest approach for creating these structures, its success relies on the precise management of specific variables: size and density of the colloidal spheres, and sedimentation rate. Despite its simplicity, the sedimentation method has notable drawbacks regarding structural precision, there is very little control over the quality and shape of the upper surface, as the regulation of the exact number of layers within the resulting 3D crystalline matrix is difficult to control.

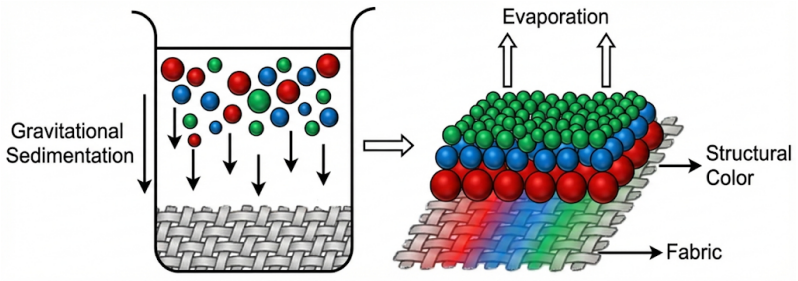


Figure 9 Schematic illustration of gravitational sedimentation of PCs. (This image was generated by GeminiPro)

- **Self-assembly under physical confinement**. [106-108] This process, which often employs centrifugation and sedimentation methods, can be optimized by introducing physical constraints, such as using substrates with epitaxial or surface relief patterns. For instance, highly ordered colloidal PC films can be achieved by confining the colloidal suspension between two substrates (Figure 10). Injecting the suspension under pressure facilitates the formation of films with low defect levels, and the application of continuous ultrasound during this infiltration process further improves the structural quality.

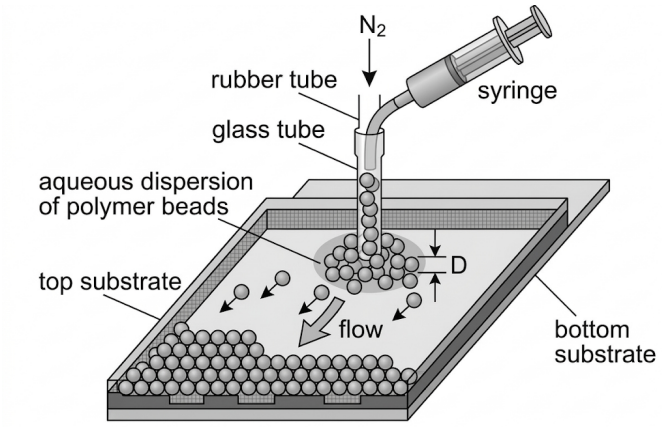


Figure 10 Schematic outline for PC self-assembly through physical confinement. (This image was generated by GeminiPro)

- **Vertical deposition**. [4, 70, 109] This method, alternatively referred to as self-assembly induced by evaporation or isothermal heating evaporation, is a prominent technique in colloidal self-assembly. It relies on the controlled evaporation of a liquid (typically ethanol or water) to facilitate the ordered rearrangement of colloidal spheres within the meniscus formed between a vertical substrate, the colloidal suspension, and the air interface. A planar substrate is introduced into a suspension of colloidal spheres, oriented either vertically or at a specific angle (as illustrated in Figure 11). As the solvent-air interface moves along the substrate surface, capillary forces acting at the liquid-air interface direct the mounting of spheres onto the substrate. During the initial formation of a monolayer, spheres are drawn to the substrate-solvent interface through capillary immersion forces mediated by the solvent meniscus. Subsequent solvent evaporation induces a convective flow of particles within the remaining suspension towards the drier, forming particle layer. This technique offers precise control over the resulting thickness and yields structures with superior crystalline quality, even when utilizing larger diameter polymeric spheres (diameters exceeding 1 μm).

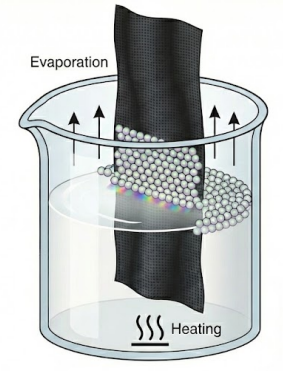


Figure 11 Schematic diagram of vertical deposition method. (This image was generated by GeminiPro)

- **Dip-drawing (or dip-coating)**. [110-113] This process is similar to vertical deposition, in which an object to be coated is immersed in a coating solution, but the substrate is drawn up at a controllable rate and heated to evaporate the solvent (Figure 12). The dried object obtains a thin film at its surface. This method has several advantages as its simplicity, quickness, low cost and environmentally friendly.

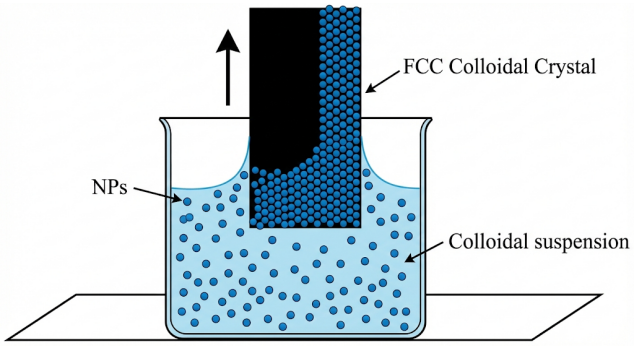


Figure 12 Scheme of dip-drawing method. (This image was generated by GeminiPro)

- **Spin coating**. [114, 115] A method of producing homogeneous thin films by rotating a suspended substrate, with the aid of a vacuum pump, for a period of time until the desired film thickness is achieved. A specified quantity of solution is deposited onto to substrate before rotation. The substrate is then dried or cured.

- **Electrophoretic deposition**. [116, 117] This method facilitates the formation of colloidal monolayers using charged polymer colloids with varying lattice structures. The specific patterns of the electrode substrates are critical, as they determine the resulting structures of the colloidal crystals grown upon them. The electrophoresis process is conducted utilizing two electrodes, which can be arranged in either a horizontal or a vertical configuration. (Figure 13).

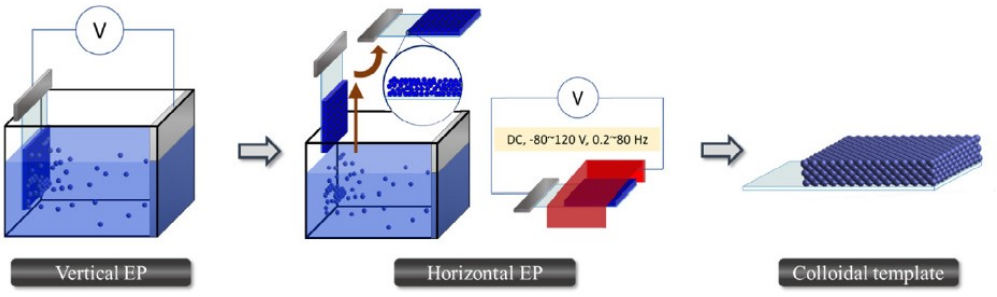


Figure 13 A schematic of the processing steps involved in electrophoresis (EP) to fabricate colloidal crystals. [116] Copyright with permission from Elsevier.

Self-assembled nanostructures with large areas or designed shapes can be prepared at low cost. In addition, depending on the interactions between the colloidal particles, the colloidal structures can be dramatically affected and modulated by applying an additional external field (sensoring). Colloidal crystals typically have only a single, incomplete light-blocking characteristic (pseudo PBG) because of unavoidable flaws that form during their creation and the naturally low refractive index of the tiny spheres they are made of. However, their regular pattern is still effective enough to produce specific quantum optical phenomena. [118, 119]

Other techniques have also been explored, such as auto cloning processes and colloidal and block copolymer self-assembly, among others, [120-126] showing potential applications in sensors, laser engraving, light-emitting diodes and electronic devices. [7, 64, 97, 100, 127-129]

Although many structural PC optical devices have been reported, this area of research still faces many challenges. It is still a challenge to manufacture large PCs with a well-defined stopband, due to the difficulty in reaching PCs with combined properties of homogeneously well-ordered latex assembly, without breaks in large areas, reduced void fraction and sufficient thickness. This is of particular importance for improving the resolution and sensitivity of PC-based devices and the extension of PC applications to various advanced optical filters. Reducing the dependence on the diffraction color angle is particularly important for obtaining wide viewing angles. In addition, to make optical/electrical devices using PCs, synthetic PCs need to be modeled in the form of microphotonic crystal with optically functional planarized architectures. In this case, the PC material must be sustainable enough to efficiently control diffraction at rapid time scales, which is still a major challenge. In addition, the pseudogap only inhibits spontaneous emission in a certain direction. PCs with full PBG and highly ordered structure over a large area is the long-term goal. [118, 119]

Bearing in mind that one of the main objectives of this project is that the entire process of production and application of photonic crystals is as ecological as possible, the dip-drawing method will be preferred for the deposition of PCs, as it is the fastest and most easily adaptable method to the textile industry.

2.1.6. Plasma radiation technology

Plasma technology has assumed great importance among all processes for changing available textile surfaces. [130-137] It is a dry, ecological and suitable method for the worker, which allows changing the surface without changing the properties of different materials. Plasma is an electrically ionized gas and contains a significant number of electrically charged particles that are not bound to an atom or molecule, as well as in the form of free radicals. Free electrical charges make the plasma an electrical conductor,

internally interactive and strongly responsive to electromagnetic fields. Although there are many types of plasma in nature (it is estimated that plasmas are more than 99% of the matter that makes up the visible universe), plasmas can also be effectively produced in the laboratory and in industry. For the modification of the surface of the polymers, the power is usually obtained from an electric field. This is responsible for the acceleration of electrons, which collide with atoms or molecules producing new charged particles, such as ions, atomic molecules, free radicals, electrons and photons. [138, 139]

In terms of the classification of different types of plasma, they can be classified, in a simplistic way, into two categories, thermal and non-thermal. [140-142]

Thermal plasma can be generated artificially namely through electrical discharges, laser and microwave discharges. The temperatures reached are extremely high (a few thousand degrees Celsius), they are characterized by the condition of thermal balance between all the different species contained in the gas, so that no textile material would be able to withstand such temperatures. Non-thermal plasmas are those in which the thermodynamic balance between electrons and particles of higher mass (neutral atoms or molecules, ions and fragments of neutral molecules) is not achieved. The temperature of the electrons is higher than the temperature of other particles, thus being a suitable method for the modification and processing of surfaces of textile materials, since most of them are temperature sensitive polymers. [141]

It has been shown that such forms of discharge have the main advantage of inducing significant surface chemical and morphological modifications, thus improving hydrophilicity and making fibers more accessible to various chemical species, without changing the bulk material properties. [132]

2.1.7. Biopolymers applied to textiles

Currently, great attention is given to biopolymers due to their biocompatibility, biological functions and, consequently, to their potential application in the biomedical and pharmaceutical fields. Biopolymers can be divided into three major groups: polynucleotides (ribonucleic acid and deoxyribonucleic acid), polypeptides and polysaccharides (Figure 14). In the last group are includes alginates, microbial cellulose, chitin and chitosan. Other important biopolymers such as soybean, sodium alginate, polylactic acid, bacterial polyester and cellulose are used in several industries, mainly in medicine, surgery and healthcare fields. One of the few disadvantages of using biopolymers is the inferior performance when compared to oil-based polymers, exhibiting lower heat and moisture resistances. [143, 144]

Some examples of commercially available biopolymers include: Ingeo (Natureworks), a biodegradable thermoplastic polyatide produced from corn; Lenpur produced from wood pulp of harvested white pine

tree clippings; and Tencel/ Lyocell produced by Lenzing from wood pulp of beech and eucalyptus trees. [145]

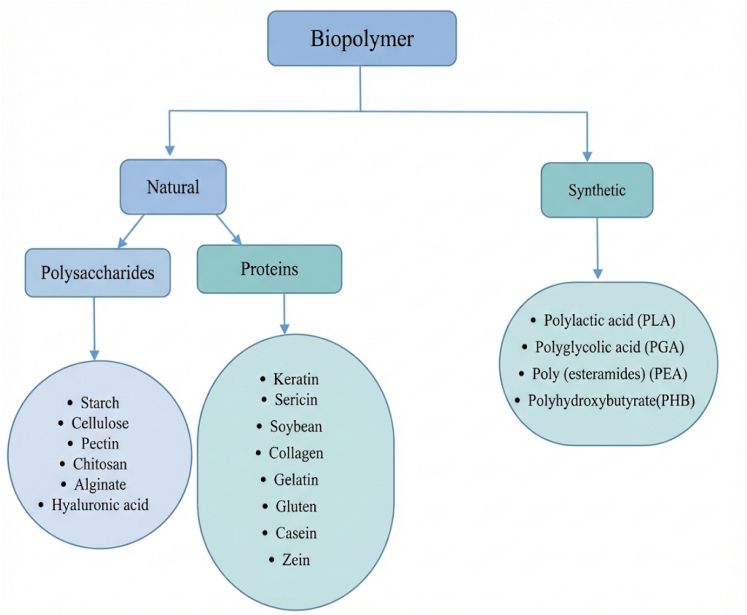


Figure 14 Classification of biopolymers and their origins. (Adapted from [146])

Aware of the environmental impact produced by synthetic polymers, the use of more profitable and environmentally friendly biological materials (biopolymers), such as starch, whey or chitosan, could be a solution to gradually replace synthetic polymers, thereby reducing their carbon footprint. [147] For example, keratin from chicken feathers has been used as an alternative sizing agent to polyvinyl alcohol (PVA). [148] PVA does not degrade and persists in textile effluent, and it is a high contributor for the BOD load.

In view of these ecological and environmental concerns, natural biopolymers are the only suitable and renewable products that have the potential to become a key resource in the development of sustainable bioactive textile products. [149] Recently, the use of natural biopolymers has been preferred for modifications to textile substrates. Generally, the natural polysaccharides used for the functional finishing of textiles are abundantly available as waste and are environmentally friendly. As a result, a variety of environmentally benign technologies are expanding rapidly for their versatile applications in the textile industry. Biopolymers derived from agricultural feed or marine food resources have several advantages, such as abundant availability, biocompatibility and biodegradability and, therefore, ecological security. [150]

In textile finishing, the incorporation of natural polysaccharides is a fairly recent concept. This was caused by the recognition that its unique properties can be applied to different areas of application, such as aroma, insect repellent, fire retardant, UV blocking, water resistance and antimicrobial finishes that have become popular recently. [151]

The flexibility of the fabrics, texture, fiber/yarn structure and roughness, which give a floating and complicated appearance to the fabric surface, makes the production of structural colors in these materials much more complex than on smooth, compact and uniform surfaces. [152] Due to these limitations, very few articles have been published on the self-assembly of photonic crystals and their application in flexible textiles. Most studies have focused on silk and polyester fabrics, discarding the hypothesis of application on cotton and other cellulosic substrates. [65] Thus, it is essential to effectively adhere the matrix coating to the photonic crystals so that the fabric works as expected. Since cotton fibers are negatively charged due to the presence of carboxyl and hydroxyl groups, it is often necessary to functionalize their surface with cationic charges. Chitosan is the deacetylated derivative of chitin and represents an interesting alternative to compounds commonly used to functionalize cotton due to the presence of protonated amino groups. It is mainly obtained by alkaline deacetylation of chitin, being chemically composed of units of glucosamine and N-acetylglucosamine linked by ß-1-4 glycosidic bonds. Being non-toxic, biodegradable, biocompatible and resistant to microbes has given it enormous potential in a wide range of scientific areas, such as biomedical, food, agricultural, cosmetic, textile, pharmaceutical and other industries. [144, 149]

Yavuz reported the structural coloration on the surface of cotton fabric using self-assembled colloidal photonic crystals, where the fabric is able to exhibit a different iridescence at different viewing angles changing to a shorter wavelength at as the viewing angle increases from 0° to 90°. The colloidal photonic crystals were efficiently deposited by the electrostatic self-assembly technique on a cotton fabric coated with chitosan. The crosslinking promoted by glutaraldehyde allows a durable chemical bond and longer washing durability between cotton, chitosan and photonic crystals. [152]

Xiaodi Shi coated cotton fabric with polydopamine (possesses highly sticky properties), a derivative of mussel protein, to obtain structural color with improved fastness and mechanical strength. Polydopamine presented a black color after polymerization, essential to enhance PCs chroma, improving the color saturation on cotton fabrics. [153]

Biopolymer usage in textile processes is exciting and innovative but will require some acceptance time by the textile industry.

3

Materials and Methods

3.1. Materials and Chemicals

Commercial black polyamide (PA) plain fabric (61.50 g/m^2), white polyester (PES) plain fabric (Lemar–Leandro Magalhães de Araújo (Filhos), Lda, Guimarães, Portugal, 100 g/m^2) and white cotton (CO) plain fabric (Lameirinho Indústria Têxtil SA, Guimarães, Portugal, 140 g/m^2) were used for dyeing processes and PC coating. Dianix disperse dyes (DyStar, Porto, Portugal), Serilene disperse dyes (FOCOR, Porto, Portugal) and Coralene disperse dye (Impocolor, Grijó, Portugal) were used to dye polyester fabrics (Table 2). Reactive dye Novacron Black NS (Huntsman Performance, Leça da Palmeira, Portugal) was used to dye cotton fabrics.

Table 2 Disperse dyes utilized for polyester and photonic crystal dyeing processes.

Dye name and code	Color	PES dyeing	PC dyeing
Coralene Black MD (CB)	Black	✓	×
Dianix Brilliant Violet R (DBV-R)	Violet	✓	✓
Seriline Royal Blue ADS (SRB-ADS)	Blue	✓	✓
Green Seriline HWF (GS-HWF)	Petrol blue	✓	×
Yellow Seriline ADS (YS-ADS)	Yellow	✓	✓
Orange Seriline ADS (OS-ADS)	Orange	✓	×
Red Seriline ADS (RS-ADS)	Pink	✓	×
Red Dianix K-3G (RD-K3G)	Red	✓	✓
YS-ADS:SRB-ADS (1:1, GD11)	Green	✓	✓

Polyester and cotton dyeing were carried out in an Ibelus C-720 (Pregitzer&Ca, LDA, Guimarães, Portugal) dyeing machine. In cotton dyeing, NaOH (Fisher Chemical, USA), Na_2CO_3 (Scharlau, Barcelona, Spain) and NaCl (Panreac, Barcelona, Spain) were used as auxiliaries in the dyeing process. Non-ionic detergent Diadavin UN (Tanatex Chemicals, Santo Tirso, Portugal) was utilized for post-dyeing fabric washing, as European Colourfastness Establishment (ECE, Charles Small, Vila Nova de Famalicão, Portugal) detergent was utilized for washing fastness assays.

For PC synthesis, styrene (St), methyl methacrylate (MMA), butyl acrilate (BA), butyl methacrilate (BMA,) acrylic acid (AA), sodium dodecylsulphate (SDS), ammonium bicarbonate (NH_4HCO_3), sodium persulfate ($Na_2S_2O_8$), potassium persulfate ($K_2S_2O_8$) and other analytical grade reagents were purchased from Sigma–Aldrich Quimica S.L. (Lisbon, Portugal) and used without further purification. For the synthesis of SiO_2 particles, tetraethyl orthosilicate (TEOS) 98% and $NH_3.H_2O$ 25% were purchased from

Merck S.A. (Lisbon, Portugal) and EtOH 96% was acquired from Enzymatic (Santo Antão do Tojal, Portugal). Kraft lignin (KL) powder was kindly provided by Vigo University. KL was produced via acidic precipitation of black liquor derived from the Kraft pulping process of *Eucalyptus globulus*, sourced and supplied by Ence (Pontevedra, Spain). [154]

Biopolymers sodium alginate and cellulose acetate were acquired from Panreac (Barcelona, Spain).

Commercial finishing agents EDOLAN, TANACOAT, TANAFINISH and TANAPUR were kindly supplied by Tanatex (ADI Group, Porto, Portugal), while Acronal S790 was supplied by BASF (BASF Portuguesa S.A., Lisbon, Portugal). Sylgard 184 silicone elastomer kit was purchased from Dow Chemicals (Dow Europe GmbH, Wiesbaden, Germany).

3.2. Fabrics Characterization

Polyamide, polyester and cotton fabrics were characterized according to the International Organization of Standardization (ISO) as follows (n=3).

- ISO 7211-2:1984 – Textiles – Woven fabrics – Construction – Methods of analysis – Part 2: Determination of number of threads per unit length.
- ISO 7211-3:1984 – Textiles – Woven fabrics – Construction – Methods of analysis – Part 3: Determination of crimp of yarn in fabric.
- ISO 7211-5:2020 – Textiles – Methods for analysis of woven fabrics construction – Part 5: Determination of linear density of yarn removed from fabric.

Thickness measurements were performed with an electronic digital micrometer (Mitutoyo) in 5 different points of the fabric, for all fabrics (n=3).

3.3. Photonic crystal synthesis

3.3.1. P(St-MMA-AA)

Monodisperse composite latex nanospheres of P(St-MMA-AA) were synthesized by soap free emulsion copolymerization. Briefly, St (20 g), MMA (1 g), AA (1 g), distilled water (dH2O, 100 mL), SDS (0-0.004 g), and ammonium bicarbonate (0.50 g) were added sequentially to a three-necked flask equipped with an N_2 inlet, a reflux condenser and a magnetic stirrer. Reaction of the mixture was initiated at 70 °C for 30 min. Following the addition of an aqueous solution of sodium persulfate ($Na_2S_2O_8$, 0.48 g dissolved in 15 mL dH_2O), polymerization was carried out at different temperatures, for 5 h and fixed stirring speed,

in order to obtain a homogeneous latex with monodispersed particles. P(St-MMA-AA) photonic crystals were used without further purification.

3.3.2. SiO_2

SiO_2 microspheres were synthesized using a modified Stöber method. [155] In a first instance, SiO_2 solution was prepared in a round bottom flask containing $NH_3.H_2O$ and EtOH. This mixture was then homogenized for 5 min at 300 rpm. Subsequently, TEOS was added and the reaction was maintained at room temperature for 1 h with stirring at 300 rpm. The SiO_2 particles were collected by centrifugation (Gyrozen 1248R, Seoul, South Korea) (4000 rpm for 10 min) and washed with EtOH to remove unreacted TEOS and NH_3. This process was repeated three times. Adjustments of reagents, stirring and time were performed in order to obtain different sized SiO_2 particles.

3.3.3. Kraft Lignin

Kraft lignin (3.2 wt%) was dissolved in an EtOH/MeOH solvent system at a 1:1 (v/v) ratio under continuous stirring at 500 rpm until partially dissolved at room temperature. The resulting mixture was then centrifuged at 4,000 rpm for 10 minutes. Following centrifugation, dH_2O, equivalent to twice the volume of the initial KL solution, was gradually added dropwise to the KL solution, at 750 rpm. After all dH_2O was added, the solution was continuously stirred at room temperature for 1 minute, resulting in a final concentration of approximately 1 wt%. KL particles were used without further purification.

3.4. Dyeing Processes

3.4.1. Cotton dyeing

Cotton plain fabric was dyed with Novacron Black NS at 6% over fiber weight (ofw). The dyeing bath was composed by 100 g/L of NaCl, 5 g/L of Na_2CO_3, 3 mL/L of NaOH 50%, with a liquor ratio of 1:20. The dyeing program (Figure 15) started at room temperature (~20°C) and then was raised to 60°C, which was maintained for 90 min. After cooling to 50°C, cotton fabric was rinsed in cold water to remove hydrolyzed dye from the fabric's surface, washed at 100°C for 20 min with detergent Diadavin UN 1 g/L to remove the remaining hydrolyzed dye in the fabric's interior, rinsed again with cold water and then dried in an oven at 40°C.

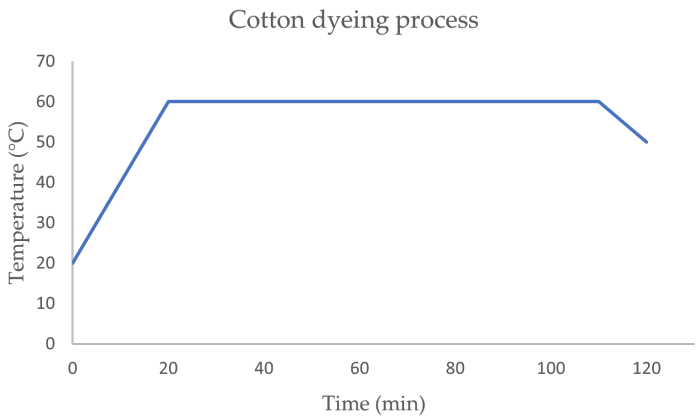


Figure 15 Dyeing process used for CO at 60°C.

3.4.2. Polyester and P(St-MMA-AA) dyeing

Polyester plain fabric was dyed with the following dyes at 3% ofw, with a liquor ratio of 1:30: CB, DBV-R, SRB-ADS, GS-HWF, YS-ADS, OS-ADS, RS-ADS, RD-KSG and GD11. The dyeing process (Figure 16) started at room temperature (~20°C), with a subsequent raise of the temperature in several steps: to 60°C with a rate of 3°C/min and kept at 60°C for 10 min; to 90°C with a rate of 2°C/min and kept at 90°C for 30 min; to 130°C with a rate of 1.5°C/min and kept at 130°C for 45 min. The cooling was performed in two steps, from 130°C to 80°C with a rate of 2°C/min and then from 80°C to 50°C with a rate of 2.5°C/min. Finally, the PES fabrics were rinsed with hot water followed by rinsing with cold water and dried in an oven at 40°C. P(St-MMA-AA) photonic crystals were dyed using the same temperature and rate conditions. 20 ml of disperse solution of 210 nm PCs (green color, 15 wt%) were dyed with disperse dyes DBV-R, SRB-ADS, GD11, YS-ADS and RD-K3G at 2% concentration. 210 nm PCs were also dyed with RD-KSG at 0.5 and 1% concentration. No further purifications were performed.

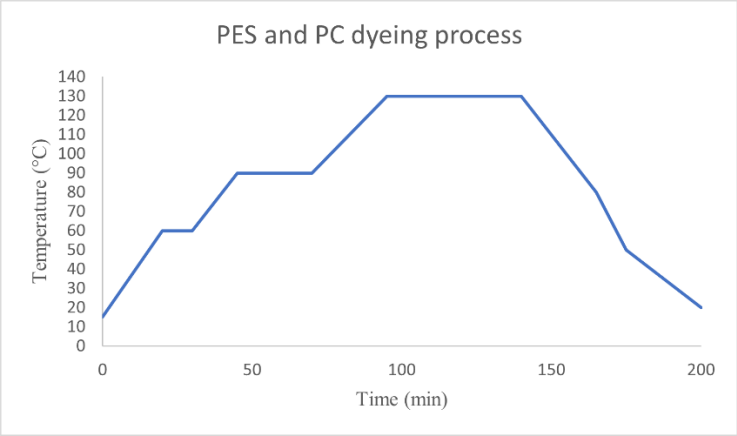


Figure 16 Dyeing process used for PES and P(St-MMA-AA) PCs at 130°C.

3.5. Photonic crystal deposition on fabrics

3.5.1. P(St-MMA-AA) deposition by dip-drawing method

A piece of fabric, 3 x 3 cm, was dipped in the P(St-MMA-AA) disperse solution (15 wt%) for 10 seconds, slowly removed and dried in a petri dish at 40 °C for 15-25 minutes. Fabrics were used without any further modifications for the subsequent tests and measurements.

3.5.2. SiO_2 and KL deposition by gravitational sedimentation method

A piece of fabric, 3 x 3 cm, was placed in a petri dish and submerged in the SiO_2 or KL disperse solution. For SiO_2, the petri dish was placed in an oven at 40 °C for 30 min to evaporate the solvent. As for KL, solvent evaporation was performed at room temperature for 24h.

3.6. P(St-MMA-AA) PCs mixture

Different sized P(St-MMA-AA) PCs (170, 190, 210 and 250 nm) were premixed in different proportions of volume (1:1, 1:3 and 3:1) before being applied through dip-drawing method in PA fabrics.

3.7. Adhesive synthesis

Adhesive synthesis was performed through emulsive polymerization, in a round bottom flask with magnetic stirring. Briefly, 0.6 g of SDS were mixed in 100 mL of dH2O at 200 rpm for 20 min. Then, 4.65 mL of MMA, 4.5 mL of BMA or BA and 0.1 g of $K_2S_2O_8$ (polymerization initiator) were added to the previous mixture. The resulting solution was heated to 85 °C and maintained at this temperature for 5 hours. The resulting polyacrylate adhesives, P(MMA-BMA) and P(MMA-BA), were used without further purification.

3.8. Plasma discharge for textile surface activation

Surface activation experiments were performed using an atmospheric pressure plasma jet (Plasmatreat, model PTU1212, Germany). The system was applied to the treatment of dyed PES and CO fabrics, aiming to modify surface properties by increasing surface energy. The plasma was generated at atmospheric pressure using compressed air as the process gas, operating at an input power of approximately 520 W and a voltage of about 280 V, with a compressed air flow rate of 45 L/min. Treatments were carried out with the plasma jet operating at a scanning speed of 5 m/min, maintaining a treatment distance of 5 mm between the jet nozzle and the fabric surface, and using a track pitch of

13 mm. Under these operating conditions, effective and reproducible surface treatments were achieved, suitable for the experimental evaluation of plasma-induced activation on textile substrates.

3.9. Application of adhesives and finishing agents

PA, PES and CO fabrics covered with P(St-MMA-AA) PCs were immersed in either commercial finishing agents or synthetized adhesives, and then padded (Padder BHP, Roaches, UK) at a 2 bar pressure and speed of 4 m/min at room temperature. In the case of Sylgard™ 184, 1 wt% of a curing agent was added to the silicone gel, mixed and placed in ultrasound bath to remove bubbles. After the textile coating, samples were dried at 40 °C and thermoset between temperatures of 80 to 100 °C (depending on the information provided in each technical datasheet) for 5 min. P(MMA-BMA) and P(MMA-BA) adhesives were not thermoset. For Sylgard™ 184, thermoset time was 3 hours (80 °C).

3.10. Reflectance measurements

3.10.1. Spectrophotometry with integrating sphere

PC coated fabrics were analyzed by UV/Vis spectrophotometry using a Shimadzu UV-2600 (Shimadzu Corporation, Kyoto, Japan), to calculate CIEL*a*b* color coordinates through its reflectance analysis, within the wavelength range from 200 to 800 nm. These were also analyzed with a spectrophotometer (Cary 5000) equipped with an integrating sphere (DRA 2500), within the wavelength range from 250 to 2500 nm (NUV-VIS-NIR). However, only the wavelength region 350–750 nm (VIS) was analyzed in this work. Directional Hemispheric Reflectance (DHR) was both measured at a fixed angle of incidence of 8 degrees (total DHR, without polarizer) and at different angles of incidence (α_i), from 12 to 80 degrees, for both s- and p-polarized light.

3.10.2. Scatterometry

For color characterization of the fabric samples, scatterometry measurements were first performed giving the In-Plane Bidirectional Reflectance Distribution Function (IP-BRDF). These measurements were performed using a modified set up, based on an RC2 ellipsometer (J.A. Woollam Co. Inc.), comprised of a spectrometer, light source, and goniometer. The measurements were made at incident angles $30° \leq \alpha_i \leq 70°$ in steps of $10°$. For each incident angle the angle of observation was varied according to $0° \leq \alpha_o \leq 70°$ with varying steps. That is, each sample was measured with 20 settings of the incident and observation angles. Measured reflectance values were interpolated to cover the whole range of

observation directions with 1° resolution. The light source used for these measurements was D_{50} illuminant. A schematic of the experimental setup with angle notation is shown in Figure 17.

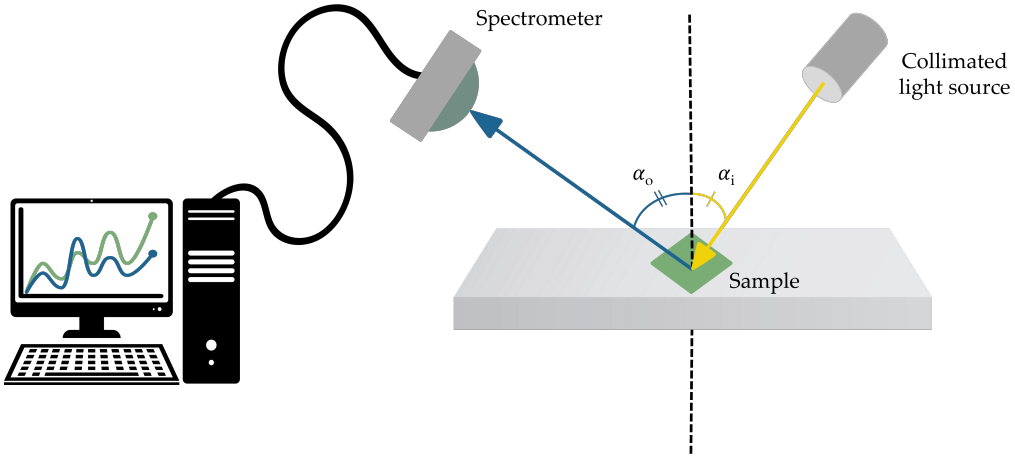


Figure 17 Schematic of IP-BRDF setup.

3.10.3. Conversion of data to 3D color coordinates and IP-BRDF imaging

Since the experimental set up is using a spectrometer with unknown spectral sensitivity, a simple procedure of conversion to color coordinates was performed. The angularly varying spectral intensity of the white reference (99% Spectralon) was first recorded using the spectrometer. Then spectral reflectance values for the white reference were measured, and its reflectance was calculated as the ratio between two signals (Signal_white/Signal_lamp), with exposure time factor included. After collecting reflectance in arbitrary units for the measured samples, a normalization was made by dividing with the white reference signal (IP-BRDF_sample = Signal_sample/Signal_white). Finally, the obtained reflectance values were converted to the color coordinates under the assumption of illuminant (D_{50} or Illuminant A), CIEL*a*b*. [156]

3.11. Scanning electron microscopy and scanning transmission electron microscopy

Three different SEM equipment were used throughout the thesis. Morphological analyses of P(St-MMA-AA) PCs and PC-coated fabrics were carried out scanning transmission electron microscopy (STEM) and by scanning electron microscopy (SEM), respectively, with an ultra-high resolution field emission gun (FEI NOVA 200 Nano SEM). PC-coated fabric samples were covered with a thin film of gold/palladium (80:20) in a 208HR high-resolution sputter coater (Cressington) coupled to an MTM-20 high-resolution thickness controller (Cressington).

For cross section analysis of PA fabrics with mixed PCs, a GeminiSEM 560 Zeiss field-emission SEM (Oberkochen, Germany) was utilized, operating at an accelerating voltage of 2kV. P(St-MMA-AA)coated fabrics were sputter-coated with a platinum layer of 5 nm, using a Leica EM SCD500 coater (Wetzlar, Germany).

Morphological characterization of KL and SiO_2 PCs was performed using SEM, with a FlexSEM 1000 microscope (Hitachi, Tokyo, Japan) operating at an accelerating voltage of 10 kV. Prior to image acquisition, particles were mounted on conductive carbon adhesive tape and sputter-coated with a gold layer of 7.5 nm for 90 s, using a Quorum Mini QS coater (London, UK).

PC size analysis was performed in software ImageJ (version 1.54g), where at least 100 measurements were performed for each sample, and results reported as the mean ± standard deviation.

3.12. Fourier-transform infrared spectroscopy with attenuated total reflectance

Fourier transform infrared (FTIR) spectroscopy, Shimadzu IRAffinity S1 (Shimadzu Corporation, Kyoto, Japan), equipped with a horizontal Attenuated Total Reflectance (ATR) accessory (Norleq, Porto, Portugal), was employed for a chemical characterization of synthesized PCs. Spectra data were acquired with 45 scans at a resolution of 4 cm^{-1}, within the spectral range of 4000 to 500 cm^{-1}.

3.13. Surface Roughness analysis

Surface roughness was measured with a HANDYSURF+ 35/40/45 (ACCRETECH) rugosimeter. Calibrations parameters and calculations were defined according to standard ISO 1997/2009, using a Gaussian filter. Roughness average (Ra) measurements were performed at a speed of 0,6 mm/s for a length of 10 mm. Each Ra value is an average of 12 points measured along the 10 mm of fabric. Measurements were performed only in P(St-MMA-AA) coated fabrics, in triplicate for each sample.

3.14. Differential scanning calorimetry

The thermal properties of P(St-MMA-AA), SiO_2 and KL PCs were analyzed using differential scanning calorimetry (DSC). The DSC thermograms were obtained using DSC-822e equipment (Mettler-Toledo International Inc, Switzerland). Samples with ~6 mg were placed in an aluminum pan. The samples were then heated from 25 to 500 °C, with a heating rate of 10 °C/min, using a nitrogen flow rate of 200 mL/min. The results were evaluated using LAB Mettler Star SW 8.1 software (Mettler-Toledo International Inc, Switzerland).

3.15. Simultaneous thermogravimetric analysis

The simultaneous thermogravimetric analysis (STA) of the synthetized PCs (~6 mg) were conducted using the STA 7200 system from Hitachi (TA Instruments, Newcastle, UK). The thermal evaluation was performed within a temperature range of 25 to 600 °C for P(St-MMA-AA) PCs, and of 25 to 1100 °C for SiO_2 and KL PCs, under a controlled heating rate of 10 °C/min and a nitrogen flow rate of 200 mL/min to prevent oxidation. The thermogravimetric data were interpreted by examining the percentage of mass loss as a function of temperature, providing insights into the material's decomposition profile and thermal degradation behavior.

3.16. Dynamic light scattering and Zeta potencial

The determination of PCs particle size, PdI and zeta potential were carried out using dynamic light scattering (DLS) using a NANO ZS Malvern Zetasizer (Malvern Panalytical Ltd., Malvern, UK) at a controlled temperature of 25 °C. The size and PdI were assessed in dispersions diluted at a 1:1000 ratio for KL, 1:100 for P(St-MMA-AA) and at 5 wt% for SiO_2. P(St-MMA-AA) and KL PCs were dispersed in dH_2O and SiO_2 PCs were dispersed in EtOH. Each sample underwent three independent measurements, and the results were reported as the mean ± standard deviation. Data analysis was performed using Malvern Dispersion Technology Software with a high-resolution multiple narrow modes approach.

3.17. Digital photographs

Digital photographs were taken with a Canon EOS 750D digital camera. The images of PC coated fabrics were acquired in a light chamber under a D65 light source. In the case of the multi-angle photographs, the sample was set at 3 different angles (Figure 18) while the camera maintained the same distance (50 cm). No adjustments of pixels, color, brightness and contrast were applied to the images. The photographs produced were parts of larger images that were selected without obscuring, eliminating or misrepresenting any information that was present in the originals.



Figure 18 Sample holder with 30, 45 and 70° angles, used for structural color photographic documentation, a) front view and b) side view.

3.18. Angular support design

The sketching and design of a new angular support for the observation of structural colors was performed in the software SolidWorks 2024. The different components were design separately, being assembled afterwards to form the final prototype (See Annexes, Figure A1). This new sample holder allows the observation and documentation of structural colors at 19 different angles, in opposition of the current holder, which only possesses 3 different angles.

3.19. Standard Methods for color fastness

Light fastness (adapted from ASTM G154 – 06)

To evaluate UV light fastness, PA coated samples with P(ST-MMA-AA) were exposed to UV radiation for 24, 48, 76 and 168 h at 50 °C, without condensation. The assay was performed using QUV equipment (Q-Lab, Westlake, OH, USA).

Washing fastness (ISO 105-C06:2010)

The washing fastness PC coated samples was evaluated based on the ISO 105-C06:2010 standard (Tests for color fastness—Color fastness to domestic and commercial laundering). Briefly, samples (4 × 10 cm) were sewn to the multifiber adjacent fabric and immersed in 150 mL of washing bath containing 4 g/L of ECE detergent. The washing procedure was evaluated at 40°C for 30 min using an Ibelus C-720 machine. Subsequently, samples were rinsed with distilled water and dried in an oven at 40°C.

4

Photonic crystal synthesis and characterization

Part of this chapter was based on the following publication:

(Paper) **Fernandes, Rui D.V.**; Gomes, Pedro; Zille, Andrea; Souto, A. P.. "The influence of chemical reaction conditions upon poly(styrene-methyl methacrylate-acrylic acid) synthesis: Variations in nanoparticle size, colour and deposition methods". *Coloration Technology* (2020) 136, 101-109. doi: 10.1111/cote.12452

4.1. Synthesis of poly(styrene-methylmetacrylate-acrylic acid) (P(St-MMA-AA)) PCs

For the spherical particle synthesis of P(St-MMA-AA) PCs (Figure 19) the time of reaction was maintain equal to the previously optimized time of 5h. [6, 152] Further increase of time did not improve monomer conversion significantly and can cause heterogeneous nucleation if the monomer feed rate was much lower than the polymerization rate. [157, 158] To measure the size of the produced particles by the several reactional conditions, DLS and STEM techniques were used, as well as zeta potential to confirm the stability of the solutions.

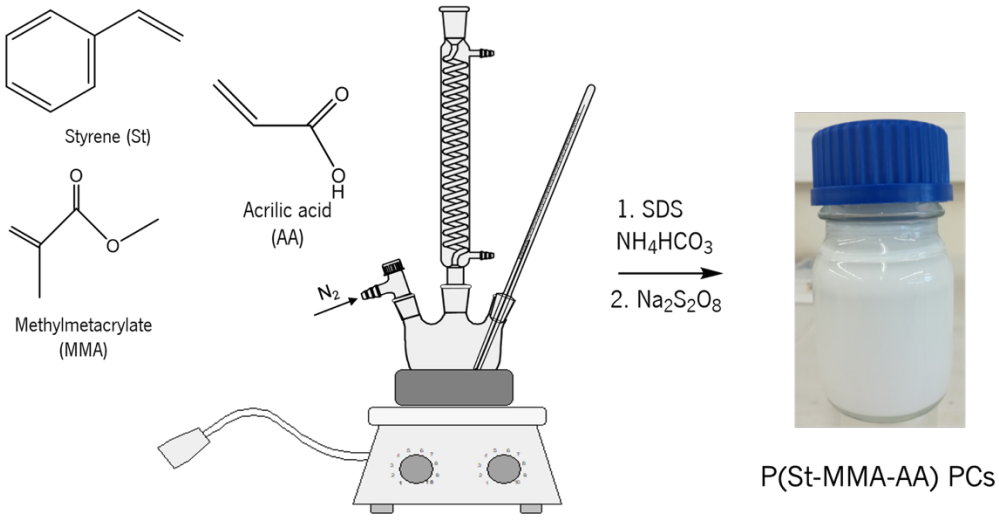


Figure 19 Reaction setup for P(St-MMA-AA) PC synthesis.

Zeta potential of the spheres was recorded between -39 ± 0.6 to -50 ± 2.9 mV (zeta potential augmented with PC size increment) indicating the good stability of the colloidal suspension. The calculated polydispersity index (PdI) of P(St-MMA-AA) spheres was determined to be inferior to 0.1 confirming their highly monodispersity, uniformity and propensity for generating highly ordered structures. However, since DLS technique is performed in solution, where particles are swollen, the observed average diameters and respective associated standard deviations were also calculated by STEM (dried particles) (Table 3).

Table 3 P(St-MMA-AA) PCs size analysis comparison between DLS and STEM of the tested reactional conditions.

Temperature (°C)	Stirring (rpm)	Size DLS (nm)	PdI	Size STEM (nm)
90	300	192.3 ± 3.9	0.03 ± 0.02	164.5 ± 4.5
80	300	215.7 ± 7.0	0.02 ± 0.01	189.0 ± 5.7
70	300	230.1 ± 5.8	0.03 ± 0.02	209.8 ± 8.2
65	300	257.2 ± 5.9	0.10 ± 0.03	226.4 ± 7.9
60	300	317.9 ± 5.8	0.09 ± 0.03	262.8 ± 11.1
80	400	215.2 ± 9.0	0.04 ± 0.03	191.8 ± 9.1
80	200	201.0 ± 9.0	0.04 ± 0.02	165.0 ± 9.9
Monomer adjustment	-	277.6 ± 7.4	0.07 ± 0.04	260.7 ± 9.5

P(St-MMA-AA) synthesis at 80 °C and 300 rpm (~190 nm) was used as a control parameter reaction in order to evaluate the differences obtained when temperature/stirring speed is altered. Thus, at higher temperatures (90 °C) smaller PCs nanospheres can be obtained, with a size around 170 nm. As the temperature is lowered, bigger size nanoparticles are obtained, ~210 nm at 70 °C, ~230 nm at 65 °C and ~250 nm at 60 °C.

As expected, the decrease of the reaction temperature from 90 to 60 °C significantly decrease the conversion of the monomers at the end of the polymerization leading to an increase of the PCs size and also slightly narrowing the nanosphere size distribution. [158] Higher reaction temperatures lead to degradation and polydisperse nanosphere distribution due to the instability of the monomer bulk phase polymerization. Furthermore, lowering the temperature to 60°C promoted particle agglomeration. Raising the stirring speed to 400 rpm did not significantly alter the particle sizes. On the other hand, when the stirring speed was lowered to 200 rpm smaller nanoparticles were obtained (~170 nm). Also, the stirring rate can have important effects in the PCs size, however it is more difficult to steadily control since it produces a complex chaotic environment that is also function of the used temperature. Nevertheless, it was possible to observe that the increase from 300 to 400 rpm at high reaction temperature did not have significant impact on the PCs sizes. On the other hand, at 200 rpm the nanosphere size decreased. This effect can be attributed to the low amount of surfactant used in the reaction mixture. In these conditions, due to a higher stability provided by the lower stirring velocity, the monomer did not polymerize on the surface of the seed latex nanosphere but in the monomer droplets produced by stirring. However, due to

the absence of the stabilizing properties of the surfactant the formed PCs are not able to reach high degree of polymerization maintaining a low size. [159] To overcome the agglomeration problems observed at 60°C, different ratios of the three monomers, St:MMA:AA, namely, 20:1.25:1, 20:1.5:1, 20:1.75:1, 20:2:1, 20:4:1, 20:1:2, 10:1:1, were tested to optimize the obtention of 250 nm spheres. With these monomer variations it was possible to conclude that an increment of MMA in the ratio allowed the formation of 250 nm PCs, at 300 rpm and 70 °C. Increasing MMA ratio from 1 to 1.25 or AA ratio did not form the pretended size, whilst an increase of MMA to 1.5 up to 4 formed 250 nm spheres. Decreasing the ratio of St from 20 to 10 also allowed the formation of 250 nm spheres, meaning that the proportion St:MMA is the critical factor to obtain larger particle sizes with higher temperature conditions. Figure A2 illustrate the color differences between synthesis after PCs were applied onto PA substrate.

To quantify the percentage of P(St-MMA-AA) photonic crystals in the obtained colloidal solution, a determined volume was dried in an oven at 40° C. The PC powder was then weighted, being the total mass extrapolated for each synthesis. In average, a 15 wv% mass of PCs was obtained.

STEM analysis (Figure 20) at high magnification (200.000×) confirms that the P(St-MMA-AA) latex spheres are composed by shell rich in poly(acrylic acid) (PAA) and poly(methyl methacrylate) (PMMA) covering the polystyrene (PSt) domains in the core as previously observed. [6] This can be observed in Figure 20a,c,d where the PSt can be easily identify as the darker core surrounded by a lighter shell of PAA and PMMA. The STEM images also confirm the highly monodisperse PC suspensions and the reproducibility of the synthesis method in obtain specific sphere sizes with a very few nanometer differences in diameter.

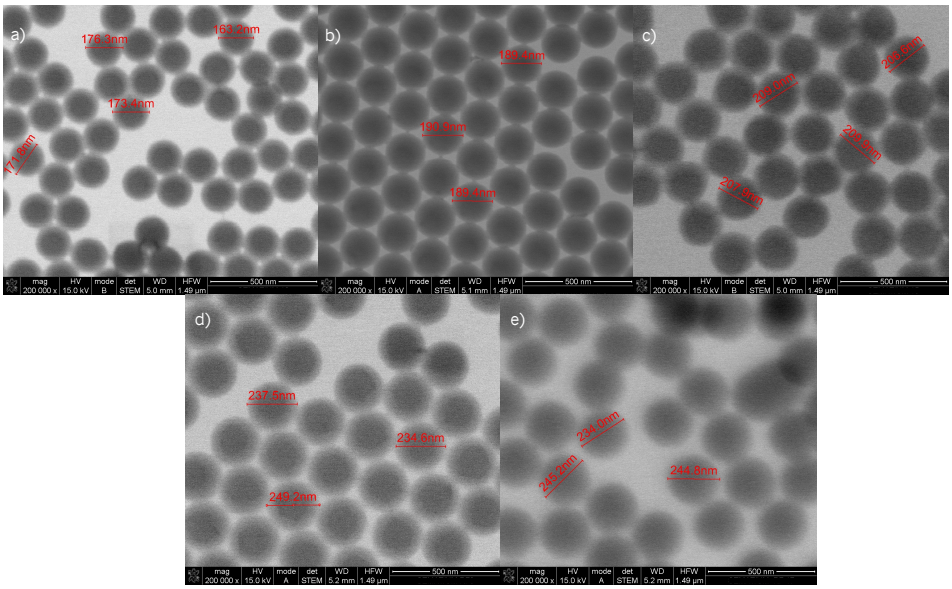


Figure 20 STEM micrographs (200.000 × magnification) of a) ~170, b) ~190, c) ~210, d) ~230 and e) ~250 nm P(St-MMA-AA) spheres.

The chemical composition of the obtained spheres was confirmed by ATR-FTIR, where the spectra of the synthetized spheres is not only the sum of the singles reagents but also the proof of the reaction among the constituent materials (Figure 21). There is a significant reduction of the peaks associated to the alcoholic or ether C-O stretching between 1050-1100 cm^{-1} as well as the disappearance of the C-O peak associate to the acid groups of AA between 1200 and 1300 cm^{-1}. The small peak at 1728 cm^{-1} indicates the presence of carboxyl groups on the surface of the P(St-MMA-AA) nanospheres. The peak at 1601 cm^{-1} is associated with the C=C stretching vibrations of the benzene ring of the styrene while the peaks at 1493 and 1452 cm^{-1} are related to the CH_2 scissoring and CH_3 asymmetric stretching or deformation of the C–H bonds in the methyl groups. The peaks at 1028 cm^{-1} and 756 cm^{-1} were assigned to the C–O–C symmetric stretching vibrations and CH_2 rocking in-plane bending of the MMA, respectively. [104, 109, 160]

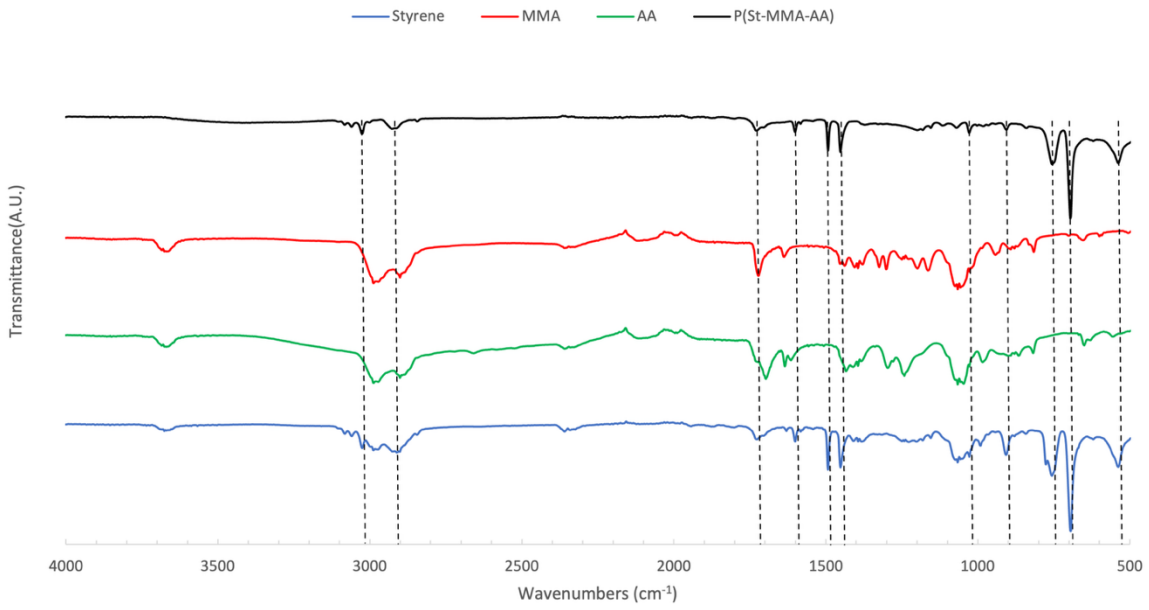


Figure 21 ATR-FTIR spectra from styrene (St), methylmethacrylate (MMA), acrylic acid (AA) and poly(styrene-methylmethacrylate-acrylic acid) (P(St-MMA-AA)).

To understand the thermal behavior of P(St-MMA-AA) PCs thermal analyses (DSC and STA) were performed on P(St-MMA-AA) samples prepared with different reactional conditions. Independently of the size of the spheres, P(St-MMA-AA) PCs present similar DSC thermograms, with energies and peak temperatures within the same values. P(St-MMA-AA) samples exhibit a thermal peak at 108°C, with enthalpy energies between -1 and -3 $J.g^{-1}$, meaning that it is a low-energy endothermic peak corresponds

to a glass transition. [6, 161] The prepared PC spheres are heat stable, provided they are handled in the glass transition temperature range, i.e., between 105-110°C (Figure 22).

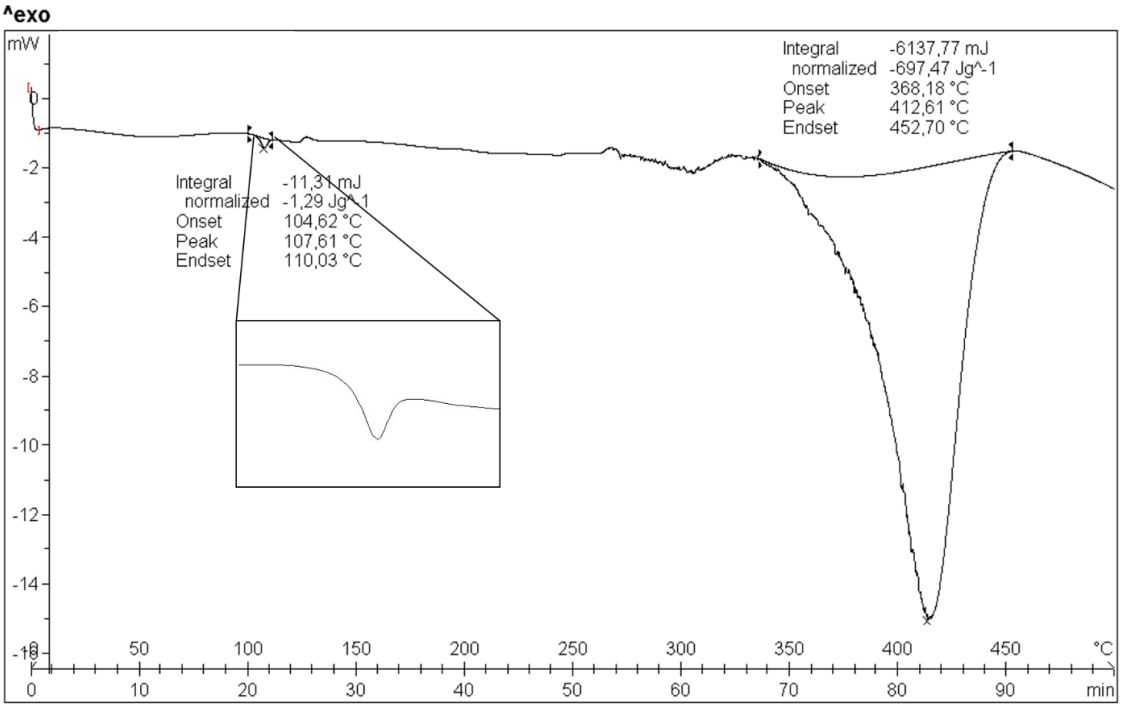


Figure 22 DSC thermogram of P(St-MMA-AA) PCs.

The DSC thermogram also showed another peak at 413 °C, with enthalpy energies between -677 and -775 $J.g^{-1}$, a high-energy endothermic peak corresponding to a melting point or a decomposition temperature of the photonic crystals. If a cooling curve from 500 °C to 0 °C had been performed, we could determine the nature of this peak without resorting to other instrumental methods of thermal analysis. Since this cooling was not performed, thermogravimetric analysis was performed to complement the information acquired from the DSC curve.

Analyzing the STA curves (Figure 23), it was possible to confirm that the endothermic peak at 413 °C in the DSC thermogram is a degradation peak, since there is a mass loss of approximately 84% within this temperature, at which DTG reaches its maximum peak. There was practically a total mass loss above 800 °C (99.8%). [6, 162]

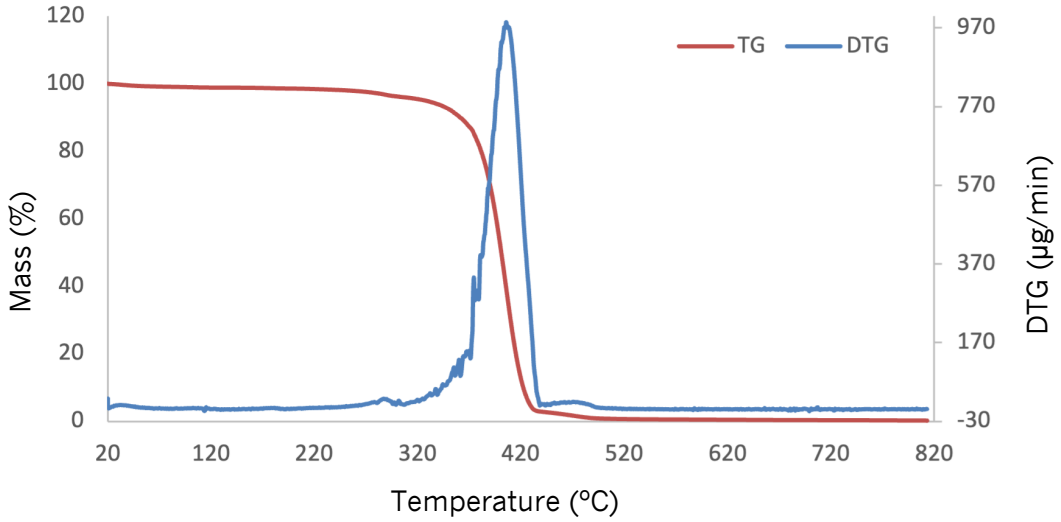


Figure 23 STA curve of P(St-MMA-AA) PCs.

The performed morphological, chemical and thermal characterization confirmed the uniformity and stability of the reactional conditions utilized to synthetize P(St-MMA-AA) PC spheres, which were then used for fabric coloration without further purification.

4.2. Synthesis of SiO_2 PCs

SiO_2 microspheres were synthesized as described in Chapter 3.3.2.. In the initial experiments, SiO_2 particle formation was not being complete, so reaction times of 2, 6 and 24 hours were tested. However, even with this augment in reaction time, spherical particles were not produced. Thus, several ratios of TEOS/NH_3.H_2O/EtOH and stirring speeds (200, 300, 500 and 750 rpm) were tested to obtain the desired microspheres, within the range of sizes to produce structural color (typically between 200-300 nm). [163] Overall, maintaining a stirring speed of 300 rpm for 1h at 30 °C (Figure 24), a TEOS/NH_3.H_2O/EtOH ratio of 1:2:20 produced 468±42 nm PCs (SiO_2-1), a ratio of 2:1:20 produced 307±6 nm PCs (SiO_2-2) and 1:4:40 ratio produced 429±12 nm PCs (SiO_2-3), being PC size assessed by DLS measurements, where PdI of these samples was registered at 0.15. Zeta potential of SiO_2 PCs incremented with an increment in particle size, which was registered between -17.9 ± 0.2 and -9.9 ± 0.7 mV.

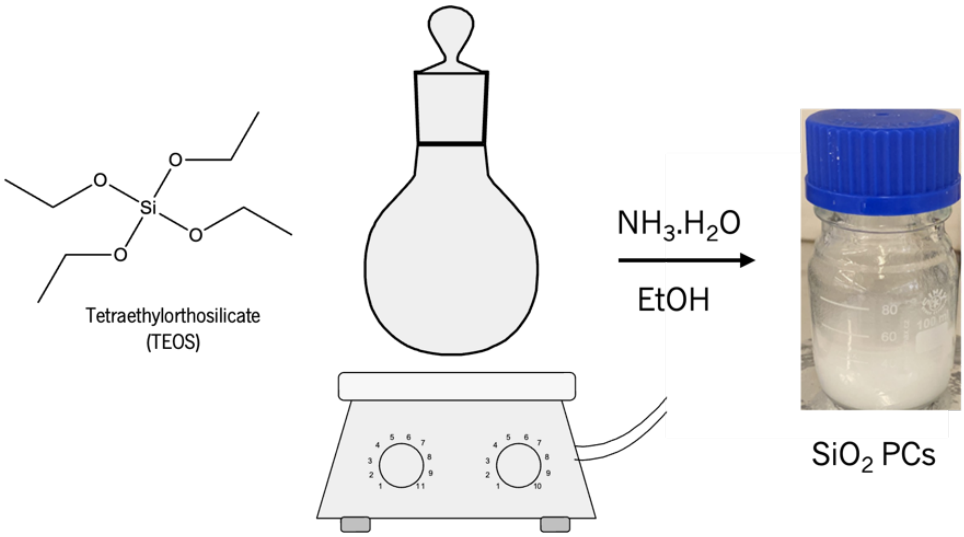


Figure 24 Reaction setup for SiO_2 PC synthesis.

The obtained results are not in conformity with the literature, as an increase in TEOS concentration should have produced larger spheres. [164, 165] Here, the lowest TEOS ratio produced the larger spheres, as the highest TEOS ratio used produced smaller spheres. SEM analyses (Figure 25) were performed to compare dried particle size to DLS measurements.

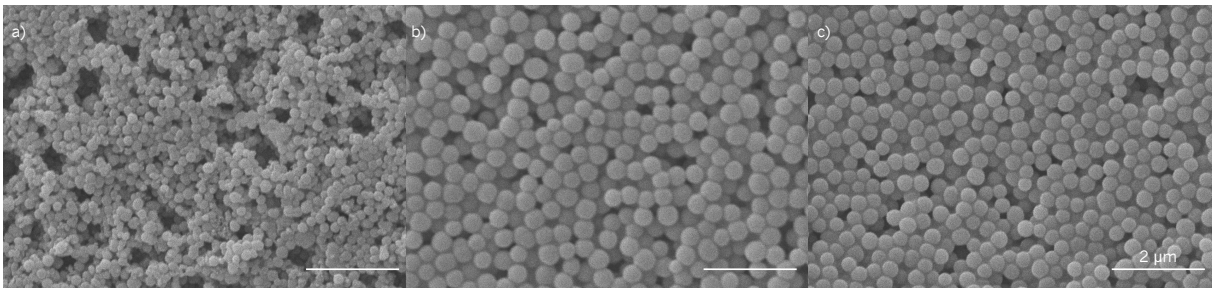


Figure 25 SEM micrographs (40000× magnification) of the obtained SiO_2 particles with different ratios of TEOS:NH_3.H_2O:EtOH, a) 1:2:20 (SiO_2-1), b) 2:1:20 (SiO_2-2) and c) 1:4:40 (SiO_2-3).

Comparing SEM sizes to the ones obtained by DLS, SiO_2-1 presented a reduction in size of ~60 nm (407±40 nm), while SiO_2-2 and SiO_2-3 presented reductions of ~90 nm (213±17 nm) and ~100 nm (327±25 nm), respectively. These results confirmed the inconsistency in the obtained sizes, as SiO_2-1 reactional conditions should have generated sizes between the sizes of SiO_2-2 and SiO_2-3. Furthermore, the self-assembly of these spheres did not present a structured arrangement, as seen in P(St-MMA-AA) PCs, where a hcp arrangement was present. Nevertheless, the produced SiO_2 PC spheres were characterized, to an extent.

ATR-FTIR analysis of the initial reagents was not performed due to its toxicity (ammonia) and susceptibility to humidity (TEOS), as this analysis is made in "open air". ATR-FTIR of the synthesized SiO_2 spheres is presented in Figure 26.

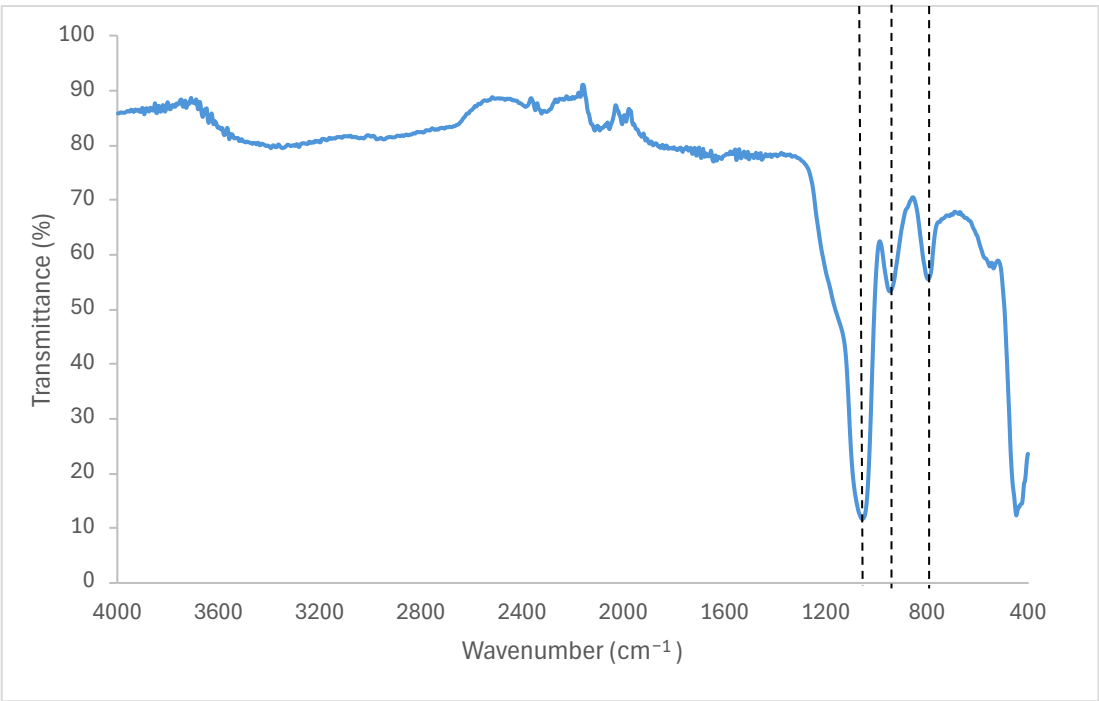


Figure 26 ATR-FTIR of SiO_2 PCs.

The peak at 1049 cm^{-1} is related to the asymmetric stretching of Si-O-Si bonds, peak at 945 cm^{-1} is associated to Si-OH bond stretching of the silanol groups, while the peak at 800 cm^{-1} is attributed to symmetric stretching/bending of Si-O-Si, often assigned to tetrahedral SiO_2. Finally, peak at 447 cm^{-1} is attributed to rocking motion of the Si-O-Si bridging bond. [166-168]

Regarding the thermal behavior, DSC curve of SiO_2 PCs (Figure 27) presents an endothermic band at 106 °C, with an associated energy of 173 $J.g^{-1}$, typical of physically adsorbed water desorption. A very broad band appears from 240 to 370 °C, with an energy of 39 $J.g^{-1}$, possibly associated to slow process of silanol condensation (dehydroxylation), where Si-OH are converted into a Si-O network. To confirm this, STA analysis was performed (Figure 28), showing an initial 7% loss of mass attributed to water evaporation (25-110 °C) and a residual 5% loss from 110 to 1100 °C, thus confirming the occurrence of a dehydroxylation process. [169-172] Thus, DSC and STA analysis showed the high thermal stability of the synthesized SiO_2 PCs.

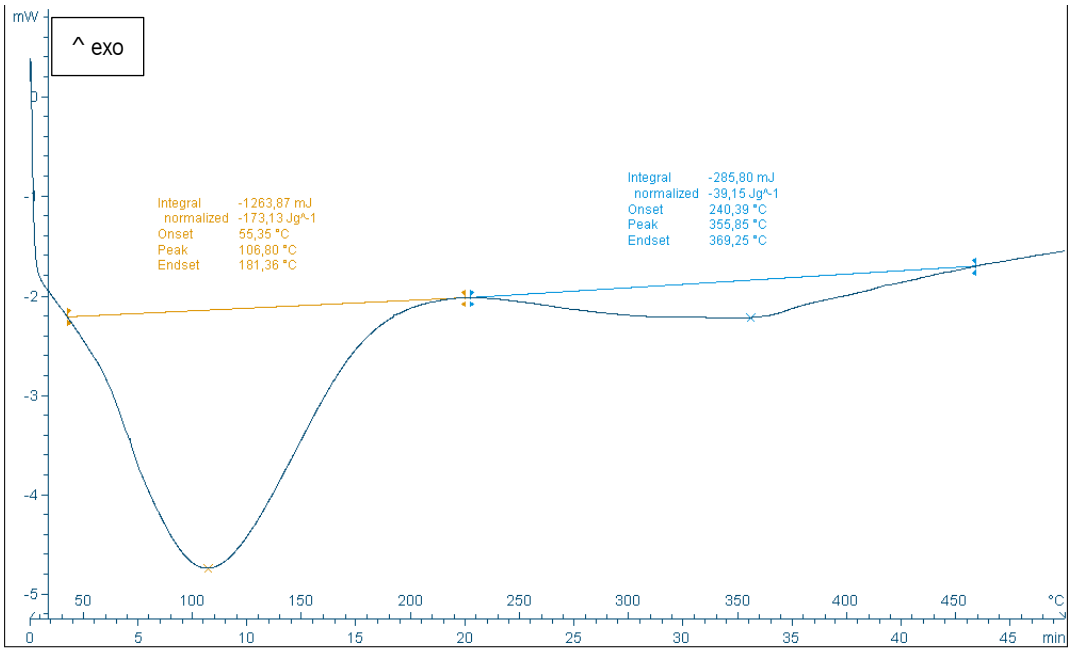


Figure 27 DSC thermogram of SiO_2 PCs.

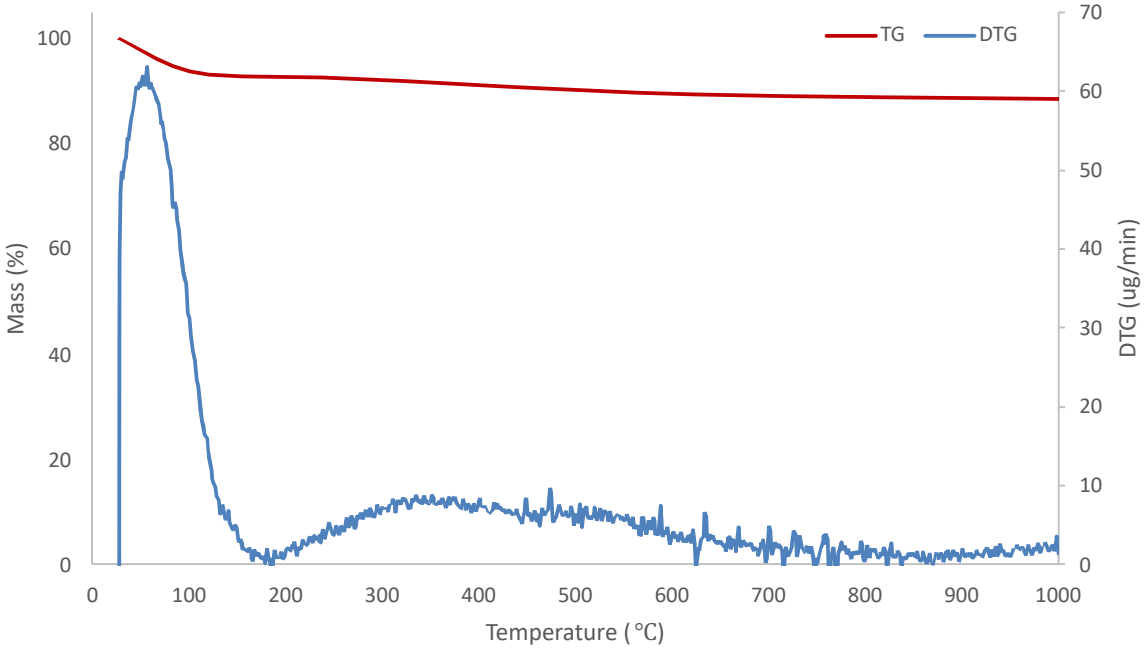


Figure 28 STA curve of SiO_2 PCs.

Although there were inconsistencies in the synthesis of these spherical particles it was still possible to perform morphological, chemical and thermal characterization, confirming the obtention of SiO_2 PC spheres and their high thermal stability. SiO_2 PCs used for fabric coloration without further purification.

4.3. Synthesis of KL PCs

KL spheres were synthetized via a solvent-antisolvent methodology as represented in Figure 29. KL initial concentration was set around 3 wt%. When the water was added the final concentration was around 1 wt% (10 mg/mL). KL PCs were then characterized via morphological, chemical and thermal assays.

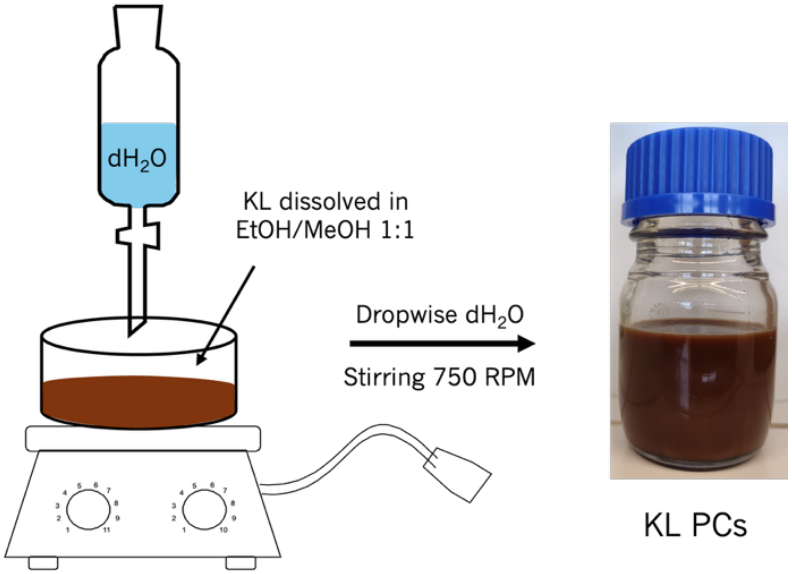


Figure 29 Reaction setup for KL PC synthesis.

ATR-FTIR analysis chemically proved the presence of KL after solvent-antisolvent synthesis. Peaks between 3400–3200 cm^{-1} correspond to the O–H stretching vibrations, while bands centered around 2935 and 2839 cm^{-1} arise from C-H stretching in aromatic methoxyl groups and in methyl and methylene groups of side chains. Peaks at 1600, 1514, 1454 and 1423 cm^{-1} correspond to aromatic skeletal vibrations combined with C–H in-plane deformation, C–H deformations of methyl and methylene, aromatic skeletal vibration breathing with C=O stretching, and C=O stretching (conjugated), respectively. The peak at 1321 cm^{-1} is attributed to the C–O stretching of syringyl (S) ring units, highly characteristic of hardwood lignins. On the other hand, the peak at 1211 cm^{-1} typically arises from C–C, C–O, and C=O stretching from guaiacyl (G) units and phenolic OH groups. S unit aromatic C–H in-plane deformations appear at 1109 cm^{-1}, C–O(H) and C–O(C) stretching associated with primary alcohols and aliphatic ethers appear at 1028 cm^{-1}, while C–H out-of-plane bending from S units appear at 827 cm^{-1}. [173-176]

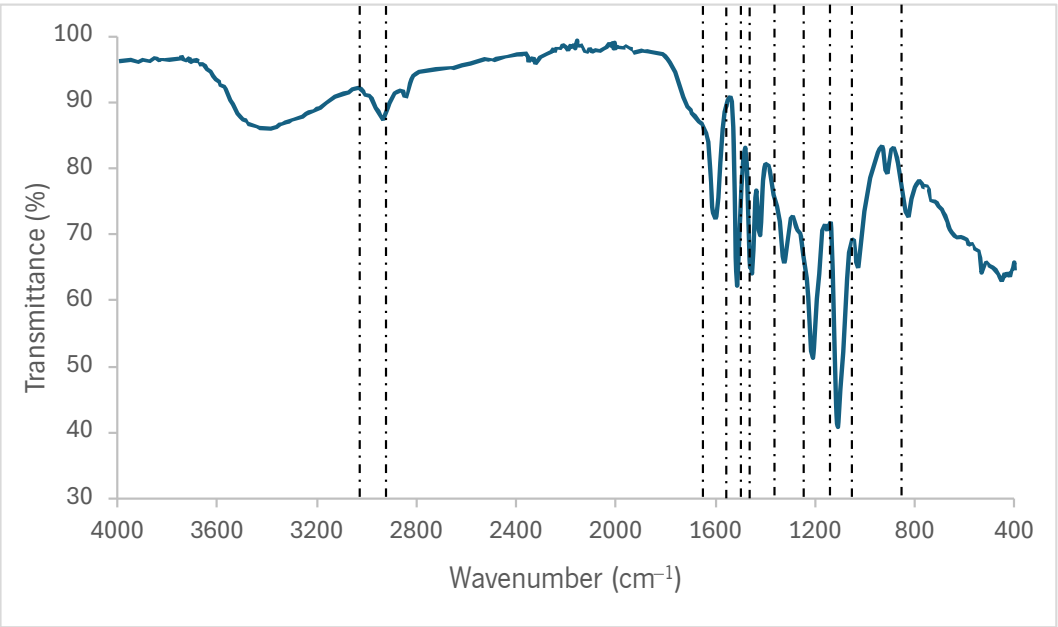


Figure 30 ATR-FTIR of KL PCs.

As for size determination, DLS and SEM were utilized to evaluate particle size in both wet and dry states. DLS analysis displayed a particle size average of 667.0 ± 17.1 nm with a PdI of 0.14 ± 0.06, indicative of good size uniformity and homogeneity. Zeta potential of KL particles was registered at -45.8 ± 0.6 mV, indicative of high dispersion stability. [177] As for SEM, the average size was lower, 507.7 ± 105.2 nm, but its standard deviation was much higher than the one seen in DLS measurements. The higher standard deviation observed can be explained by lignin's nature, as lignin is prone to aggregate. As seen in Figure 31, KL seems to present a thermoplastic behavior, even when dried at room temperature or under vacuum conditions, thus contributing to the high standard deviation observed in SEM measurements. [178, 179] Nevertheless, the obtained sizes are consistent with the ones reported in the literature, as other authors also obtained 500 nm particles at a lignin concentration of 10 mg/mL, using other methodologies and solvents. [180, 181]

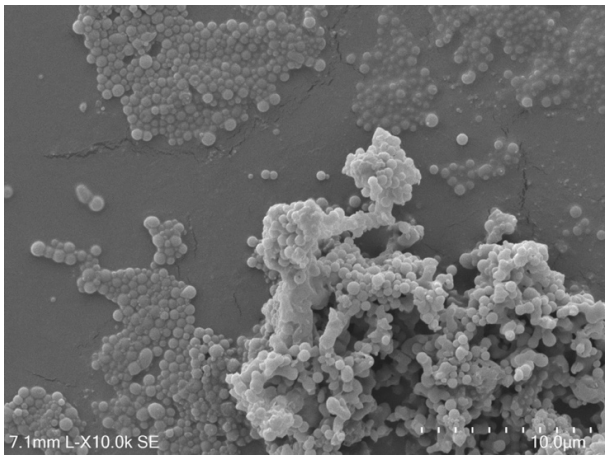


Figure 31 SEM micrograph (magnification of 10000×) of KL PCs.

Thermal characterization of KL spheres performed by DSC (Figure 32) showed an endothermic band at 80 °C referent to water evaporation, followed by two low energy endothermic events. The first event, at 149 °C, can be attributed to a glass transition temperature, which may differ depending on lignin's nature, as it is influenced by its polymeric chains (length and stiffness) as well as the rotational freedom of molecular moieties. The second event, at 191 °C, is often classified as a softening temperature, the temperature at which the molecular mobility becomes high enough for viscous flow. [182-184] Regarding STA analysis (Figure 33), it was registered a residual mass loss of 5% from 20 to 240 °C. At this temperature, KL starts its degradation process, registering a 50% mass loss at 500 °C (DTG maximum peak at 385 °C). After this temperature, lignin continues to carbonize, registering a final residual content of 36%. [183, 185]

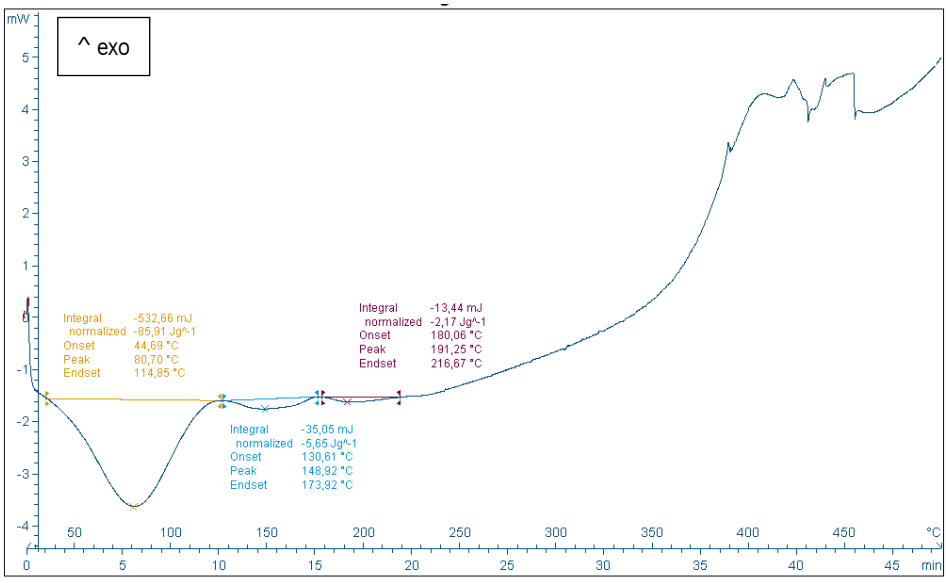


Figure 32 DSC thermogram of KL PCs.

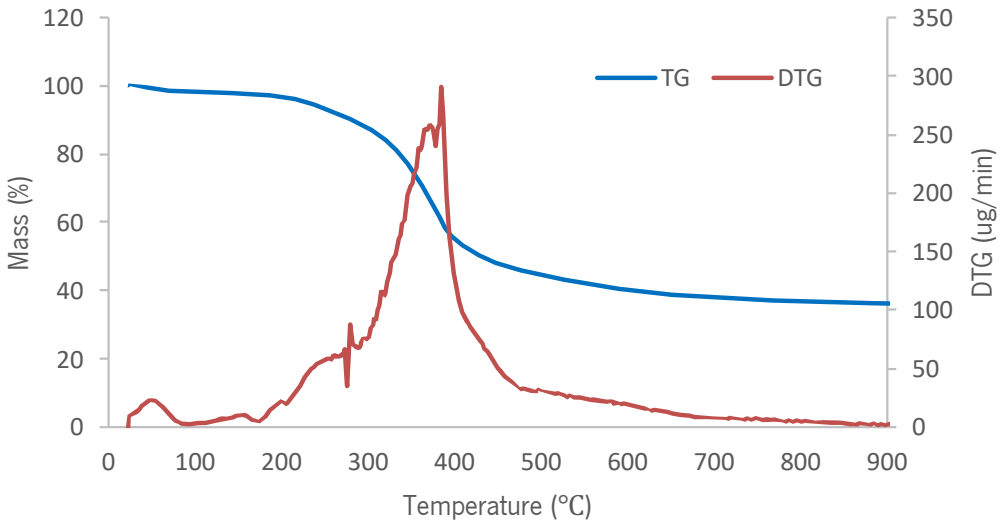


Figure 33 STA curve of KL PCs.

The performed analysis showed that KL particles present good morphological and thermal properties, suitable for garment application. KL PCs were used for fabric deposition without further purifications.

5

PC deposition onto textile substrates

Parts of this chapter were based on the following publications:

(Paper) **Fernandes, Rui D.V.**; Gomes, Pedro; Zille, Andrea; Souto, A. P.. "The influence of chemical reaction conditions upon poly(styrene-methyl methacrylate-acrylic acid) synthesis: Variations in nanoparticle size, colour and deposition methods". *Coloration Technology* (2020) 136, 101-109. doi: 10.1111/cote.12452

(Paper) **Fernandes, Rui D.V.**; Pranovich, Alina; Valyukh, Sergiy; Zille, Andrea; Hallberg, Tomas; Järrendahl, Kenneth. "Iridescence Mimicking in Fabrics: A Ultraviolet/Visible Spectroscopy Study". *Biomimetics* (2024) 9, 71. doi: 10.3390/biomimetics9020071

This chapter had the support of Linköping University (LiU) and the Swedish Foundation for Strategic Research (SSF), grant number RIF21-0026.

5.1. P(St-MMA-AA) deposition onto polyamide, polyester and cotton fabrics

After PC synthesis was performed, the next step involved their deposition in different textile substrates. Different deposition techniques were performed for the coating with P(St-MMA-AA), SiO2 and KL PCs.

To understand if any type of textile substrate is suitable (without any pretreatment) to mimic the structural colors found in nature, all three fabrics were characterized, in terms of thickness, linear density of the yarns (measured in Tex, where 1 Tex = 1 g per 1 km) at warp and weft, and number of yarns per centimeter at warp and weft (Table 4), before any procedure was performed on the fabrics.

Table 4 Fabrics characterization according to the ISO standards.

Property Measured	Polyamide	Polyester	Cotton
Structure	Plain weave	Plain weave	Plain weave
Mass per area (g/m²)	61.5	100	140
Thickness (mm)	0.11	0.25	0.30
Yarn linear density (Tex)	3 at weft 5 at warp	8 at weft and warp	20 at weft and warp
Number of yarns/cm	45 at weft 70 at warp	32 at weft and warp	30 at weft 40 at warp

To enhance the chroma (color intensity, saturation, or purity) from the structural colors, cotton and polyester fabrics were dyed black, as previously described, whereas black polyamide fabric was commercially available. [40, 51, 54, 186, 187] Then, P(St-MMA-AA) photonic crystals with five different sizes (170, 190, 210, 230 and 250 nm) were applied by dip coating onto polyamide, polyester, and cotton fabrics, to produce violet, blue, green, green-red and red structural colors, respectively. As seen in Figure 34, the polyamide samples exhibit brighter colors than polyester and cotton samples. Upon ocular inspection of all three fabric samples, PA samples are the only ones to have a visible iridescent effect. Furthermore, cotton samples exhibit a milky aspect at the fabric's surface.

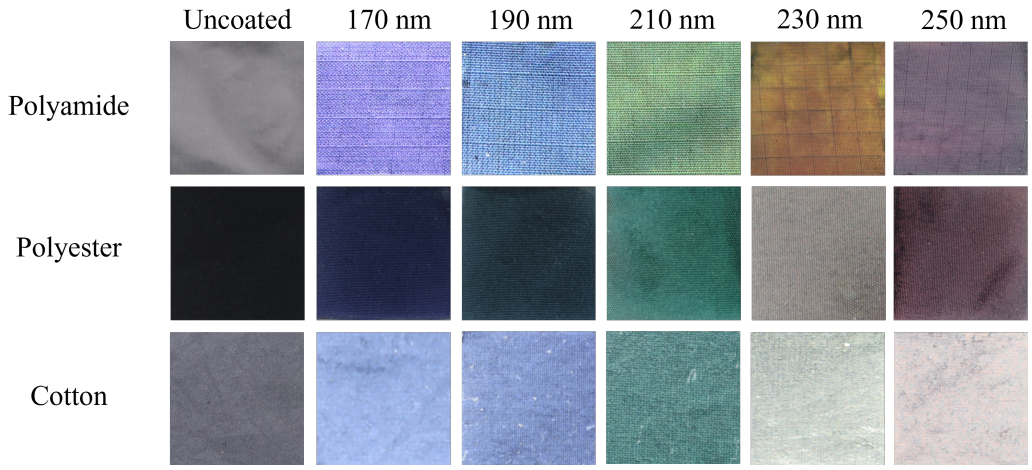


Figure 34 Digital photographs of uncoated polyamide (PA, L* = 21.11, a* = 0.52, b* = −1.13), polyester (PES, L* = 20.36, a* = −0.34, b* = −3.13) and cotton (CO, L* = 21.19, a* = 0.80, b* = −3.97) fabrics, and PA, PES and CO fabrics coated with 170, 190, 210, 230 and 250 nm PCs. **Note:** the uncoated PA and CO appear grey in photographs but are black.

Since all three fabrics have the same plain structure, differences in the sample's chromaticity are probably due to the fiber's type and linear density (g/m^2). As both polyamide and polyester are synthetic fibers, the difference in color must be related to the linear density of the fabrics and consequently, surface roughness. Fabrics composed of natural fibers, such as cotton, usually have a rougher surface than synthetic ones. To assess these assumptions, SEM and surface roughness measurements were performed on all three fabrics, for both coated and uncoated samples. Figure 35 shows SEM micrographs of the fabrics utilized for PC deposition at different magnifications, whereas Figure 36 denotes the same fabrics coated with 190 nm PCs.

When analyzing the SEM micrographs, uncoated fabrics seems to show an increase of surface roughness, with polyamide being the smoothest, followed by polyester and cotton. To confirm these visual assumptions, the surface roughness average (Ra) of uncoated fabrics was measured with a HANDYSURF+ rugosimeter.

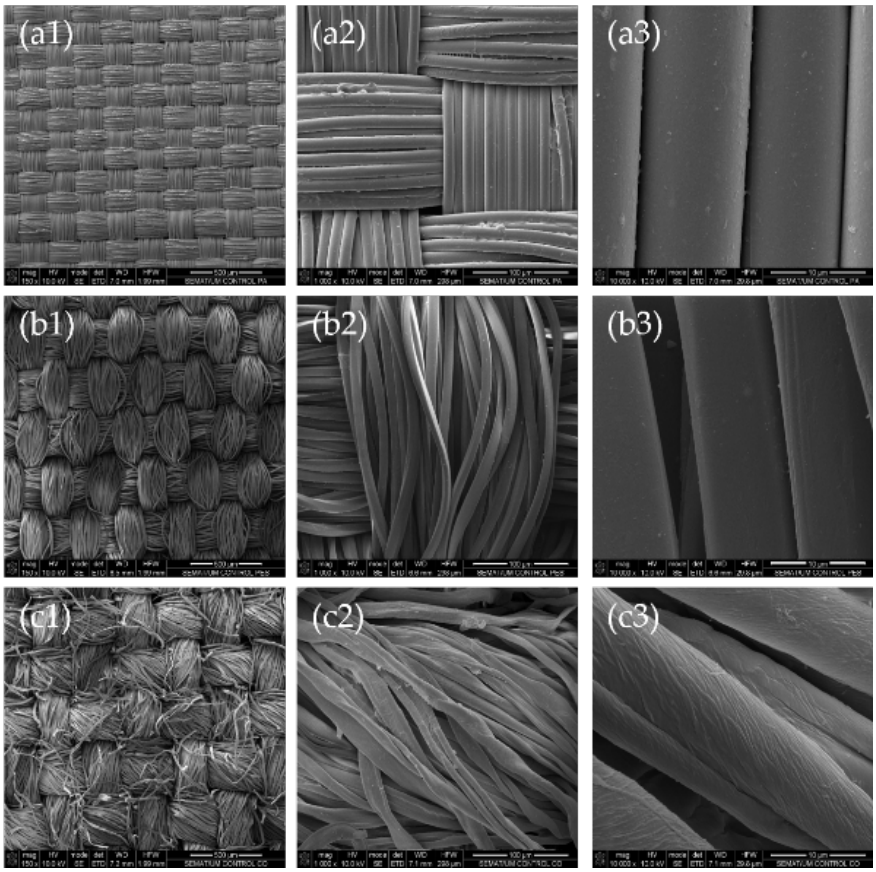


Figure 35 SEM micrographs of polyamide (row a), polyester (row b) and cotton (row c) uncoated fabrics at 150x (a1, b1, c1), 1000× (a2, b2, c2) and 10,000× (a3, b3, c3) magnifications.

The results are presented in Table 5, along with the surface roughness of PC coated fabrics. Surface roughness values are in agreement with SEM micrographs, where polyamide is in fact the smoothest fabric with an Ra of 6.33 ± 1.99 μm, followed by polyester with an Ra of 16.43 ± 5.51 μm and cotton, the roughest fabric with an Ra of 17.43 ± 6.27 μm. Polyamide SEM analysis also showed that, the levelling agent used in the dyeing process may created a coating, but due to its dimension, was assumed to not affect surface roughness, taking in account the relative dimension of the PCs. After PC coating, polyamide and cotton fabrics maintained their Ra values. Polyester Ra increased by 3 μm after the PC coating, which is less than one third of the diameter of one individual thread (~10 μm) of the fabric's yarn (~250 μm warp, ~200 μm weft), thus this increase may be disregarded. Since SEM micrographs of PES samples showed a very well-organized structure, it was expected that these samples should present bright colors and iridescence.

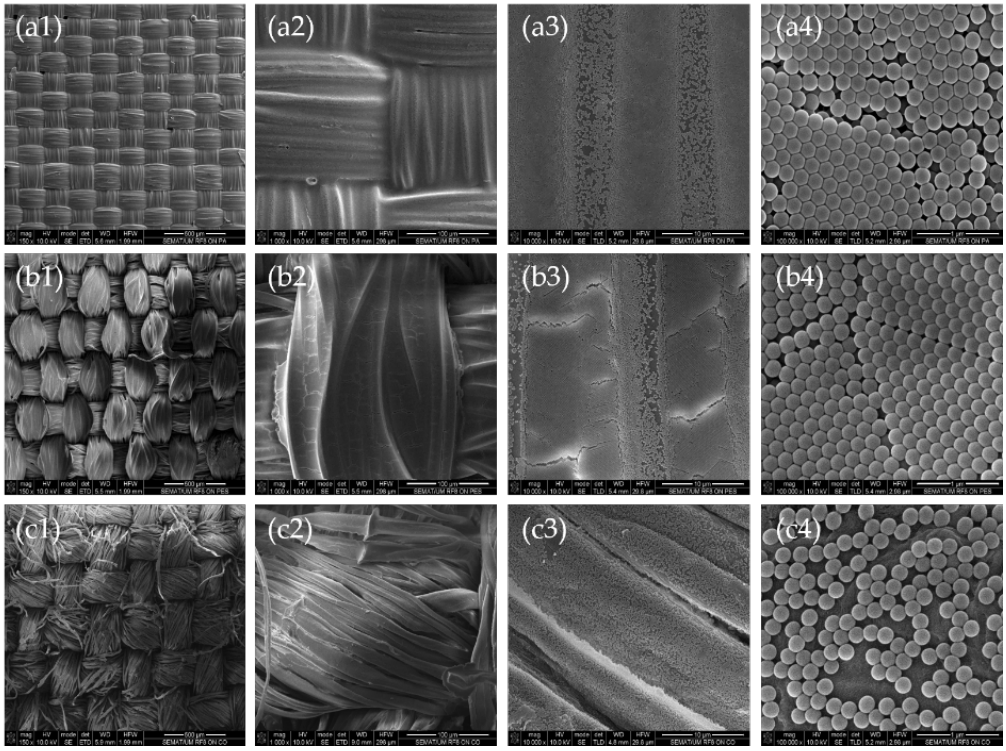


Figure 36 SEM micrographs of polyamide (row a), polyester (row b) and cotton (row c) coated fabrics with 190 nm PCs at 150× (a1, b1, c1), 1000× (a2, b2, c2), 10,000× (a3, b3, c3) and 100,000× (a4, b4, c4) magnifications.

Table 5 Surface roughness (Ra) measurements values of uncoated and PC coated fabrics (n = 3).

Fabric	Ra of Uncoated Fabrics (μm)	Ra of PC Coated Fabrics (μm)
Polyamide	6.33 ± 1.99	6.77 ± 1.35
Polyester	16.43 ± 5.51	19.91 ± 3.73
Cotton	17.43 ± 6.27	17.17 ± 5.47

However, this was not the case, probably due to the roughness factor. Instead, the PA samples were the brightest, with the most intense color and the only ones to present visible iridescence from ocular inspection. Since all three fabrics have the same plain structure, the factors that are influencing structural coloration are the thickness, yarn Tex and the tightness of the weave. The combination of all these factors will affect the fabric surface roughness, which should be as low as possible for a good and uniform photonic crystal deposition. Thus, after analyzing these fabric properties it is concluded that a lower fabric thickness, low yarn Tex and a tight weave will produce fabrics with lower surface roughness. If fabric thickness is low, there will be less PC spheres needed to fill gaps between fibers, thus more spheres are available to form a more uniform and flat coatings. Yarns with low Tex values are thinner, smoother and with less fibrils on its surface, thus roughness can be minimized, to an extent, without compromising its

physical and mechanical properties. Furthermore, in tighter weaves the gaps between the fibers are smaller, leading to a higher fabric cover, which will diminish surface roughness and increase the surface area for a better PC deposition, without defaults/cracks in its structure. These conclusions are in agreement with the studied performed by Li *et al*, where polyester and silk substrates with different structures, plain and twill, were analyzed for PC deposition purposes and, consequently, optimization of structural color. [54] It was observed that plain structures were preferred over twill structures, for both polyester and silk, due to the higher covering factor of this type of structure. Plain structures with tighter weaves lead to fabrics that are more compact, flat, and dimensionally stable, which demonstrated to be better for the obtention of good structural colors. Furthermore, yarn diameter and yarn density were determinant factors to obtain the best structural color possible. Thus, it is of high importance to know what are the characteristics of the textile substrate used for PC biomimicry. [188, 189]

After comprehending photonic physical behavior in different types of fibers, the PC-coated polyamide, polyester and cotton fabrics were analyzed by UV/Vis reflectance measurements for each color/particle size (Figure 37).

The PA samples produced sharp reflection peaks in the visible wavelength region, except for the red sample, where the peak is very weak for all three fabrics. In most cases, the CO samples have higher reflectance as compared to PA and PES since the self-assemble structures in these samples are not uniform, giving them a whiter appearance, due to higher light scattering on the fabric surface. Also, in CO samples, the highest reflection peak has a small hypsochromic (blue) shift when compared to PA samples. For PES samples, intensity reflectance is comparable to violet, green and red PA samples, always with a slight blue shift in terms of maximum reflection peak, as in CO samples.

Interestingly, in the fabrics coated with 230 nm PCs (green-red sample), the reflection peak appears in the green region for CO and PES, while in PA the peak appears in the red region. Thus, it can be assumed that, since SEM and roughness analysis showed that PA is the best substrate of all three fabrics for PC deposition, the main reflected color produced by the photonic structure is red. This could be used as a preliminary indication whether the self-assembly of PCs is good or not. By observing when the reflected color does not match between fabrics with PCs of the same size, the use of more expensive techniques such as SEM can be reduced.

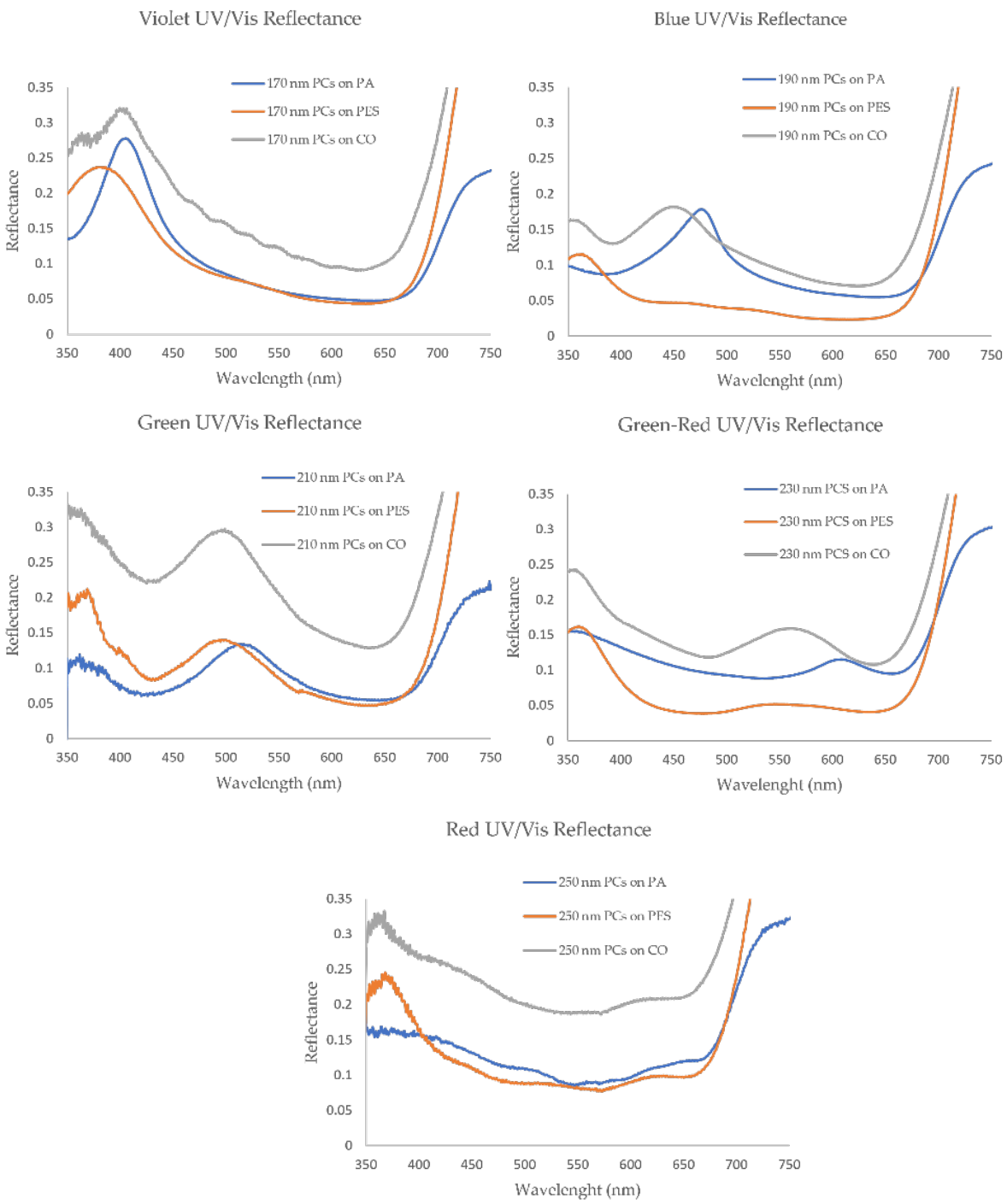


Figure 37 Fixed angle of incidence (8°) UV/Vis reflectance (DHR) spectra for (a) 170, (b) 190, (c) 210, (d) 230 and (e) 250 nm P(St-MMA-AA) PCs in polyamide, polyester and cotton fabrics.

Since only the coated PA fabrics presented iridescence (by ocular inspection, Figure 38), angle-dependent UV/Vis reflectance measurements were done on only these samples.

The measurements were performed for all five different colors, with both s- and p-polarized light. With this analysis it was possible to observe the reflection peak movement while changing the angle of incidence

of light. PA samples coated with 190 (blue) and 230 nm (green-red) PCs presented the most interesting results, which will be discussed in more detail below.

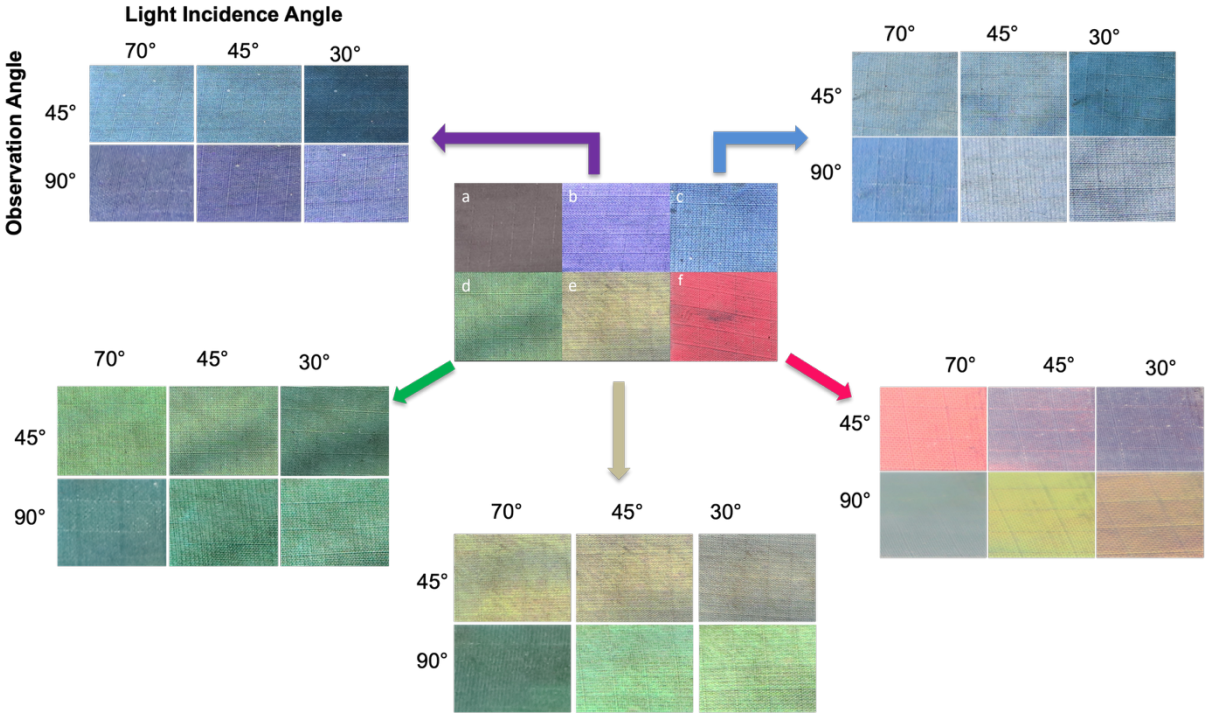


Figure 38– Photographs of a) PA uncoated fabric, PA coated with P(St-MMA-AA) photonic crystals with different sizes, b) 170 nm, c) 190 nm, d) 210 nm, e) 230 nm and f) 250 nm, and the observed iridescent effect in each sample.

For PA coated with 190 nm PCs, for s-polarized light measurements, the initial reflection peak (α_i = 12°) appears at a wavelength of 475 nm (blue region), which moves with a hypsochromic shift as the α_i increases. At α_i = 80°, the reflection peak is located at a wavelength of 400 nm (violet region) (Figure 39). This behavior occurs similarly for p-polarized light, with the exception that above an α_i of 70° the reflection peak is no longer visible. Furthermore, in s-polarized light, a second reflection peak starts to appear at 610 nm (red region), from α_i of 50° to 80°, indicating that, at higher α_i, the final color observed is the result of the addition of two separate colors (violet and red). This phenomenon is not observed in the p-polarized light measurements.

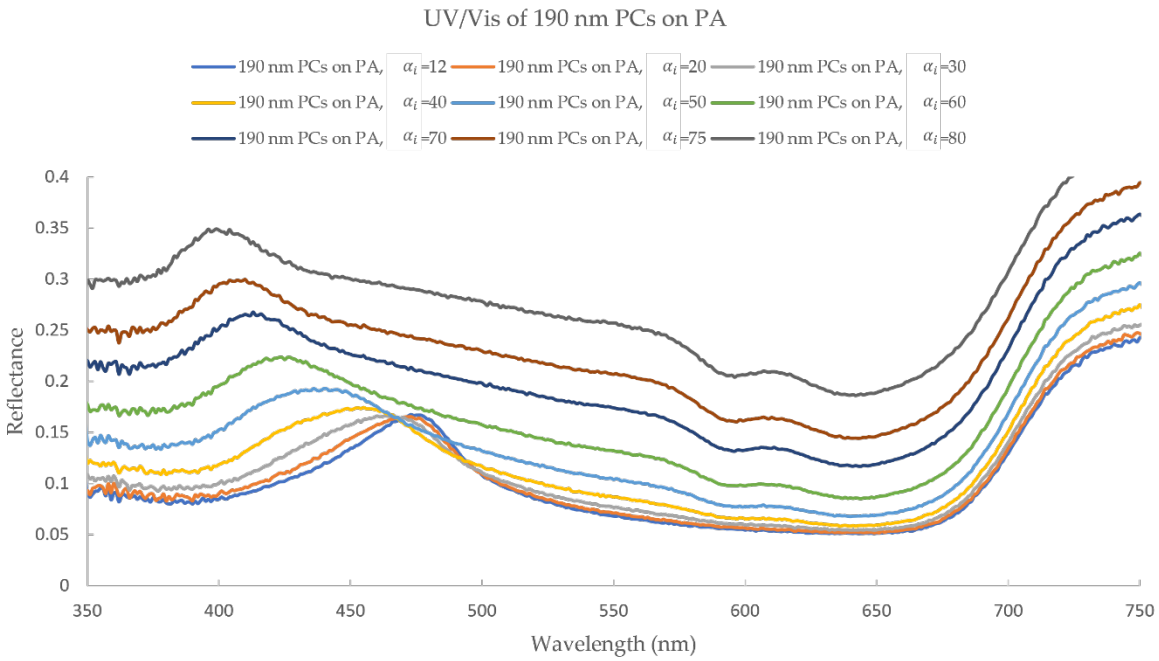


Figure 39 UV/Vis reflectance (s-polarized light) spectra analysis of PA coated with 190 nm PCs, with α_i ranging from 12° to 80°.

In order to present the color appearance of the fabrics, scatterometry (or angular resolved reflectance spectroscopy) was recorded giving IP-BRDF data. With this technique it was possible to observe color shifts as the angle of incidence α_i, and angle of observation α_o changes. As seen in Figure 40 (top), the initial color at an α_i = 30° is slightly green (at a low α_o) and gradually changes to blue and violet as α_i and α_o increase. At a maximum α_i and α_o, color sample is greyish, almost white, where the luminosity parameter L* increases drastically at these angles. This was observed for every sample tested. The IP-BRDF measurements are in alignment with the data observed in the UV/Vis spectra, thus validating both techniques for iridescence characterization. Color coordinates in a 2D CIEL*a*b* space are presented in Figure 40 (bottom), where the arrows represent the movement direction, from low to high α_o. L* varied between 30 and 55, except at higher α_i and α_o, which were above 80. This was also observed in the other PA samples.

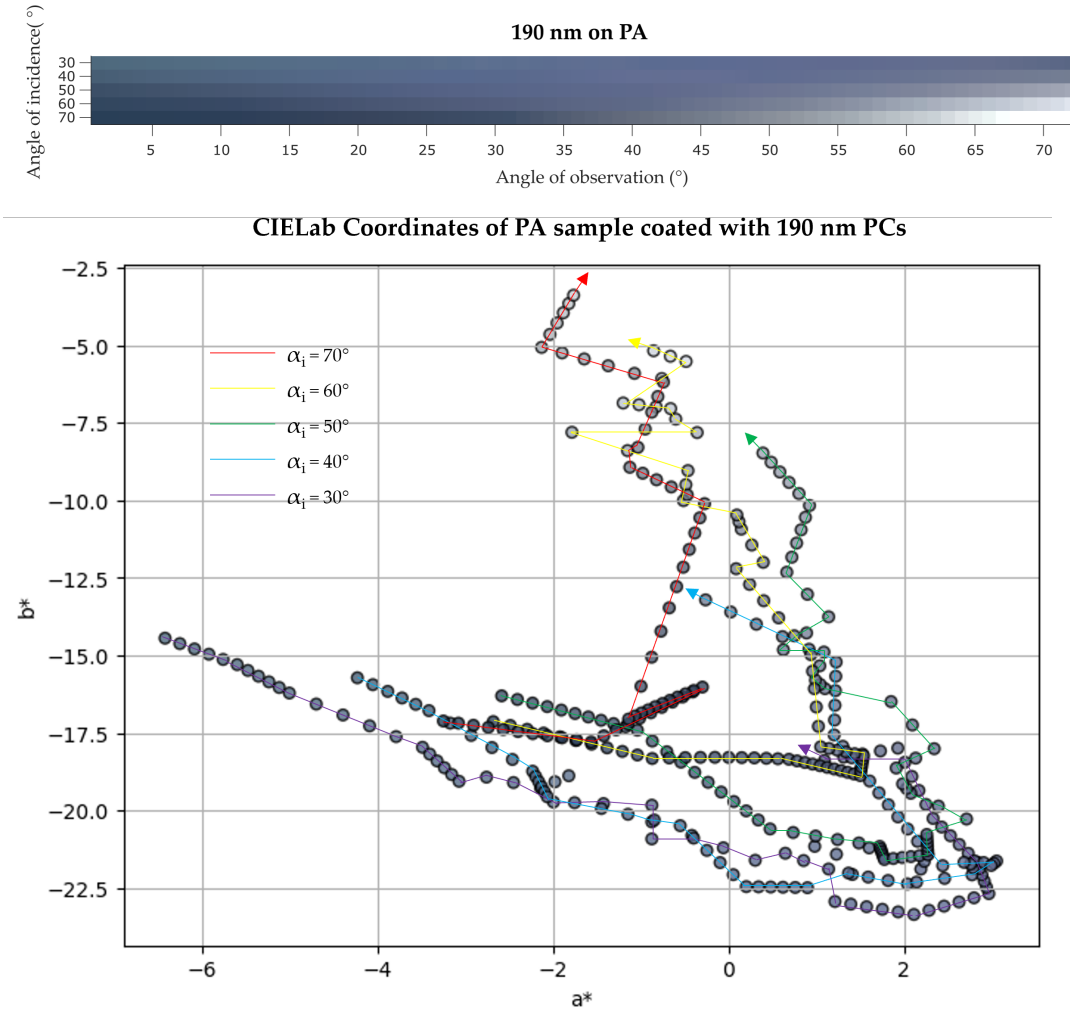


Figure 40. (top) IP-BRDF measurements of PA coated with 190 nm PCs, α_i = 30° to 70° and α_o = 0° to 70°; (bottom) 2D representation of color coordinates movement in CIEL*a*b* space, where the arrows represent the direction from low to high α_o (0° to 70°) for each α_i (30° to 70°).

The s-polarized light measurements of the PA sample coated with 230 nm PCs showed a single reflection peak for α_i = 12° at 610 nm (Figure 41). As the α_i increases, this peak stays unaltered at 610 nm and other reflection peaks start to appear. At α_i = 50° a new peak appears at 560 nm and, as the α_i increases to 80°, this peak is divided in two, where the first peak maintains its wavelength at 560 nm and a second one is formed at 500 nm. Similarly to the previous sample, this phenomenon is not noticeable in the p-polarized light measurements, where the peak at 610 nm fades away above α_i = 50° and the formation of new reflection peaks is not observed.

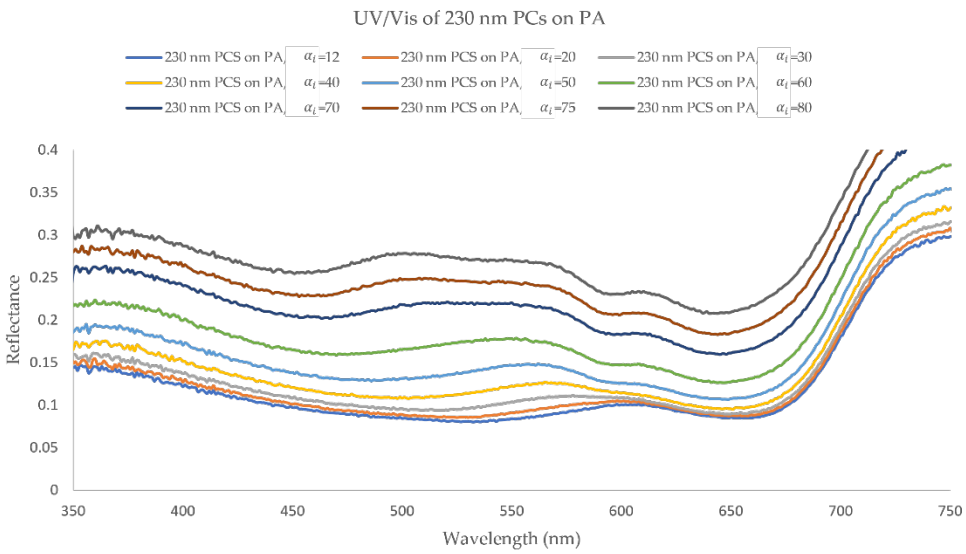


Figure 41 UV/Visible reflectance (s-polarized light) analysis of PA coated with 230 nm PCs, with α_i ranging from 12° to 80°.

The IP-BRDF measurements of the same sample (Figure 42, top), show that for low α_o the color is mainly red, for every α_i. From α_i above 50°, at mid to high α_o, the color changes to green. Once again, this is consistent with the angle-dependent UV/Vis data where a new peak appears at 560 nm (green region) at the same α_i. Furthermore, this confirm the previous assumptions made in the fixed angle UV/Vis analysis, where the red color was dominant. As for CIEL*a*b* coordinates (Figure 42, bottom), L* varied between 38 and 58, and color is observed to be greener (lower a* values), yellower (higher b* values) at low α_o and bluer at high α_o (lower b* values).

UV/Vis reflectance measurements for PA samples coated with 170, 210, and 250 nm PCs were also performed. The UV/Vis data of these samples is briefly discussed along with IP-BRDF measurements and color coordinates analysis present below (Figures 43–45). A summary of the UV/Vis peaks changes according to α_i is also presented in Table 6.

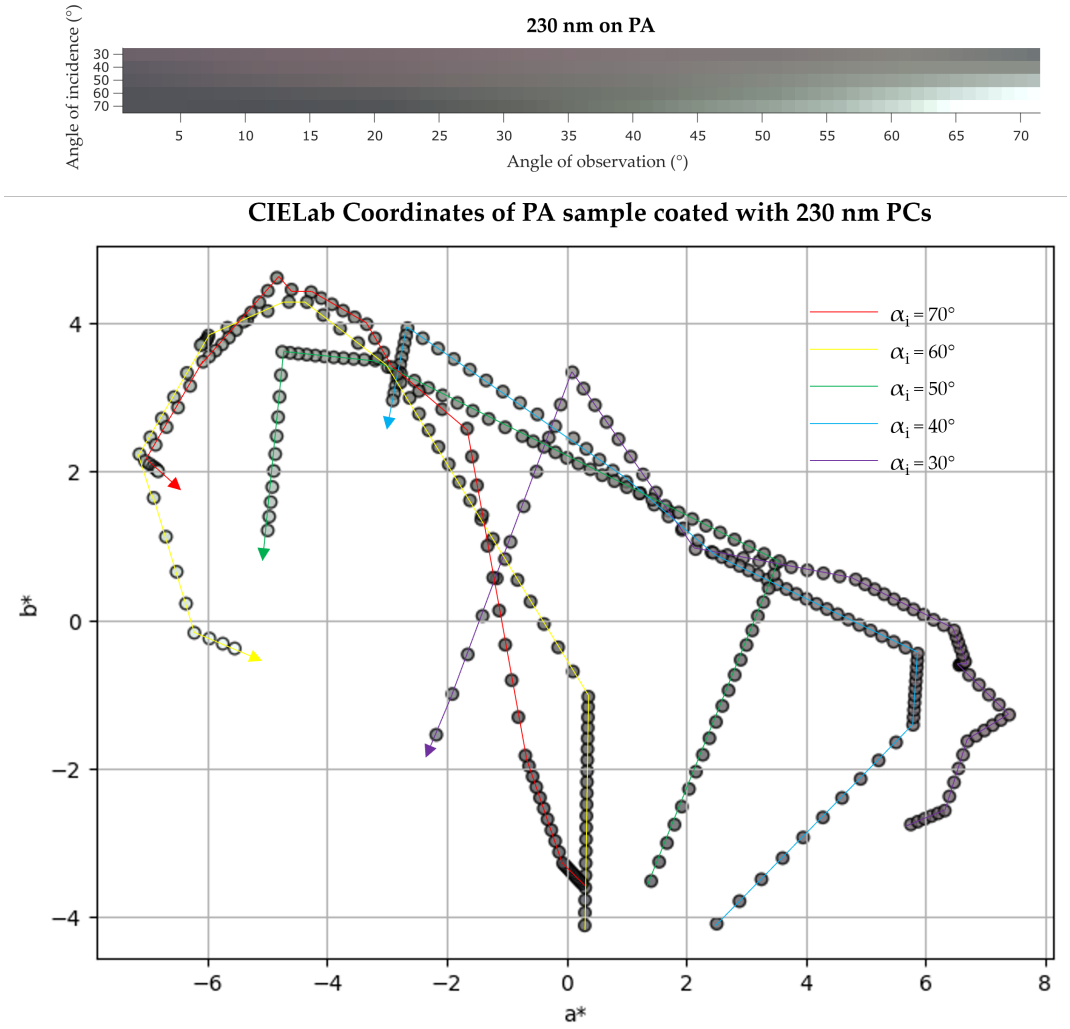


Figure 42 (top) IP-BRDF measurements of PA coated with 230 nm PCs, α_i = 30° to 70° and α_o = 0° to 70°; (bottom) 2D representation of color coordinates movement in CIEL*a*b* space, where the arrows represent the direction from low to high α_o (0° to 70°) for each α_i (30° to 70°).

The PA sample coated with 170 nm PCs showed a small color change, the violet color (UV/Vis reflection data showed a peak at 405 nm for α_i = 20°) becomes lighter with higher α_o and darker at higher α_i (the peak at 405 nm shifted to 385 nm with increasing α_i). Again, at a maximum α_i and α_o the sample color is basically grey, with L* parameter much higher than observed at other angles (L* ranged between 31 and 66). In the 2D color space, a yellower and greener color is obtained.

Table 6 UV/Vis reflectance peaks of PA coated samples with 170, 210 and 250 nm PCs according to changes in the angle of incident light (α_i).

α_i	170 nm PCs on PA UV/Vis Peak (nm)	210 nm PCs on PA UV/Vis Peak (nm)	250 nm PCs on PA UV/Vis Peak (nm)
12°	406	510	641
20°	405	510	639
30°	397	506	639
40°	394	504	636
50°	393	503	633
60°	389	499	627
70°	387	495	622
80°	385	490	619

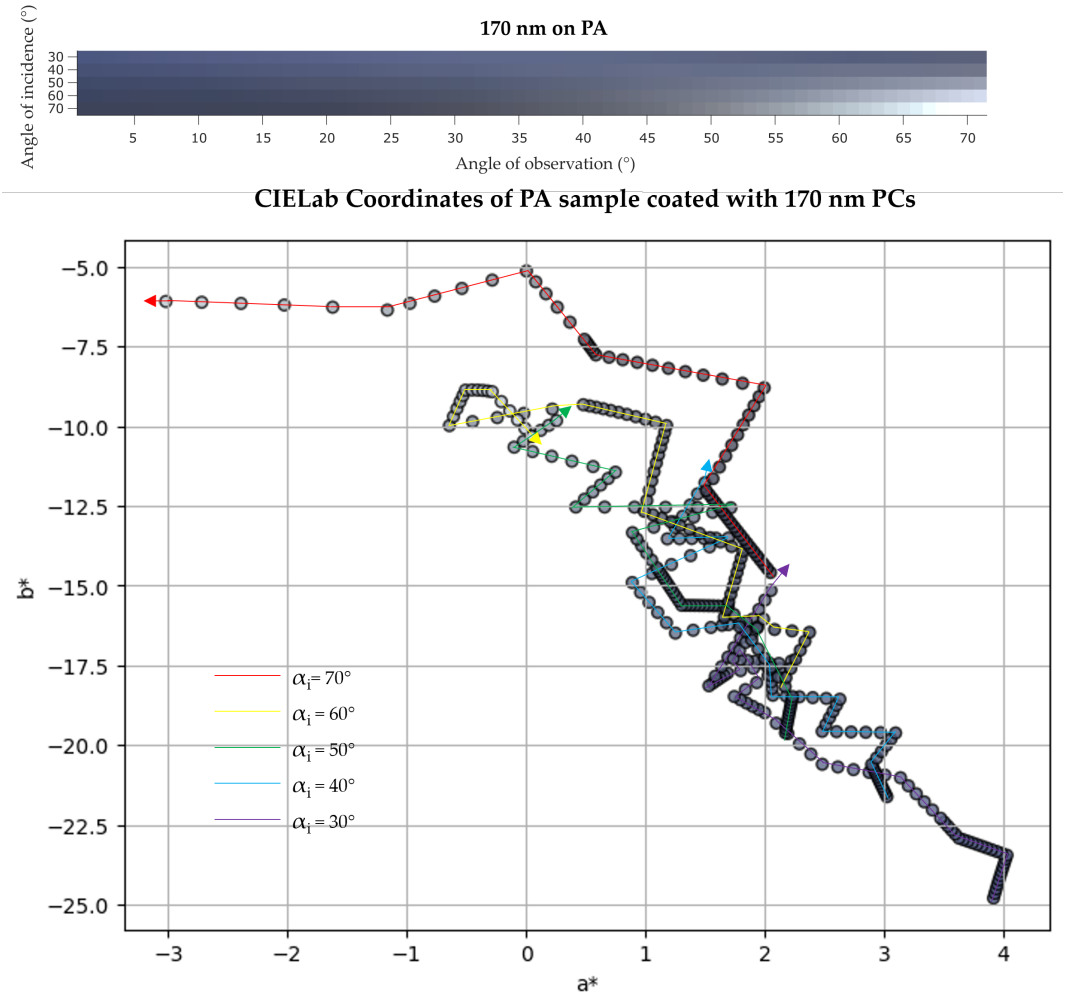


Figure 43 (top) IP-BRDF measurements of PA coated with 170 nm PCs, α_i = 30° to 70° and α_o = 0° to 70°; (bottom) 2D representation of color coordinates movement in CIEL*a*b* space, where the arrows represent the direction from low to high α_o (0° to 70°) for each α_i (30° to 70°).

The PA sample coated with 210 nm PCs showed a color change from green (UV/Vis reflectance data showed a peak at 510 nm for α_i = 20°) to blue (the peak was slightly shifted to 490 nm for higher α_i and α_o). This is consistent with the observed color coordinates, showing sample color getting bluer and redder as α_i increases. The luminosity varied between 34 and 63.

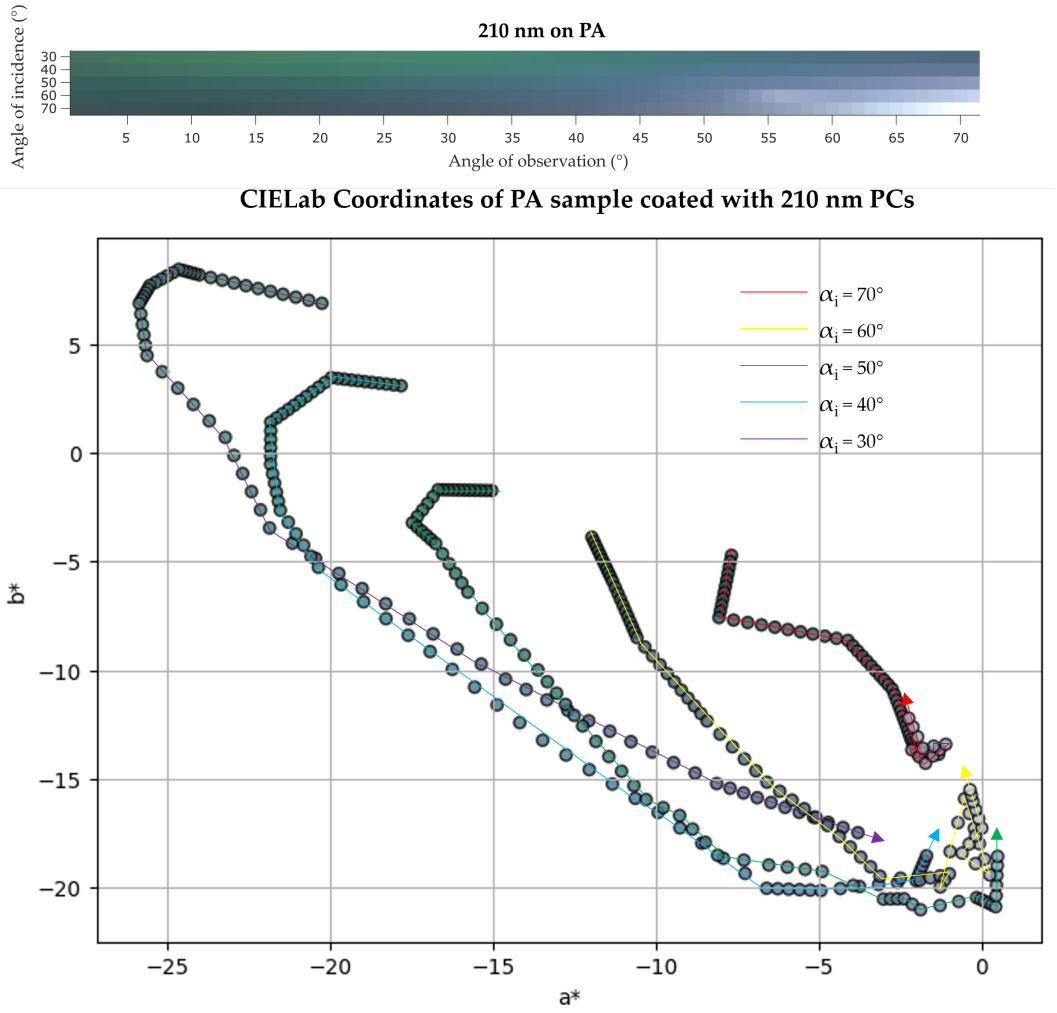


Figure 44 (top) IP-BRDF measurements of PA coated with 210 nm PCs, α_i = 30° to 70° and α_o = 0° to 70°; (bottom) 2D representation of color coordinates movement in CIEL*a*b* space, where the arrows represent the direction from low to high α_o (0° to 70°) for each α_i (30° to 70°).

Finally, the PA sample coated with 250 nm PCs showed a color change from brown-red (UV/Vis reflectance data showed a peak at 640 nm for α_i = 20°) to green (a very weak peak appeared at 520 nm for α_i above 60° and the peak at 640 nm slightly shifted to 620 nm at higher α_i). Analyzing the color space coordinates, it can be observed that at low α_i and α_o, sample color is getting redder and slightly yellower. Then, at α_i above 50° and high α_o, the sample color gets greener and yellower, which

is in accordance with UV/Vis reflectance measurements. In terms of luminosity, this sample presented the highest values of all five samples, with L* values ranging between 48 and 80.

Overall, in all PA coated samples was observed a hypsochromic color shift as the αi increased, in both UV/Vis and IP-BRDF analysis. PA samples showed a wide variety of colors, able to emulate the iridescent effects observed in nature.

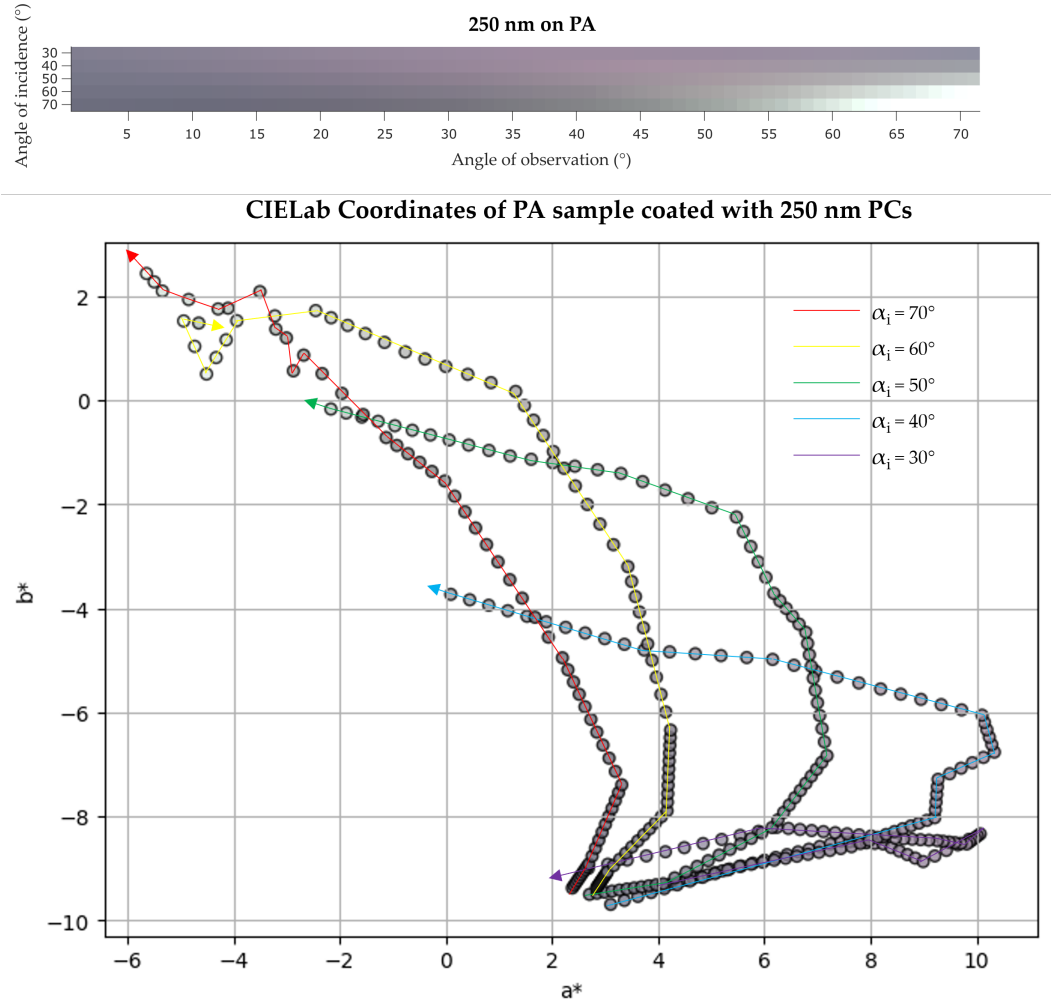


Figure 45 (top) IP-BRDF measurements of PA coated with 250 nm PCs, α_i = 30° to 70° and α_o = 0° to 70°; (bottom) 2D representation of color coordinates movement in CIEL*a*b* space, where the arrows represent the direction from low to high α_o (0° to 70°) for each α_i (30° to 70°).

Since polyester and cotton fabrics did not present iridescence by ocular observation, the highly time-consuming polarized UV/Vis reflectance measurements were not performed for these samples (only 2 samples per day could be measured). In the contrast, the IP-BRDF measurements using the presented methodology, allowed around 20 measurements per day. Thus, IP-BRDF was performed for the PES

(Figure 46) and CO (Figure 47) samples, to confirm if some iridescence still could be present in these samples. IP-BRDF of PES coated samples showed major alterations in terms of color, as compared to the PA samples, especially for the sample coated with 210 nm PCs, where color changed from green to blue. At high α_i and α_o a more reddish color can be observed. Also, all PES samples present a lower luminosity parameter L*. The lack of coating uniformity in the PES samples may be the reason for these changes of color and luminosity, as the measured area probably had less photonic crystals, thus the IP-BRDF measurement were affected by a higher percentage of fabric color rather than PC color. This was observed in the samples with 190 and 230 nm PCs. As for samples with 170 and 250 nm PCs, they maintained their color but with darker hues, which is in agreement with the photographs (Figure 34) taken of these samples. Thus, although the self-assembly on PES samples is not as good as in the PA samples, it is possible to affirm that iridescence is present and being most pronounced in the sample coated with 210 nm PCs.

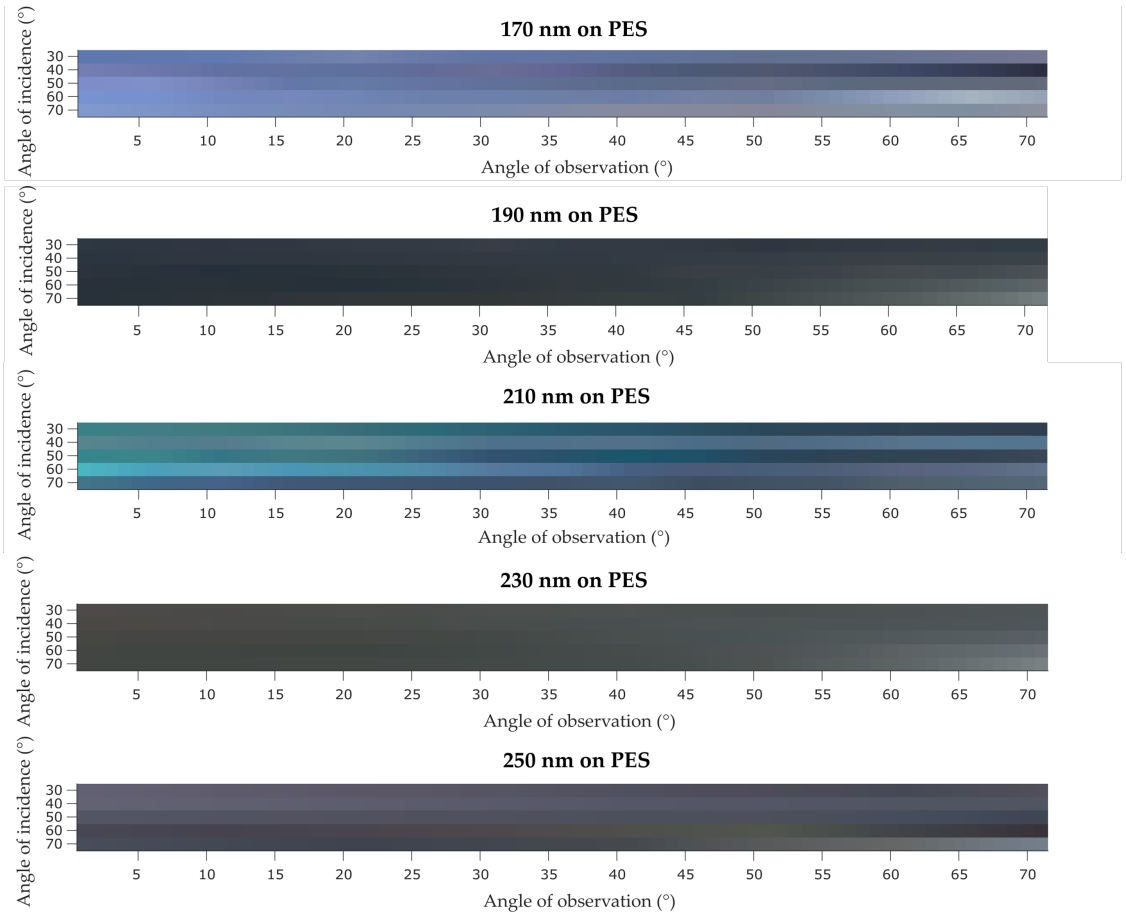


Figure 46 IP-BRDF measurements of PES coated samples.

As for the coated CO samples, all presented a higher luminosity parameter due to the milky aspect on their surfaces as seen in the photographs (Figure 34). Again, when comparing with PA the CO sample with largest color change was the sample coated with 210 nm PCs. In general, the color changed from blue to red at α_i 50° and 70° at higher α_o. The CO sample coated with 230 nm PCs also has a major change when compared to the respective 230 nm PA sample, where the color is mostly green in CO, whereas in PA was mostly red. Overall, the color is changing as α_o is increasing for all CO coated samples, confirming an iridescent effect also in these samples. To optimize/improve the structural color on PES and CO samples it will be necessary to do a pre-coating (with biopolymers or conventional finishing agents) of the fabrics in order to smooth their surface. [190-192]

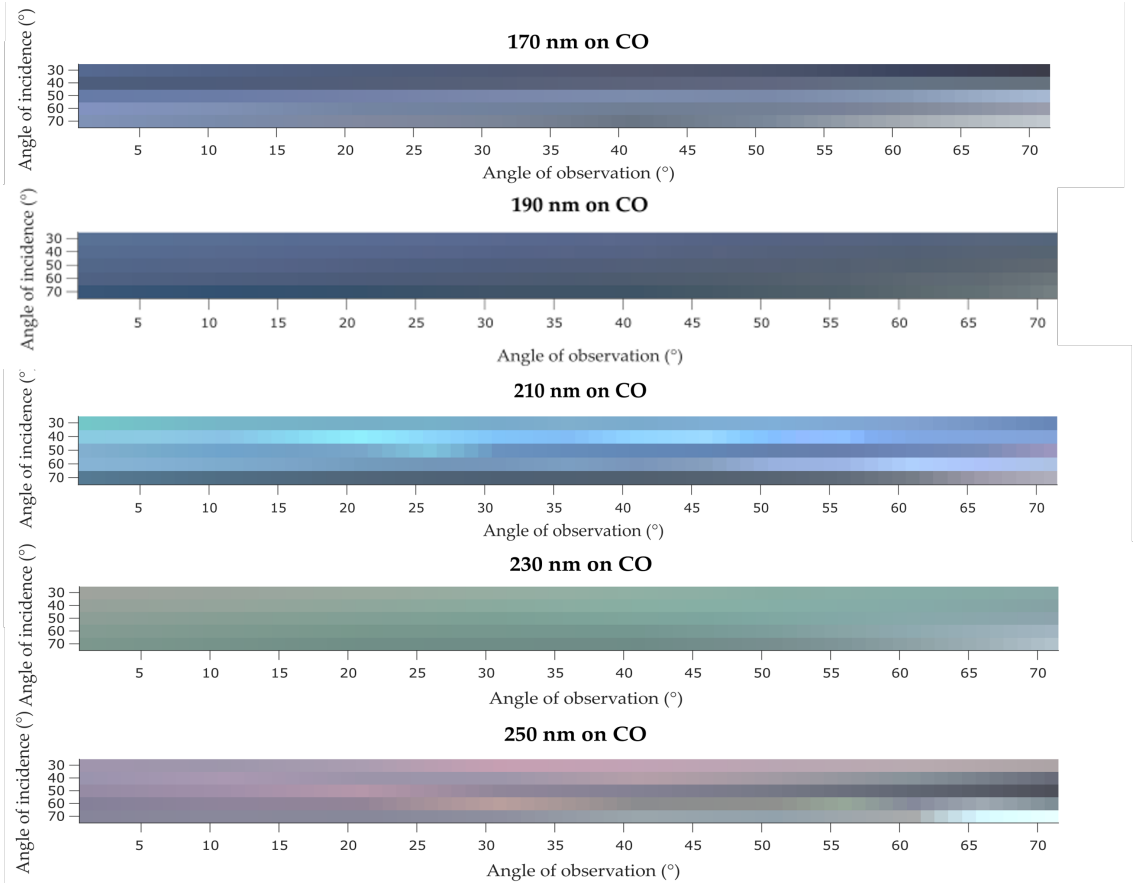


Figure 47 IP-BRDF measurements of CO coated samples.

To further understand the structural color behavior in textiles, IP-BRDF simulations were performed using a different light source. Human color perception varies with different light sources, as their wavelengths are emitted in different regions of the visible spectra. As such, when illuminated with different light sources, the wavelength of the light reflected by the fabric's surface will change and color

perception is different for each illuminant. This is of highest importance to further understand PC color behavior in textiles and, to the author knowledge, there are no such studies made envolving textiles. One of the few articles found in the literature report the usage different light source illumination of PCs, where polystyrene microspheres were 3D-printed onto a black cardboard substrate. [43] The 240 nm PS microspheres presented a green color under a D_{65} light source, a bluish color under cool white fluorescent illuminant, and a yellowish color under illuminant A (IA).

Using IA as light source, simulations were made for the PA samples (since they had better results than both the coated PES and CO samples) and compared with the experimental data obtained for PA samples under D_{50} light source. These simulations showed that, overall, there were minor differences in terms of color, where the L* parameter was practically the same ($\Delta L^* < 1$, where $\Delta L^* = |L_{D50} - L_{IA}|$) for most of the PA coated samples under both D_{50} and IA light sources. The sample coated with 210 nm PCs showed $\Delta L^* = 2$. A brief comparison of CIEL*a*b* color coordinates (a* axle – green/red, b* axle – blue/yellow) for both light sources is presented in Table 7.

Table 7 Differences in CIEL*a*b* color coordinates of PA coated samples under D_{50} and IA light sources illuminations. Δa_{avg} and Δb_{avg} are the overall averages of the modular difference for all α_i and α_o between a* and b* under D_{50} and IA for each PA coated sample. $\Delta a_{avg} = |a_{D50} - a_{IA}|$; $\Delta b_{avg} = |b_{D50} - b_{IA}|$.

Sample	Overall Color Changes under IA	Δa_{avg}	Δb_{avg}
PA with 170 nm PCs	Greener	5–6 (low α_o); 1–2 (high α_o)	<1 (low and high α_o)
PA with 190 nm PCs	Greener	1–3 (low α_o); 4–6 (high α_o)	<1 (low and high α_o)
PA with 210 nm PCs	Redder and bluer	3–5 (low α_o); 0–2 (high α_o)	3–5 (low and high α_o)
PA with 230 nm PCs	Yellower	<1 (low and high α_o)	0–2 (low and high α_o)
PA with 250 nm PCs	Greener	0–2 (low and high α_o)	~1 (low and high α_o)

The PA samples under IA light source illumination are generally greener and yellower, with the exception of the sample coated with 210 nm PCs which is redder and bluer. In terms of the a* axis, the 210 nm coated sample is redder at α_i from 30° to 50° and greener at α_i above 60°. Samples coated with 230 and 250 nm PCs are in general greener except at high α_o, where they are slightly redder. In terms of the b* axis, samples coated with 170 and 250 nm PCs are slightly yellower, and sample coated with 190 nm PCs is slightly bluer. These results are in agreement with the study mentioned previously, where color

under IA is greener and yellower when compared with color under D_{50} light source. [43] These color changes are almost imperceptible even by color coordinates analysis, where color differences (Δa and Δb) in most cases are lower than 5 measuring units, in a total range of 256 units for each axle.

Although PES and CO did not present iridescence by ocular inspection, it was still possible to obtain fabrics with solid colors, suitable to substitute the usage of conventional dyes. Thus, structural coloration can be used as a more sustainable method of fabric coloration.

5.1.1. PCs as water/humidity sensors

Analyzing P(St-MMA-AA) PCs sizes by DLS and STEM, it was noticed a size difference when the PCs are in dry or wet state. Furthermore, and when deposited onto polyamide, different structural colors were reflected within a difference of 20 nm in particle size. So, P(St-MMA-AA) PCs deposited onto PA substrates were tested to evaluate their ability as hydrosensors. A droplet of water was applied in the fabric's surface and, as the P(St-MMA-AA) spheres swell, a change in color was observed (Figure 48). As expected, violet color changed to blue, blue to green and green to yellow-red. No color changes were observed for red structural color since it is the last color of the visible spectrum, red sample only got a darker hue as it got wet.

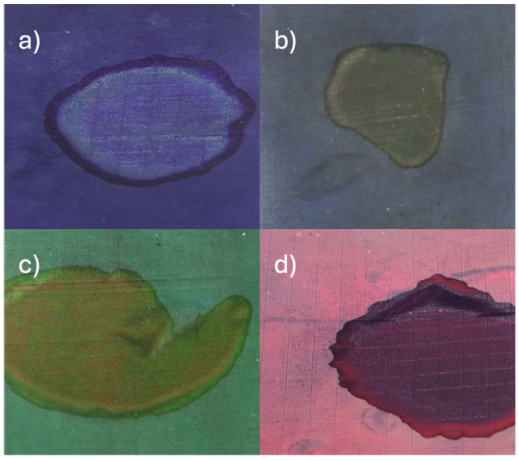


Figure 48 Structural color changes when P(St-MMA-AA) PCs are in dry/wet state on PA substrates.

However, when the wetted area is small, water marks are visible upon drying (Figure 49). These water marks can be completely removed once the sample is wetted again in its totality.

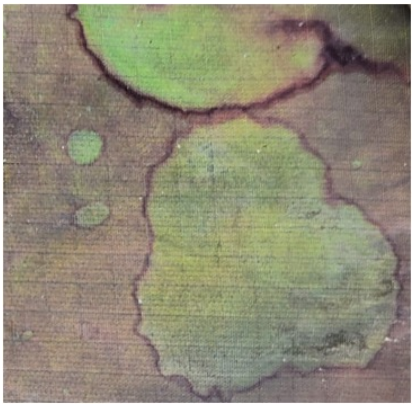


Figure 49 Water marks left on the P(St-MMA-AA) structure upon drying after being partially wetted.

These changes were also observed when samples were exposed to water vapor, meaning that these fabrics, not only could be more eco-friendly in terms of coloration and effluent generation, but also be utilized as sensors in environments to detect high humidity percentages or extreme humidity variations.

5.1.2. Color fastness assays

Light and washing fastness tests were performed on PA substrate with P(St-MMA-AA) PCs, where color changes were registered. Regarding light fastness tests (QUV), two different structural colors were used, blue and green, over a period of 168 hours (1 week). Photographs were taken at 0, 24, 48, 76 and 168 h, to document color change over time (Figure 50). As expected, there were minor changes in color, since P(St-MMA-AA) PCs are known for having excellent light fastness properties. The observed changes by ocular inspection, are mainly a decreased in brightness. Color coordinates analysis (0 and 168h) showed that the UV radiation had little impact in the blue sample, as L* remained practically the same, a* and b* were slightly (2 units) redder and bluer, respectively. As for the green sample, changes were more noticeable, where L* decreased from 49 to 40, turning the sample into a darker hue of the original color, a* diminished 7 units (from 23 to 16) becoming redder and b* was reduced in 10 units (from 21 to 11) becoming bluer than the original color.

Regarding washing fastness, in previous tests, [193] chitosan and polyvinyl alcohol were evaluated as coating agents to improve washing fastness of structurally colored fabrics. Unfortunately, these polymers were completely removed, as well as the color, after one washing cycle. Other biopolymers such sodium alginate (2 wt%) and cellulose acetate (7 wt%) were also studied for this purpose. Similar results were obtained, as alginate and color were completely washed away. As for cellulose acetate, the solvents used to dissolve it (acetone or acetonitrile), also dissolved P(St-MMA-AA) PCs, making this biopolymer unsuitable for this application.

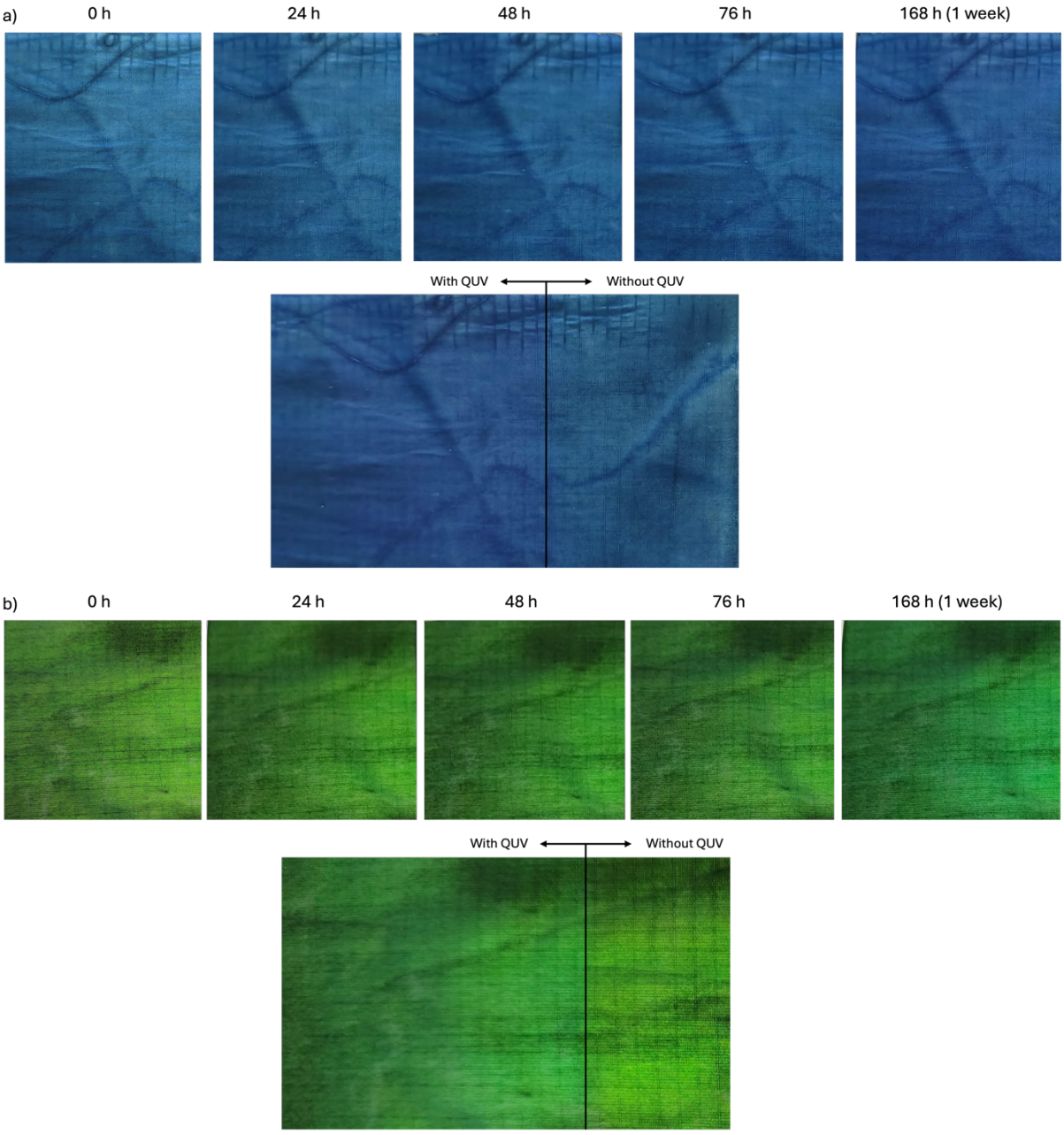


Figure 50 Evolution of color change at 0, 24, 48, 76 and 168 h, for a) blue and b) green P(St-MMA-AA) structural colors. An overall view of the substrate is presented below the times of each sample.

Due to these results, commercial finishing agents were tested, to understand what kind of polymer was the most appropriate to confer washing fastness to structurally colored fabrics. The following commercial agents were tested:

- Acronal S790 (anionic styrene-acrylic copolymer)
- TANAFINISH A (anionic silica/silicic acid dispersion)
- TANAFINISH 40119 (cationic silicon compound)
- TANACOAT SFT (aliphatic polyester polyurethane)

- TANAPUR ONE (aliphatic polyester polyurethane)
- TANAPUR EP (cationic polyester polyurethane)
- EDOLAN SN, SG, LV and RU01 (polyether-based polyurethanes)

Once again, the tested commercial products were unable to produce a durable finishing, as washed samples presented either major color changes, severe decreases in brightness, total loss of iridescence or total PC removal from the PA surface. This may be due to the blockage of PA's functional groups from the PC coating.

One last effort to overcome this issue was made through the application of Sylgard™ 184 silicone, a PDMS-based synthetic agent. P(St-MMA-AA) coated fabrics were immersed into Sylgard™ gel, submitted to padding, dried and thermoset at 80 °C for 3 hours. Figure 51 depicts samples after thermoset, showing defects (peeling) in the applied coating, before washing fastness test. It was also noticeable some loss of iridescence and brightness of these samples. The applied coating gave samples a plasticized aspect and touch. PA with 250 nm PCs (Figure 51c) was crumpled by accident, where cracks in the PC structure can be seen, meaning that this coating does not have kneading/bending fastness. Nevertheless, washed samples retained the coating and maintained its color, even in the zones where the coating was peeled off (Figure 52c).

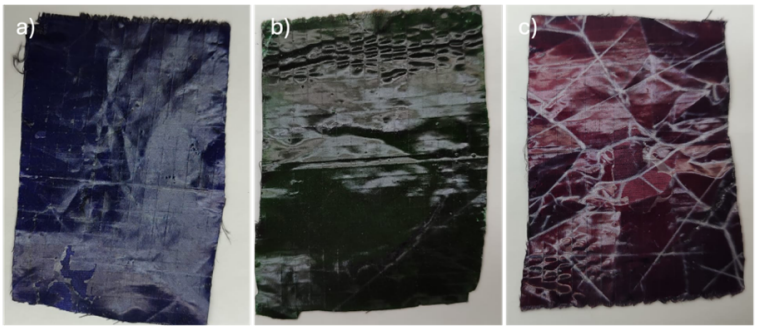


Figure 51 PA samples covered with a) 190 nm, b) 210 nm and c) 250 nm P(St-MMA-AA) PCs after being coated with Sylgard™ 184, before washing fastness test.

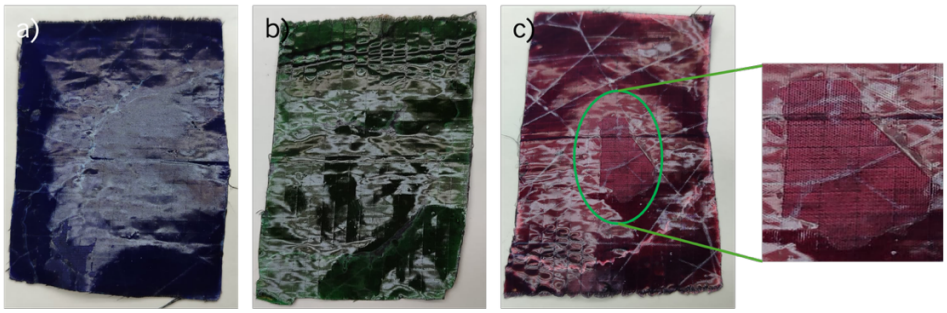


Figure 52 PA samples covered with a) 190 nm, b) 210 nm and c) 250 nm P(St-MMA-AA) PCs after being coated with Sylgard™ 184, after washing fastness test.

SEM analyses were performed to evaluate coating effectiveness, focusing in particular on the peeled-off area of the fabric. As seen in Figure 53, Sylgard™ finishing penetrated PC's structure completely and covered the fabrics with an 8.5±2.2 nm thickness coating. After washing, the coating remained unaffected overall, in both peeled and unpeeled areas. Although Sylgard™ is a not so eco-friendly petrol-based agent, it proved its capacity in retaining structural color deposited in PA fabrics, in opposition to other commercial products tested. However, PC structure is not resistant when fabric is bent. Furthermore, its plasticized aspect could compromise the physical properties of garments, as permeability to air and water vapor probably would be very low.

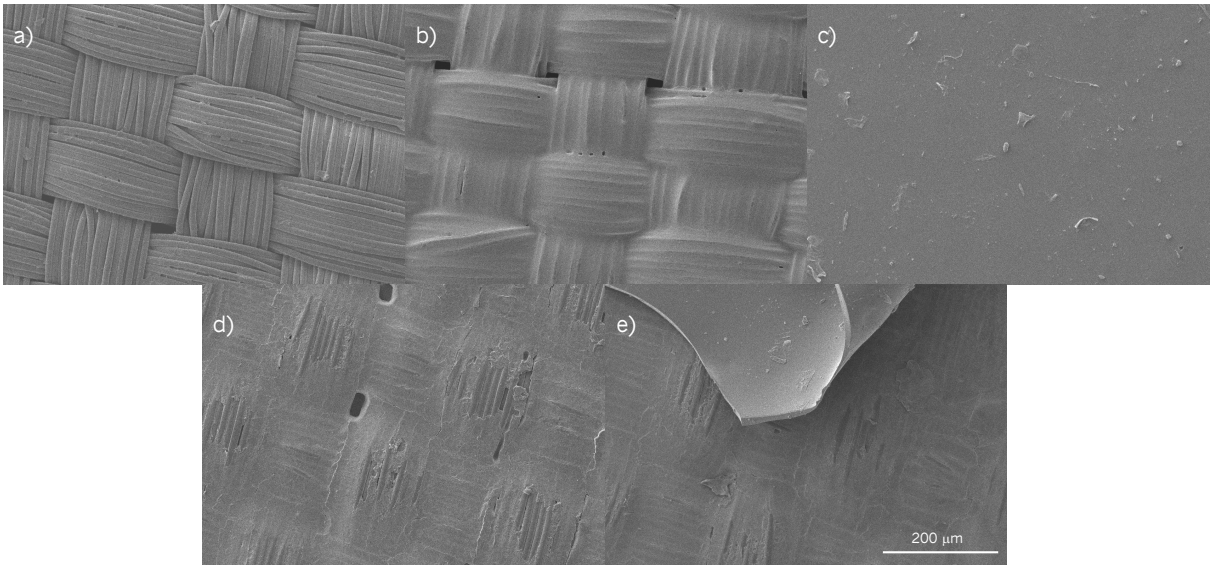


Figure 53 SEM micrographs (500× magnification) of a) uncoated PA and PA samples covered with 250 nm P(St-MMA-AA) PCs b) without Sylgard™ 184, c) coated with Sylgard™ 184, d) coated with Sylgard™ 184 in the peeled off area before washing fastness test and e) Sylgard™ 184 in the peeled off area after washing.

As such, Sylgard™ 184 pad coating should be performed under different pressure and speed conditions, focusing on the prevention of crack formation while guaranteeing good physical properties of the fabrics. Nevertheless, other coating techniques, such as knife-coating or spraying, should be explored in the future in this type of photonic structures.

5.2. Polymeric application in PES and CO fabrics for structural color improvement

The synthesis of two potential adhesives and surface smoothers, P(MMA-BMA) and P(MMA-BA) was performed to promote a more uniform PC self-assemble onto PES and CO fabrics. P(MMA-BMA) adhesive proven to be very brittle after drying, promoting cracks and peeling off the fabric's surface, thus being excluded from the assays. As BMA was replaced with BA, the adhesive was more flexible, demonstrating potential to be applied onto textiles. To potentialize the precoating to the maximum, plasma treatment was applied in both fabrics, being the precoating performed within a few hours of plasma treatment. Since the deposition of P(St-MMA-AA) PCs was already optimized in PA fabrics, the next steps focused on the deposition of SiO_2 and KL PCs onto PES and CO fabrics.

5.2.1. SiO_2 PCs deposition onto polyester and cotton fabrics

SiO_2 PCs at 3 wt% in ethanol were applied by gravitational sedimentation onto pre-coated PES and CO fabrics. As seen in Figure 54, SiO_2 PCs managed to produced different colors, but with an uneven deposition. These samples presented white agglomeration on fabric's surface, indicating that the PCs are not well organized, meaning that P(MMA-BA) pre-coating did not sufficiently decrease fabric roughness. Furthermore, the fact that red color is weaker versus blue and green colors, indicates a poorer dispersity in ethanol, possibly due to a lack in homogeneity, even though PdI value was acceptable. Dip drawing methodology was also applied, where several dippings were performed, yet it failed to produce any structural color.

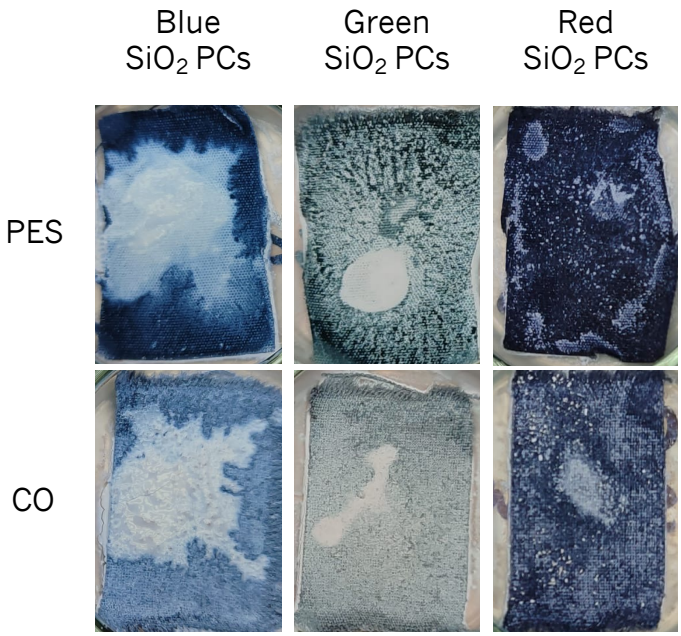


Figure 54 Blue, green and red SiO_2 PCs applied onto precoated P(MMA-BA) PES and CO fabrics.

To the author's knowledge, direct application of SiO_2 PCs onto textiles has not been reported, as authors usually functionalize SiO_2 surface to produce structural colors on textiles. This highlights the difficulty of applying pristine SiO_2 spheres on textiles. For example, Zhao and Fang functionalized SiO_2 spheres with polypyrrole to produce structural colors on white plain polyester fabrics. [167] Similarly, Deng's research group produced SiO_2/carbon composites and SiO_2/polydopamine to structurally color white cotton fabrics. [166, 194] SiO_2/polydopamine PCs were also synthetized by Li *et al* to color white polyester fabrics. [195] Alternatively to textile application, Yang *et al* produced SiO_2@Fe_3O_4 amorphous photonic films to obtain non-iridescent structural colors. Nevertheless, a revision on both the synthesis and method of application of SiO_2 PCs needs to be performed, as well as the smoothening of fabric's surface. [196]

5.2.2. KL PCs deposition onto polyester and cotton fabrics

After synthesis and characterization of KL PCs, these were dried in a watch glass (Figure 55a), where partial iridescence was observed. Then, the synthetized KL PCs were applied onto PES and CO substrates submitted to P(MMA-BA) pre-coating, to evaluate if this effect was also observed on fabrics.

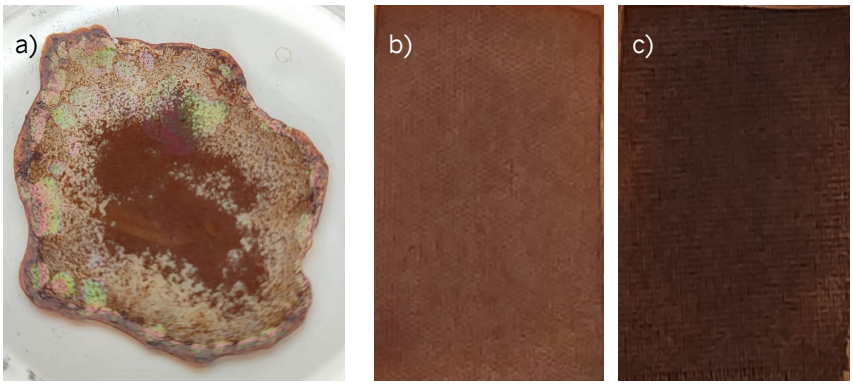


Figure 55 KL PCs deposited on a) glass substrate, b) PES fabric and c) CO fabric with P(MMA-BA) precoating.

After gravitational deposition of KL PCs onto both substrates, no iridescence was observed, unfortunately. Although the pre-coating with P(MMA-BA) helped to produce a uniform KL coating, fabric's surface was not smooth enough to promote the required hexagonal or square self-assembly structure that produce iridescence. Zhou *et al* extracted lignin from pine wood, producing lignin spheres through antisolvent methodology, using an acetone/water system. Although different sizes were obtained (100-300 nm) by adjusting the initial lignin concentration and antisolvent addition rate, PdI presented a broad range of values. Furthermore, structural color was only possible to be observed when particles were deposited in non-textile substrates. [197] Other authors produced lignin particles within the same range, through complex fractioning processes, to obtained photonic glasses. [62, 63] Photonic glasses are characteristic for having disordered structures which produce non-iridescent colors, in opposition to the periodic structure of photonic crystals, which produce bright and iridescent colors. [198]

Smaller KL PCs should be produced through the antisolvent methodology, utilizing EtOH/MeOH as solvent and water as antisolvent, by reducing the initial concentration of KL. This way, it will be possible to study the feasibility of structural color production with iridescent effects. Furthermore, the inherent brown coloration of Kraft lignin could be interfering with the reflectance of structurally produced colors, thus initial KL color should be taken in consideration in future studies. Nevertheless, the fact that KL spheres obtained through this methodology could produce an iridescent effect is a good indicator for further development of structural colors using natural organic compounds.

6

Color substrate and PC dyeing influence in structural coloration

This chapter was based on the following publication:

(Poster) **Fernandes, Rui D.V.**; Padrão, Jorge; Zille, Andrea. "Effect of color substrate in structurally colored PES fabrics". *iTechStyle Summit 2022*, Porto, 2022.

6.1. Deposition of pristine P(St-MMA-AA) PCs on PES fabrics with different colors

In the previous chapter, PCs were applied onto black substrates, as these enhance the chroma of the produced structural color. But what would happen to the structural color if substrate color was changed? In this Chapter, it was studied how the color of the substrate can alter the visual color produced by P(St-MMA-AA) photonic crystals. Although P(St-MMA-AA) PC deposition was optimal in PA, the following tests were performed in PES fabric, due to the inability to obtain the same PA fabric in undyed conditions. PES was chosen over CO due to the better structural arrangement observed in SEM micrographs (Chapter 5, Figure 36). A similar study was also performed where P(St-MMA-AA) PCs were previously dyed, applied to the different colored PES substrates and the final color evaluated. Very few reports were found in the literature for either color evaluation, reveling the necessity to explore this thematic with the present work.

PES fabric was dyed as previously described and coated with P(St-MMA-AA) PCs ranging from 170 to 250 nm by dip-drawing method. Firstly, PCs were applied with just one dipping onto black colored PES to verify the color produced by the self-assembled PC structure (as in Section 5.1.). The produced colors were also verified by UV/Vis and their CIEL*a*b* color coordinates determined (consult Annexes, Table A1). Briefly, when compared to the uncoated black substrate, 170 nm PC coated fabric was redder and bluer, 190 nm PC coated fabric was greener and bluer, 210 nm PC coated fabric was mainly greener, and 250 nm PC coated fabric was redder and slightly bluer. The luminosity parameter L* increased for all four samples, meaning that the produced colors were less dark (9 to 29% lighter) than the original black substrate. Secondly, different colored PCs were applied onto the remaining dyed PES fabrics, from violet to red, and the effect of PC color was observed for the colored substrate samples. CIEL*a*b* color coordinates were determined for all produced samples (Table A2). The luminosity parameter L* increased in almost all samples, independently of the PC color coating. As observed in Table 8, violet PCs mostly increased (redder) or maintained a* and decreased b* (bluer) parameters, as blue PCs showed a decrease in both a* and b* (greener and bluer). As for the green and red PCs, the observed effect was different for certain groups of substrate color. Green PCs showed a decreased in a* (greener) for all samples, as expected, but b* was higher (yellower) for black, violet, blue and petrol substrates and lower (bluer) for green, yellow, orange, pink and red substrates (Figure 56). In the case of red PCs, a* increased (redder) for black, blue, petrol and green substrates and decreased for violet, orange, pink and red substrates, and b* decreased (bluer) in most all substrates, except in violet, blue and petrol.

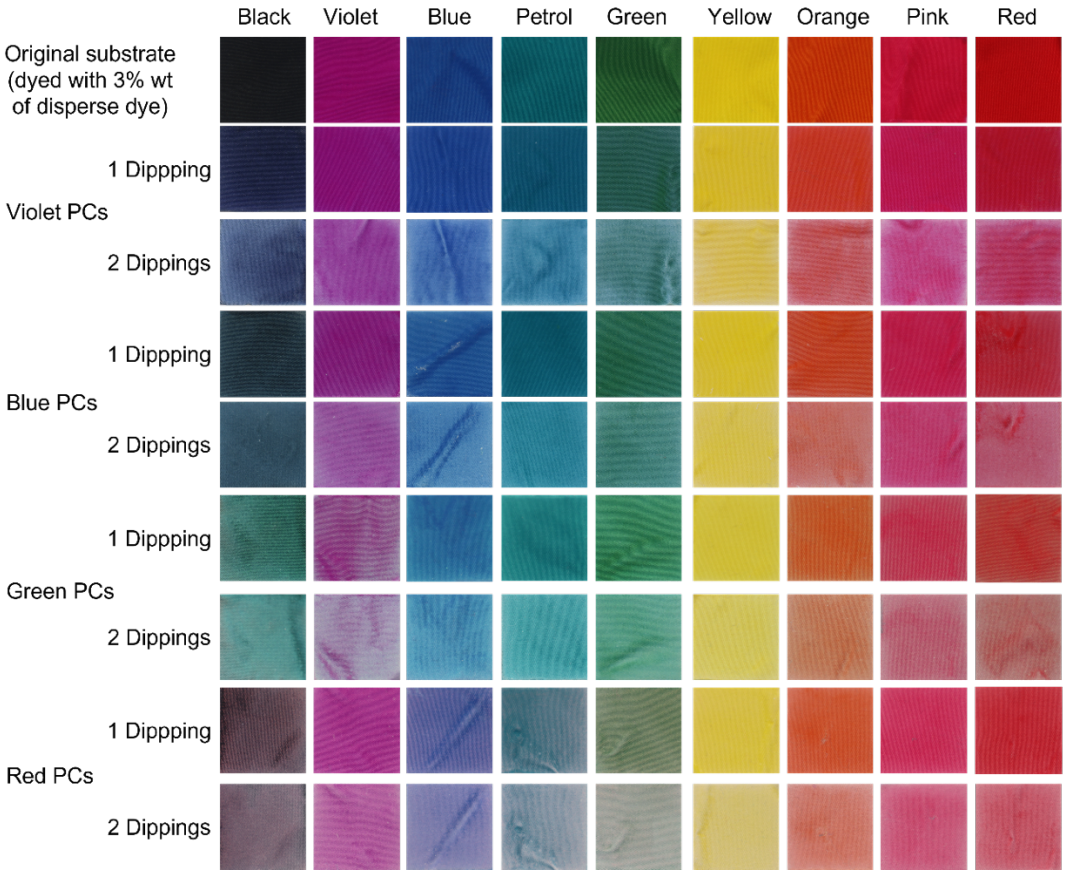


Figure 56 Photonic crystals (170 (violet) to 250 nm (red)) applied onto different colored PES fabrics, with one and two dippings.

Table 8 Effect of PC coating in CIEL*a*b* color coordinates L*, a* and b* when compared to the uncoated PES fabric. (+) increased, (-) decreased and (=) maintained.

Pristine PCs	Violet PCs			Blue PCs			Green PCs			Red PCs		
Polyester	L*	a*	b*	L*	a*	b*	L*	a*	b*	L*	a*	b*
Black	+	+	-	+	-	-	+	-	+	+	+	-
Violet	+	-	-	+	-	-	+	-	+	+	-	+
Blue	+	+	-	+	-	+	+	-	+	+	+	+
Petrol	+	+	-	+	+	-	+	-	+	+	+	+
Green	+	+	-	+	=	-	+	-	-	+	+	-
Yellow	=	=	-	+	-	-	+	-	-	+	+	-
Orange	=	=	-	+	-	-	+	-	-	+	-	-
Pink	+	=	-	+	-	-	+	-	-	+	-	-
Red	+	=	-	+	-	-	+	-	-	+	-	-

Thirdly, a second dipping was performed in order to improve PC color, which did not occur. As seen in Figure 56, after the second dipping, all samples present a milky appearance, indicating an excess of PCs on the fabric's surface. The color coordinates of these samples were determined (Table A3) and confirmed what was visually observed. L* increased even more after the second dipping and a* and b* showed a tendency to go to gray hues if continuous dippings were performed, especially in the cases were substrate color and PC color were opposites in the same CIEL*a*b* axis, red substrate coated with green PCs or green substrate coated with red PCs (Figure 57). This is in agreement with the findings of Zhao *et al*, who studied the correlation between structural colors and the base color of fabric substrates. The study showed that, when the substrate color is similar to PC color, the final color of the coated fabrics is close to the PC hue. [51] On the other hand, when substrate and PC color are complementary colors of the same CIEL*a*b* axis, the color of the assembled fabrics displays a blurry effect. [69]

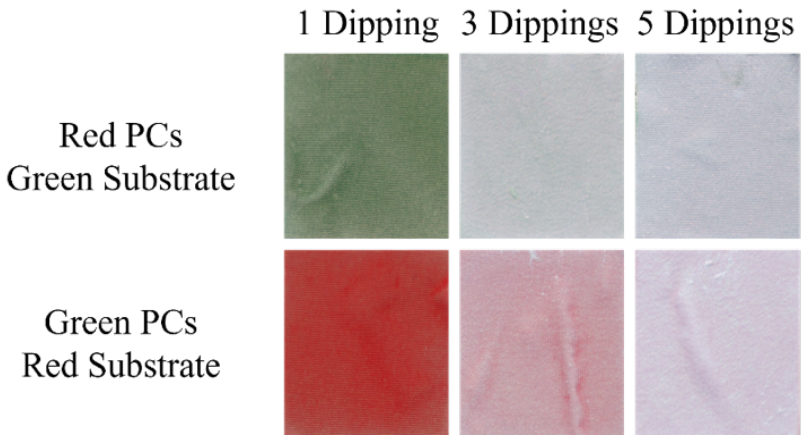


Figure 57 Effect of PC color on substrates with an opposite CIEL*a*b* axis color, with one, three and five dippings.

6.2. Deposition of dyed P(St-MMA-AA) PCs on PES fabrics with different colors

With this deeper knowledge about photonic crystals color behavior, 210 nm PCs were chosen to the next color evaluation, dyeing the photonic crystals. 210 nm PCs were selected because they stand in the middle of the visible spectrum (green structural color), thus allowing to observe either hypsochromic or bathochromic shifts. They were dyed with disperse dyes DBV-R, SRB-ADS, GD11, YS-ADS and RD-K3G at 2% concentration (Figure 58), and the effect of dye color on PC and substrate color was evaluated (Figures 59-63) (CIEL*a*b* color coordinates are presented in Tables A4-8).

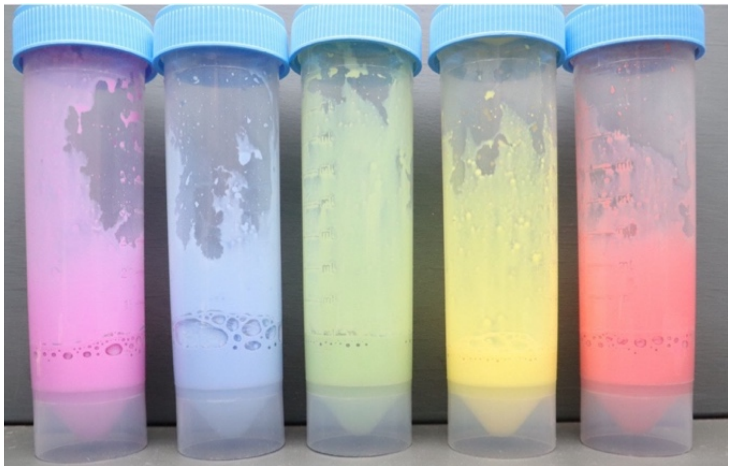


Figure 58 210 nm P(St-MMA-AA) PCs dyed with disperse dyes DBV-R, SRB-ADS, GD11, YS-ADS and RD-K3G at 2% concentration.

Tests were also performed in a white polyester fabric to check PC visibility, since undyed PCs are not visible on white substrates. Liu *et al* were able to observe structural colors in white substrates after dyeing poly(styerene-butyl acrylate-methacrilic acid) PCs with a black disperse dye. The dyed PCs were printed into fabrics by inkjet, exhibiting more vivid and iridescent structural colors, in opposition to the undyed PCs functionalized fabrics. [75] Similarly, Lu *et al* dyed SiO_2 PCs with Prussian Blue dye to obtain bright, uniform, and highly saturated structural colors, applied to white fabrics by spray coating. [199]

With one dipping, PC color was only noticeable in black polyester, whereas on the other colored samples, dye color was the main influencer on color change. Continuous dippings were performed until PC color was visually perceptive (through brightness), where a minimum of five dippings were necessary to achieve it. This constituted a problem because, with five dippings, dye color overwhelms both PC and substrate color.

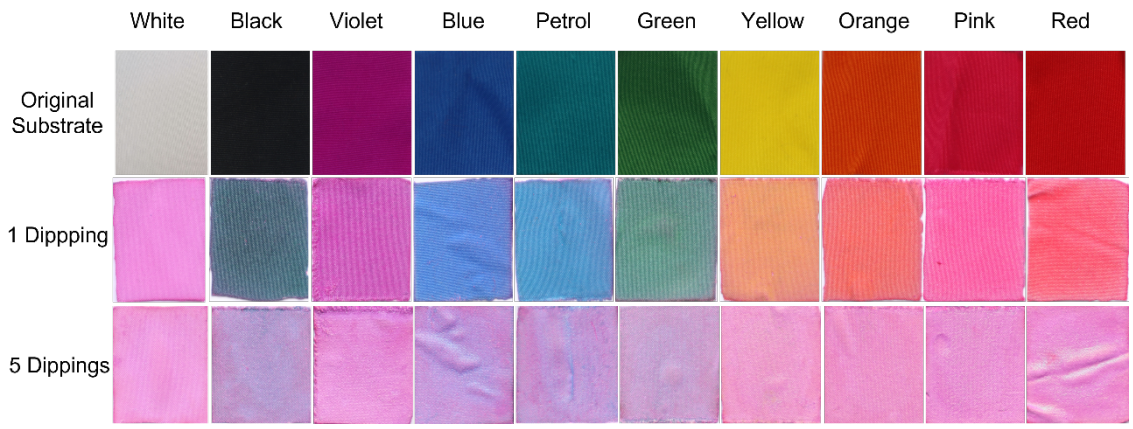


Figure 59 210 nm PCs@DBV-R (2 wt%) applied onto dyed polyester samples with one and five dippings.

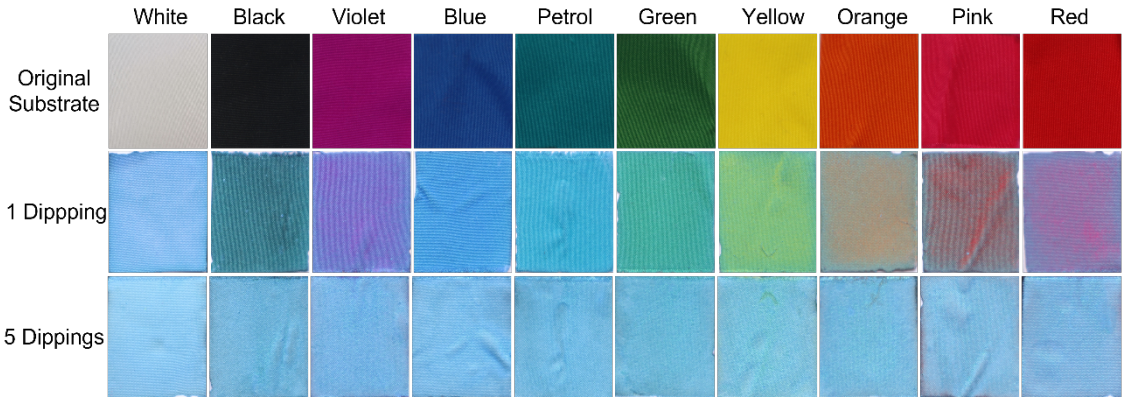


Figure 60 210 nm PCs@SRB-ADS (2 wt%) applied onto dyed polyester samples with one and five dippings.

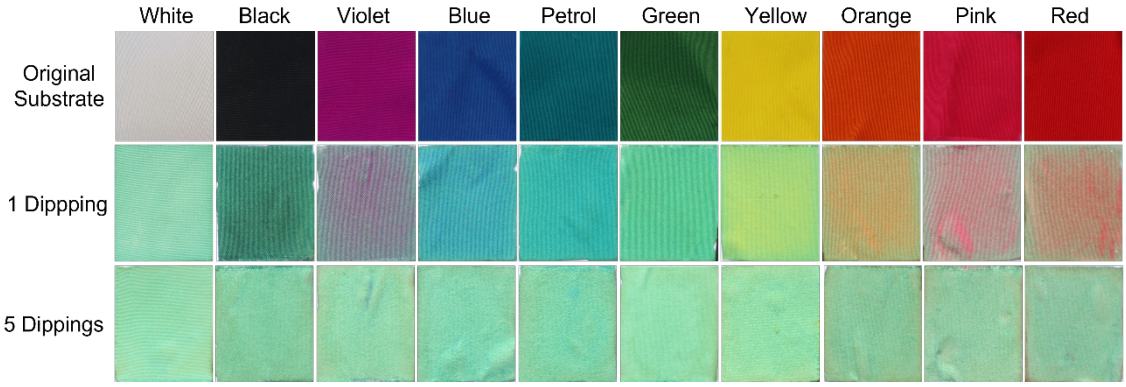


Figure 61 210 nm PCs@GD11 (2 wt%) applied onto dyed polyester samples with one and five dippings.

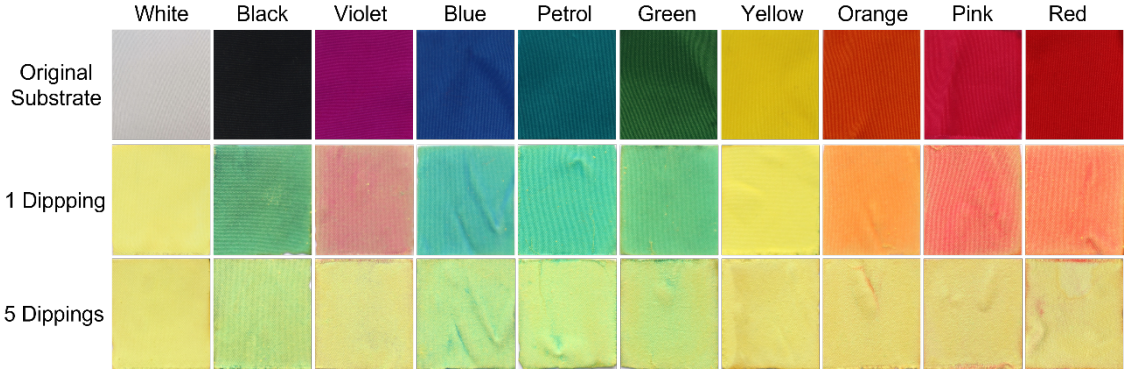


Figure 62 210 nm PCs@YS-ADS (2 wt%) applied onto dyed polyester samples with one and five dippings.

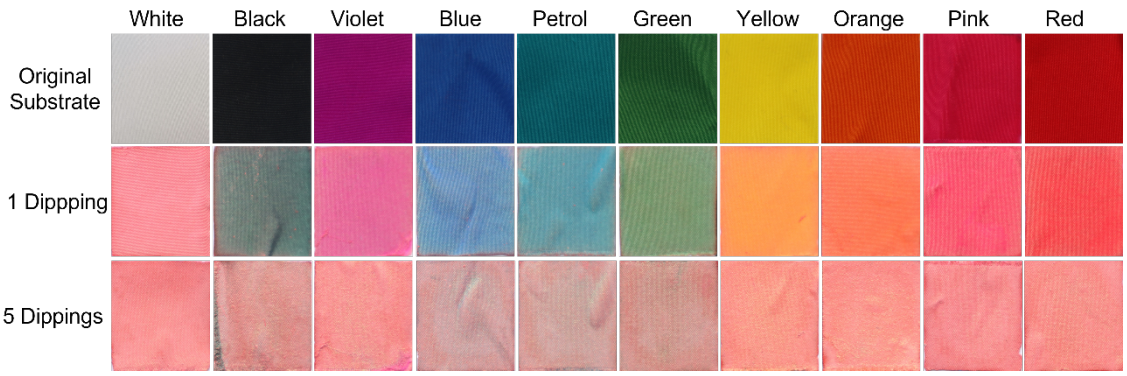


Figure 63 210 nm PCs@RD-K3G (2 wt%) applied onto dyed polyester samples with one and five dippings.

To try to overcome this issue, dye concentration was reduced, and tests performed with RD-K3G dye with 0.5 and 1 wt% (Figure 64) (CIEL*a*b* color coordinates are presented in Tables A9 and A10). For yellow, orange, pink and red substrates, reducing dye concentration had little effect on the final obtained color. As for the other remaining colored substrates, diminishing dye concentration allowed PC color to stand out, especially at 1% dye concentration. Overall, when comparing samples prepared with dyed PCs at 0.5 and 1 wt%, fabrics coated with 1 wt% dyed PCs are slightly darker, redder and yellower than fabrics with 0.5 wt% dyed PCs. Even at lower concentrations, dye effect is very pronounced. Future tests should be performed using concentrations below 0.5 wt%.

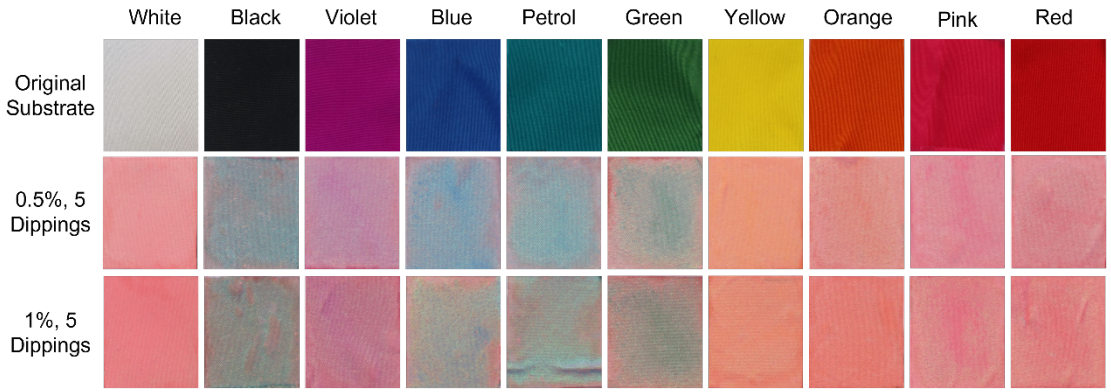


Figure 64 210 nm PCs@ RD-K3G (0.5 and 1 wt%) applied onto dyed polyester samples with five dippings.

Hu *et al* dyed polystyrene spheres with different disperse dyes (1 wt%) to construct structural colors on glass Petri dishes and quaking aspen wood surfaces. It was observed that, under specular reflection, structural coloration was dominant, whereas under diffuse reflection, dye coloration contributed more significantly, resulting in visually rich and saturated color effects. Under natural light illumination, the dyed spheres exhibited additive coloring effects, with a superior visual performance compared to undyed spheres. [200] Zhou *et al* investigated the effect of dye concentration and pH (for three different dyes) in

chitosan/polyacrylamide hydrogel films containing P(St-MMA-AA) PCs. Through the mechanochromic photonic properties of the hydrogel, it was possible to tune structural colors by pH adjustment or physical stretching of the film. These hydrogels films were produced to simulate an artificial chameleon skin with color reversibility.

Even though structural color is overwhelmed by the disperse dye, in the present work, using dyed PCs opens the possibility of refurbishing used dyed garments, independently of their previous color. If the mechanical properties of the garments are not compromised, thus making them suitable to be worn, PC deposition can be an alternative to recolor fabrics without removing the previous dye, saving time, water and energy while diminishing chemical consumption.

7

Mixture of pristine P(St-MMA-AA) PCs

This chapter was based on the following publication:

(Poster) **Fernandes, Rui D.V.**; Rodrigues, Rui; Vieira, Bárbara; Padrão, Jorge; Zille, Andrea. "Combining photonic crystals of different sizes and tuning structural colors by color addition". *Seventh International Symposium Frontiers in Polymer Science*, Gothemburg, 2023.

This chapter had the support of Linköping University (LiU) for the access to ARTEMI, the Swedish national infrastructure of advanced electron microscopy, funded by the Swedish Research Council (VR), grant number 2021-00171, and the Swedish Foundation for Strategic Research (SSF), grant number RIF21-0026.

7.1. Deposition of mixtures of pristine P(St-MMA-AA) PCs in PA fabrics

In the previous Chapters, substrate properties such as fiber type, fabric roughness and color were studied to see how they influence structural color. However, the mixture of P(St-MMA-AA) PCs has not been extensively studied in order to understand if PCs/structural color follow the principle of color addition/subtraction as common dyes, pigments or paints. To fill in a little of this scientific gap, photonic crystal behavior with premixed pristine PCs deposited in PA fabric was analyzed.

Pristine P(St-MMA-AA) PCs with different sizes, 170 nm (violet), 190 nm (blue), 210 nm (green) and 250 nm (red) were mixed in different proportions (3:1, 1:1 and 1:3) and applied onto black PA woven fabric (Figure 65). Color addition principle was denoted by the intermediate color hues/shades obtained in comparison to the original structural colors. To the author knowledge, reports on the mixture of this type of photonic crystals are not available in the literature.

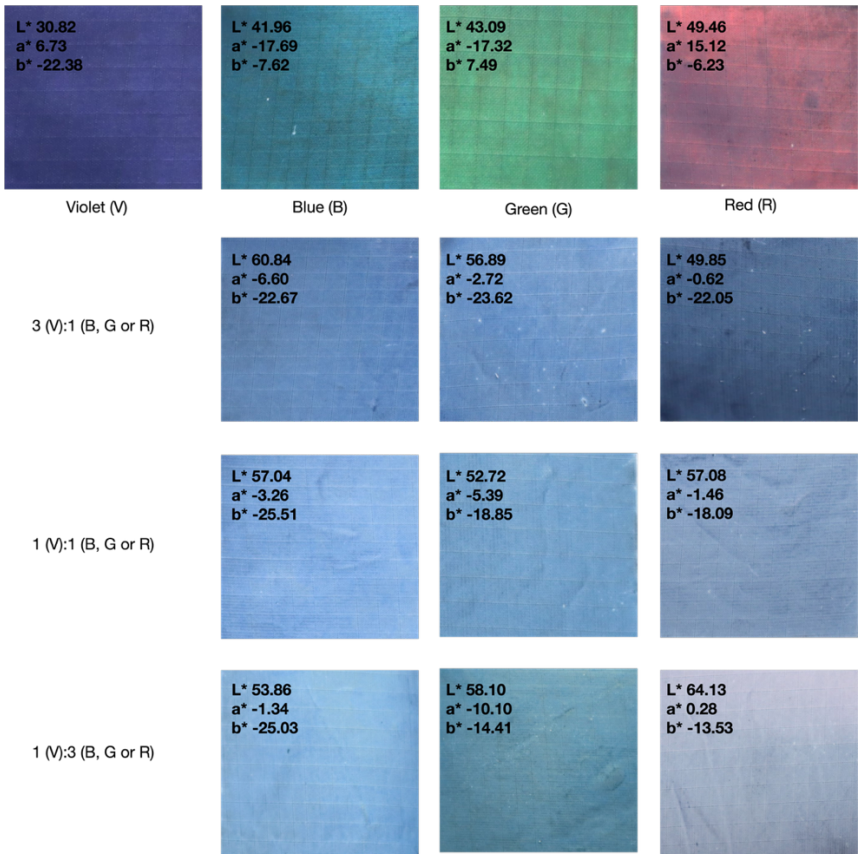


Figure 65 Photographs of mixed photonic crystals in different proportions onto PA fabric with the respective CIEL*a*b* color coordinates.

No matter the proportions, there were clear changes in the observed color, brightness, iridescence and color coordinates. Overall, L* increases, brightness is diminished and iridescence is severely reduced, in

all prepared samples. When violet is triple the proportion versus the other colors, in general a* is lower (greener, Δa between 6 and 12) and b* remains the same, originating blue hues. For violet:blue 1:3, the observed color is bluer (Δb of 3 and 18, when compared to the original violet and blue colors, respectively), whereas a* indicates a redder increase (Δa = 17) when compared to the original blue color. Regarding violet:green 1:3, and when compared to the original green color, the produced sample is redder (Δa = 7) and bluer (Δb = 21), originating a bluish-green hue. When red is triple the proportion versus violet, a* is lower (greener, Δa = 15), where b* is also lower (bluer, Δb = 7), originating a grey hue.

For proportions 1:1, the color coordinates are always closer to violet color coordinates than the other three colors, originating blue hues. This color phenomena may be attributed to the fact that, in the same volume of solution, the smaller particles are in greater number than the larger ones. To prove this hypothesis and further understand how the self-assembly and respective intermediate colors are formed, SEM was performed on the fabric's cross-section in the sample where violet and red PCs were mixed in 1:1 proportion (Figure 66). No clear structural arrangement between 170 nm (violet) and 250 nm (red) PCs was observed in the cross section, as self-assemble between the different sized PCs appears to be random, thus affecting the brightness and iridescence of the samples. The only report about PC mixing found in the literature was published very recently by Lu *et al*, where SiO_2 PCs were blended by ultrasonication and color saturation was enhanced by carbon ink addition, to obtain intermediate non iridescent structural colors. Briefly, 250 nm PCs were mixed with either 220 or 310 nm SiO_2 PCs, in several different proportions. When PCs were mixed in 1:1 proportion, SEM imaging revealed that there was not a clear structural arrangement. However, when the proportion of the bigger spheres was raised to 4:1, there was a tendency to obtain better, but not perfect, PC arrangement, before fabric deposition. [201]

From the obtained SEM micrographs, PC size measurements were performed in both the cross-section and the bottom of the fabric. Figure 67 (left, cross-section) displays an average size of violet PCs 169.2±13.2 nm and red PCs of 239.6±15.9 nm. The percentage of 67.82% and 32.18% is attributed to violet and red particles, respectively.

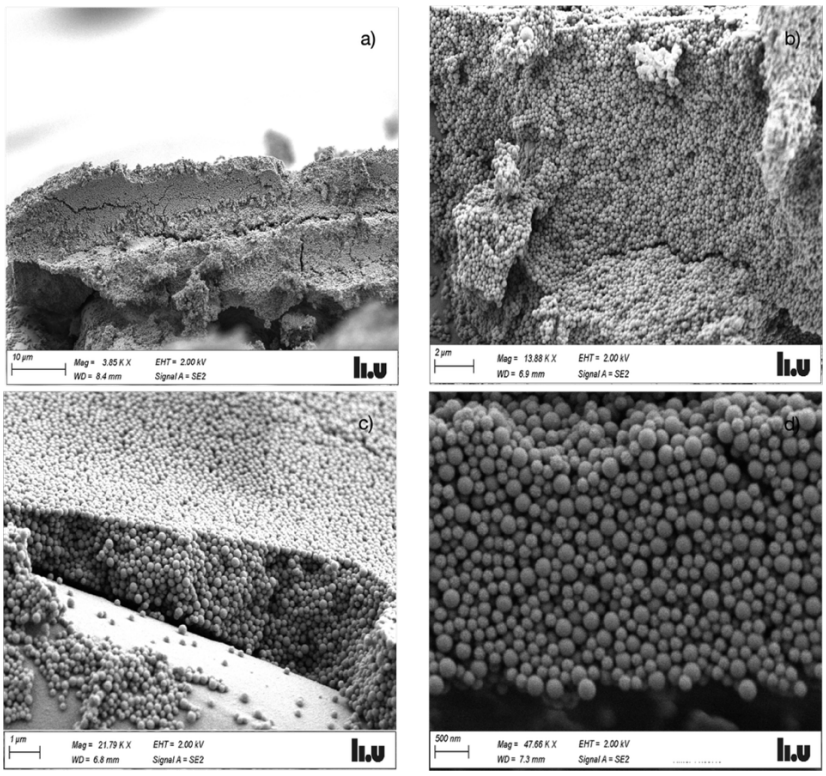


Figure 66 SEM cross-sectional micrographs of pre-mixed violet and red PCs (1:1) on PA at different magnifications, a) 4000x, b) 15000x, c) 20000x and d) 50000x.

Thus, the previous hypothesis was confirmed, since the smaller particles are in double versus the larger particles, using the same volume solution of each color. A size distribution of the PCs on the bottom of the fabric was also performed (Figure 67 (right)), denoting a percentage of 57.45% for violet PCs and 42.55% for the red PCs.

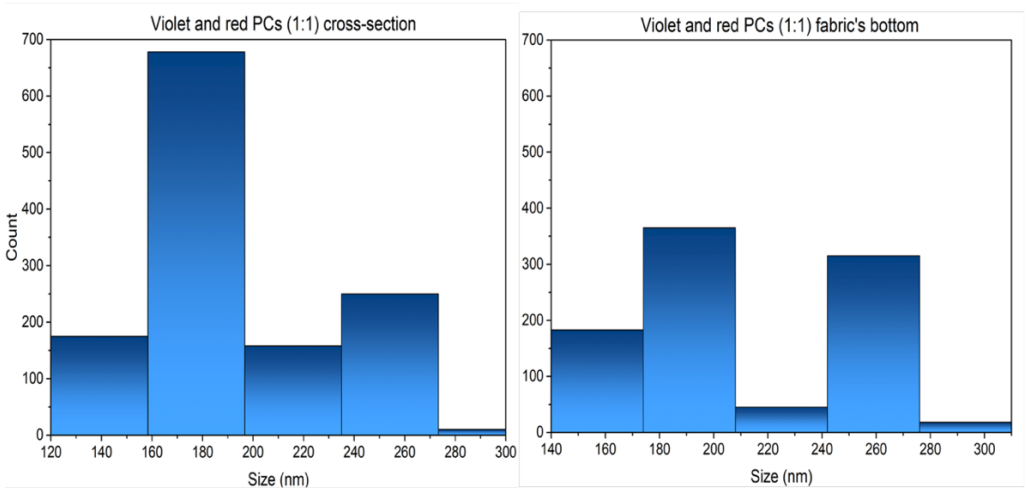


Figure 67 Particle size distribution in the cross-section (left) and on the bottom of the fabric (right). (cross section n=1271; bottom n=926)

A perfect structural arrangement of premixed PCs with two different sized is hard to obtain, unless a layer-by-layer methodology is used. [202, 203] Nevertheless, PCs can be mixed to obtain intermediate colors, following the principle of color addition, with reduced iridescence and brightness, as they are dependent of a perfect hexagonal, or at least a square structural arrangement.

8

Conclusions and Future Perspectives

8.1. Conclusions

8.1.1. Photonic crystals synthesis

Monodisperse and stable spheres of P(St-MMA-AA), SiO_2 and KL, were successfully synthesized at different sizes as confirmed by STEM and DLS analyses. For P(St-MMA-AA) sizes between 170 and 250 nm were synthetized. Small size PCs particles were obtained at high temperatures while at low temperatures particle size was increased. Higher stirring speed did not have significant influence on the nanospheres size compared to the control reaction, while lowering the stirring speed also increased the size of P(St-MMA-AA) particles, contrary to the expected. To optimize the production of red structural colors, monomer proportions were altered, instead of temperature or stirring speed.

Regarding SiO_2, although it was possible to obtain PC sizes that produced blue, green and red structural colors, the methodology used needs to be re-evaluated. The reactional conditions used to obtain the different sizes are not supported by the literature, since the obtained particles are larger than the reported and difficult to replicate, even using the same conditions. Nevertheless, these particles were able to form some coloration when applied to fabrics precoated with P(MMA-BA).

As for KL PCs, these were obtained by solvent-antisolvent methodology, with an average size of 507 nm with a PdI on the threshold of homogeneity acceptance (0.15). When applied in a glass substrate, it was possible to observe the iridescence formed by these particles. However, when deposited in fabrics precoated with P(MMA-BA), this effect was not verified. Other deposition techniques should be explored in to potentialize the application of KL PCs in fabrics since they can be the most sustainable option between the three types of synthetized PCs.

All produced PCs were properly characterized and applied onto polyamide, polyester and cotton substrates using dip-drawing and gravitational deposition methodologies.

8.1.2. P(St-MMA-AA) PCs deposition on fabrics

Polyamide fabrics covered with P(St-MMA-AA) presented the most promising results, which were able to mimic nature's iridescent effect. These samples were subjected to a more detailed analyses, in opposition to SiO_2 or KL functionalized fabrics. Polyamide's tight weave and high surface area, combined with yarns of low Tex, led to a smooth fabric surface with the lowest roughness values among the three fabrics. P(St-MMA-AA) PCs applied by dip-drawing method showed different colors according to the PCs size. SEM analysis confirmed that the self-assembled structures were mainly based on hpc arrangement with some square arrangement in the out-of-plane areas. Consequently, the PA fabric was the only one

to present a visible iridescent effect (by ocular inspection) and was further analyzed by angle-dependent UV/Vis reflectance measurements using polarized light. With this analysis it was possible to observe reflection peak shifts and the appearance of new reflection peaks when the angle of incidence was changed. Angle-dependent UV/Vis reflectance and IP-BRDF measurements were proven to be efficient methodologies to characterize iridescence in fabrics, which was also backed up by CIEL*a*b* color coordinates. Furthermore, P(St-MMA-AA) PCs can be mixed to obtain intermediate colors that follow the principle of color addition. However, iridescence is reduced as samples are opaquer, due to an imperfect structural arrangement.

PA fabrics covered with P(St-MMA-AA) PCs also displayed excellent light fastness, as minor color changes were observed after one week of continuous UV exposure, without any coating agent. As for washing fastness, several biopolymers and commercial finishing agents were tested. Almost all tested coating agents failed to retain both coating and color after washing. The exception was Sylgard™ 184, a PDMS-based agent, which was able to retain PCs at the fabric's surface, even in areas where the coating was partially peeled off. However, some loss of iridescence and brightness was verified, as well as cracks in PC structure when the fabric was bent.

Applying dyed P(St-MMA-AA) PCs to fabrics proven to be a possibility to recolor fabrics without removing the previous dye. Although the structural color and iridescence are overwhelmed by the disperse dye, especially when dye concentration is above 1 wt%, this approach can be applied to avoid the usage of stripping agents, consequently reducing chemical, water consumption and waste generation.

As for the PES and CO samples coated with P(St-MMA-AA) PCs exhibited the most color changes in IP-BRDF measurements. Overall, PES samples are darker, and CO samples have a higher luminosity parameter. This change in luminosity is due to the lack of uniformity in the PC self-assembly, which is a consequence of physical and chemical properties of these fabrics. Nevertheless, by applying P(St-MMA-AA) PCs onto these substrates, is possible to obtain solid (without iridescence) colors capable of substituting a conventional dye.

8.1.3. Main conclusions

In sum, the main conclusions of this research project are:

- An eco-friendlier alternative to dyes and pigments was achieved as three different types of photonic crystals were synthesized and characterized, where particles were obtained with different sizes, to produce a variety of structural colors
- SiO_2 and KL PC synthesis need further optimizations to produce stable structural colors

- Three textile substrates, polyamide, polyester and cotton, were tested to evaluate photonic crystal deposition and the consequent structural color. The most promising results were achieved with P(St-MMA-AA) PCs deposited onto polyamide
- UV/Vis and IP-BRDF techniques were able to ascertain the observed iridescence on P(St-MMA-AA)/PA, by band shifting at different angles of observation and incidence of light
- Sylgard™ 184 was the only finishing product capable of withstand washing fastness tests without compromising structural color and brightness
- P(St-MMA-AA) PCs can be dyed and applied onto used garments without removing the previous dye
- P(St-MMA-AA) PCs with different sizes can be mixed to produce intermediate colors, following the principle of color addition, but with some loss of brightness, due to the poorer structural arrangement.

The continuous study of photonic crystals in textiles as biomimetics is of major importance, not only for the development of advanced technical textiles but so that future generations can have more sustainable methods of coloring textiles.

8.2. Future Perspectives

The versatility of photonic crystal textiles in providing functional, sustainable, and aesthetically appealing solutions is driving ongoing research and innovation in biomimicry. As such, there is potential for improvements and, as future work, the following suggestions are proposed:

> SiO_2 PC synthesis needs to be further investigated in order to be more reliable and reproducible. Furthermore, the functionalization of these PCs should be considered, as most authors functionalize SiO_2 spheres to obtain better structural colors

> Continue to develop the studies with KL PCs, as they can be the most ecologic solution. Synthesis varying stirring speed and the addition flow rate should be performed to investigate the obtention of KL spheres with sizes capable of producing structural colors in textiles

> Continue to pursuit a suitable sustainable polymer that improve PC deposition in fabrics. Structural coloration only can be a sustainable alternative to textile dyeing if every step is as eco-friendly as possible

> If polymer precoating is not suitable/appropriate, fabrics with optimal properties for structural coloration should be weaved and produced inhouse

> Study different coating techniques such as knife coating or layer-by-layer methodology, to evaluate the possibility of obtaining organized layers of specific sizes

> Dye PCs with concentrations below 0.5 wt%, to reduce dye color influence in the final observed structural color

> Continue to pursuit an eco-friendly finishing agent that improves washing fastness without interfering with the structural color, iridescence and acting capability as sensors

> Perform life cycle analysis for each type of PC and fabric utilized

> Perform mechanical tests on the final product, ensuring its wearable viability

> Manufacture the new angular support for structural color observation, as its design has been completely finalized (see Annexes, Figure A1), allowing the photographic documentation of colors with 19 different observation angles (instead of the current 3).

Applying PCs to textiles will not only improve the quality and performance of the textiles but also contribute to a more sustainable and technologically advanced future.

Bibliography

1. Bashir, Z., et al., *Hazardous Chemicals in Textile Industries, Risk and Assessment*, in *Biocentric Approaches in Textile Waste Management*. 2026. p. 1–30. DOI: 10.1007/978-3-032-04974-2_1.
2. Parisi, M.L., et al., *Environmental impact assessment of an eco-efficient production for coloured textiles.* Journal of Cleaner Production, 2015. **108**: p. 514–524. DOI: 10.1016/j.jclepro.2015.06.032.
3. Butola, S.-u.-l.B.S., *The Impact and Prospects of Green Chemistry for Textile Technology*. 2019. DOI: 10.1016/c2017-0-01957-2.
4. Liu, G., et al., *The vertical deposition self-assembly process and the formation mechanism of poly(styrene-co-methacrylic acid) photonic crystals on polyester fabrics.* Journal of Materials Science, 2015. **51**(6): p. 2859–2868. DOI: 10.1007/s10853-015-9594-8.
5. Huang, D., et al., *Biomimetic colloidal photonic crystals by coassembly of polystyrene nanoparticles and graphene quantum dots.* RSC Advances, 2018. **8**(61): p. 34839–34847. DOI: 10.1039/c8ra07158f.
6. Yavuz, G., et al., *Dyed Poly(styrene-methyl Methacrylate-acrylic Acid) Photonic Nanocrystals for Enhanced Structural Color.* ACS Applied Materials & Interfaces, 2018. **10**(27): p. 23285–23294. DOI: 10.1021/acsami.8b03003.
7. Nucara, L., F. Greco, and V. Mattoli, *Electrically responsive photonic crystals: a review.* Journal of Materials Chemistry C, 2015. **3**(33): p. 8449–8467. DOI: 10.1039/c5tc00773a.
8. Kumar, A., et al., *Cold atmospheric plasma technology for removal of organic micropollutants from wastewater—a review.* The European Physical Journal D, 2021. **75**(11). DOI: 10.1140/epjd/s10053-021-00283-5.
9. Gururani, P., et al., *Cold plasma technology: advanced and sustainable approach for wastewater treatment.* Environmental Science and Pollution Research, 2021. **28**(46): p. 65062–65082. DOI: 10.1007/s11356-021-16741-x.
10. Al-Buriahi, A.K., et al., *Elimination of rhodamine B from textile wastewater using nanoparticle photocatalysts: A review for sustainable approaches.* Chemosphere, 2022. **287**. DOI: 10.1016/j.chemosphere.2021.132162.
11. Manzoor, K., et al., *Assessment of anaerobic membrane distillation bioreactor hybrid system at mesophilic and thermophilic temperatures treating textile wastewater.* Journal of Water Process Engineering, 2022. **46**. DOI: 10.1016/j.jwpe.2022.102603.

12. You, X., et al., *Sustainability and carbon neutrality trends for microalgae-based wastewater treatment: A review.* Environmental Research, 2022. **209**. DOI: 10.1016/j.envres.2022.112860.
13. Bilińska, L. and M. Gmurek, *Novel trends in AOPs for textile wastewater treatment. Enhanced dye by-products removal by catalytic and synergistic actions.* Water Resources and Industry, 2021. **26**. DOI: 10.1016/j.wri.2021.100160.
14. Sharma, R. and P. Malaviya, *Constructed wetlands for textile wastewater remediation: A review on concept, pollutant removal mechanisms, and integrated technologies for efficiency enhancement.* Chemosphere, 2022. **290**. DOI: 10.1016/j.chemosphere.2021.133358.
15. Faghihinezhad, M., et al., *Catalytic ozonation of real textile wastewater by magnetic oxidized g-C3N4 modified with Al2O3 nanoparticles as a novel catalyst.* Separation and Purification Technology, 2022. **283**. DOI: 10.1016/j.seppur.2021.120208.
16. Berradi, M., et al., *Textile finishing dyes and their impact on aquatic environs.* Heliyon, 2019. **5**(11). DOI: 10.1016/j.heliyon.2019.e02711.
17. Foundation, Z. *ZDHC Wastewater Guidelines Version 2.0*. 2022 [cited 2022 30.08.2022]; Available from: https://www.roadmaptozero.com/post/zdhc-releases-zdhc-wastewater-guidelines-version-2-0.
18. Yaseen, D.A. and M. Scholz, *Textile dye wastewater characteristics and constituents of synthetic effluents: a critical review.* International Journal of Environmental Science and Technology, 2018. **16**(2): p. 1193–1226. DOI: 10.1007/s13762-018-2130-z.
19. Velusamy, S., et al., *A Review on Heavy Metal Ions and Containing Dyes Removal Through Graphene Oxide-Based Adsorption Strategies for Textile Wastewater Treatment.* The Chemical Record, 2021. **21**(7): p. 1570–1610. DOI: 10.1002/tcr.202000153.
20. Fried, R., et al., *Biogenic colourants in the textile industry – a promising and sustainable alternative to synthetic dyes.* Green Chemistry, 2022. **24**(1): p. 13–35. DOI: 10.1039/d1gc02968a.
21. Chaturvedi, A., et al., *A comprehensive review on the integration of advanced oxidation processes with biodegradation for the treatment of textile wastewater containing azo dyes.* Reviews in Chemical Engineering, 2022. **38**(6): p. 617–639. DOI: 10.1515/revce-2020-0010.
22. Sela, S.K., et al., *Utilization of prawn to reduce the value of BOD and COD of textile wastewater.* Cleaner Engineering and Technology, 2020. **1**. DOI: 10.1016/j.clet.2020.100021.

23. Madhav, S., et al., *A review of textile industry: Wet processing, environmental impacts, and effluent treatment methods.* Environmental Quality Management, 2018. **27**(3): p. 31–41. DOI: 10.1002/tqem.21538.

24. Shindhal, T., et al., *A critical review on advances in the practices and perspectives for the treatment of dye industry wastewater.* Bioengineered, 2020. **12**(1): p. 70–87. DOI: 10.1080/21655979.2020.1863034.

25. Wilson, J.G., *Teratogenic activity of several azo dyes chemically related to trypan blue.* The Anatomical Record, 2005. **123**(3): p. 313–333. DOI: 10.1002/ar.1091230306.

26. Koulini, G.V., et al., *Effective degradation of azo dye from textile wastewater by electro-peroxone process.* Chemosphere, 2022. **289**. DOI: 10.1016/j.chemosphere.2021.133152.

27. Xian, Y., et al., *Urea-free reactive printing of viscose fabric with high color performance for cleaner production.* Cellulose, 2021. **28**(4): p. 2567–2579. DOI: 10.1007/s10570-021-03682-4.

28. Mukherjee, D., B. Van der Bruggen, and B. Mandal, *Advancements in visible light responsive MOF composites for photocatalytic decontamination of textile wastewater: A review.* Chemosphere, 2022. **295**. DOI: 10.1016/j.chemosphere.2022.133835.

29. Takeuchi, N. and K. Yasuoka, *Review of plasma-based water treatment technologies for the decomposition of persistent organic compounds.* Japanese Journal of Applied Physics, 2020. **60**(SA). DOI: 10.35848/1347-4065/abb75d.

30. Sanito, R.C., S.-J. You, and Y.-F. Wang, *Degradation of contaminants in plasma technology: An overview.* Journal of Hazardous Materials, 2022. **424**. DOI: 10.1016/j.jhazmat.2021.127390.

31. Wang, F., et al., *Tunable colors from responsive 2D materials.* Responsive Materials, 2024. **2**(3). DOI: 10.1002/rpm.20240007.

32. Nordén, K.K., C.M. Eliason, and M.C. Stoddard, *Evolution of brilliant iridescent feather nanostructures.* eLife, 2021. **10**. DOI: 10.7554/eLife.71179.

33. Cersonsky, R.K., et al., *The diversity of three-dimensional photonic crystals.* Nature Communications, 2021. **12**(1). DOI: 10.1038/s41467-021-22809-6.

34. Wu, P., J. Wang, and L. Jiang, *Bio-inspired photonic crystal patterns.* Materials Horizons, 2020. **7**(2): p. 338–365. DOI: 10.1039/c9mh01389j.

35. Vignolini, S., et al., *Pointillist structural color in Pollia fruit.* Proceedings of the National Academy of Sciences, 2012. **109**(39): p. 15712–15715. DOI: 10.1073/pnas.1210105109.

36. Zhang, P., et al., *Liquid crystal-based structural color actuators.* Light: Science & Applications, 2022. **11**(1). DOI: 10.1038/s41377-022-00937-y.

37. Datta, B., et al., *Socially-Directed Development of Materials for Structural Color.* Advanced Materials, 2022. **34**(20). DOI: 10.1002/adma.202100939.

38. Scharber, M.C. and N.S. Sariciftci, *Low Band Gap Conjugated Semiconducting Polymers.* Advanced Materials Technologies, 2021. **6**(4). DOI: 10.1002/admt.202000857.

39. Chen, X. and L. Tian, *Advance Materials Series: Advanced Energy Materials. Edited by Ashutosh Tiwari and Sergiy Valyukh.* Energy Technology, 2015. **3**(10): p. 1072–1072. DOI: 10.1002/ente.201500283.

40. Liu, G., et al., *Optical properties of three-dimensional P(St-MAA) photonic crystals on polyester fabrics.* Optical Materials, 2015. **42**: p. 72–79. DOI: 10.1016/j.optmat.2014.12.022.

41. Li, W., et al., *Inkjet Printing of Patterned, Multispectral, and Biocompatible Photonic Crystals.* Advanced Materials, 2019. **31**(36). DOI: 10.1002/adma.201901036.

42. Zhou, L., et al., *Facile fabrication of reactive dye@PSt photonic crystals with high contrast on textile substrates by ink-jet printing.* Materials Chemistry and Physics, 2020. **250**. DOI: 10.1016/j.matchemphys.2020.123025.

43. He, J. and X. Lv, *Structural color printing and evaluation based on 3D printing.* Pigment & Resin Technology, 2023. **53**(4): p. 502–509. DOI: 10.1108/prt-10-2022-0120.

44. Liao, J., et al., *3D-printable colloidal photonic crystals.* Materials Today, 2022. **56**: p. 29–41. DOI: 10.1016/j.mattod.2022.02.014.

45. Zhuo, Y., et al., *Photonic crystal slab biosensors fabricated with helium ion lithography (HIL).* Sensors and Actuators A: Physical, 2019. **297**. DOI: 10.1016/j.sna.2019.07.017.

46. Jee, H., et al., *Combining Interference Lithography and Two-Photon Lithography for Fabricating Large-Area Photonic Crystal Structures with Controlled Defects.* Applied Sciences, 2021. **11**(14). DOI: 10.3390/app11146559.

47. Zhu, W., et al., *High confidence plasmonic sensor based on photonic crystal fibers with a U-shaped detection channel.* Physical Chemistry Chemical Physics, 2023. **25**(12): p. 8583–8591. DOI: 10.1039/d2cp04605a.

48. Li, T., et al., *Recent advances in photonic crystal-based sensors.* Coordination Chemistry Reviews, 2023. **475**. DOI: 10.1016/j.ccr.2022.214909.

49. Zhu, K., et al., *Recent advances in photonic crystal with unique structural colors: A review.* Journal of Materials Science & Technology, 2023. **141**: p. 78–99. DOI: 10.1016/j.jmst.2022.08.044.

50. Gyu Hwang, T., et al., *Forensic-level security using non-imitable anticounterfeiting films: Humidity-sensitive 1D photonic crystals with UV-tunable color response and their encryption using small aldehydes.* Chemical Engineering Journal, 2023. **473**. DOI: 10.1016/j.cej.2023.145448.

51. Zhou, L., et al., *Study on the correlations between the structural colors of photonic crystals and the base colors of textile fabric substrates.* Dyes and Pigments, 2016. **133**: p. 435–444. DOI: 10.1016/j.dyepig.2016.06.032.

52. Wang, X., et al., *High Structural Stability of Photonic Crystals on Textile Substrates, Prepared via a Surface-Supported Curing Strategy.* ACS Applied Materials & Interfaces, 2021. **13**(16): p. 19221–19229. DOI: 10.1021/acsami.1c00176.

53. Xinyang, L., et al., *Efficient preparation of liquid photonic crystals and their application in bionic structural coloration of textiles.* Dyes and Pigments, 2023. **209**. DOI: 10.1016/j.dyepig.2022.110913.

54. Li, Y., et al., *Study on the effects of the characteristics of textile substrates on the photonic crystal films and the related structural colors.* Surface and Coatings Technology, 2017. **319**: p. 267–276. DOI: 10.1016/j.surfcoat.2017.04.017.

55. Zhou, L., et al., *Fabrication of high-quality silica photonic crystals on polyester fabrics by gravitational sedimentation self-assembly.* Coloration Technology, 2015. **131**(6): p. 413–423. DOI: 10.1111/cote.12164.

56. Liu, H., et al., *The development of lignin towards a natural and sustainable platform for optical materials.* Green Chemistry, 2024. **26**(17): p. 9281–9294. DOI: 10.1039/d4gc02944e.

57. Sipponen, M.H., et al., *Lignin for Nano- and Microscaled Carrier Systems: Applications, Trends, and Challenges.* ChemSusChem, 2019. **12**(10): p. 2039–2054. DOI: 10.1002/cssc.201900480.

58. Argyropoulos, D.D.S., et al., *Kraft Lignin: A Valuable, Sustainable Resource, Opportunities and Challenges.* ChemSusChem, 2023. **16**(23). DOI: 10.1002/cssc.202300492.

59. Liu, H., et al., *All-Lignin Colloidal Particles Enable Structural Color and Photothermal Conversion.* Small, 2025. **22**(11). DOI: 10.1002/smll.202509559.

60. Wang, J., et al., *Photonic Lignin with Tunable and Stimuli-Responsive Structural Color.* ACS Nano, 2022. **16**(12): p. 20705–20713. DOI: 10.1021/acsnano.2c07756.

61. Dghoughi, A., et al., *Synthesis of triangular lignin photonic crystal nanoparticles: Investigating solvent effects and dialysis optimization.* International Journal of Biological Macromolecules, 2025. **291**. DOI: 10.1016/j.ijbiomac.2024.139110.

62. Thalakkale Veettil, U., et al., *High-yield production of lignin nanoparticle photonic glasses.* Green Chemistry, 2025. **27**(7): p. 2130–2137. DOI: 10.1039/d4gc05797j.

63. Liu, J., et al., *Photonic crystals with rainbow colors by centrifugation-assisted assembly of colloidal lignin nanoparticles.* Nature Communications, 2023. **14**(1). DOI: 10.1038/s41467-023-38819-5.

64. Hutchings, P.B.M., *Chromic Phenomena*. 2018. DOI: 10.1039/9781788012843.

65. Yavuz, G., et al., *Structural coloration of chitosan-cationized cotton fabric using photonic crystals.* IOP Conference Series: Materials Science and Engineering, 2017. **254**. DOI: 10.1088/1757-899x/254/10/102012.

66. Hu, J., *Active Coatings for Smart Textiles*. 2016. DOI: 10.1016/c2014-0-00660-0.

67. Xuan, Z., et al., *Artificial Structural Colors and Applications.* The Innovation, 2021. **2**(1). DOI: 10.1016/j.xinn.2021.100081.

68. Feng, L., et al., *Review of recent advancements in the biomimicry of structural colors.* Dyes and Pigments, 2023. **210**. DOI: 10.1016/j.dyepig.2022.111019.

69. Yang, S., et al., *Effect of Fabric Substrate and Introduction of Silk Fibroin on the Structural Color of Photonic Crystals.* Polymers, 2023. **15**(17). DOI: 10.3390/polym15173551.

70. Liu, G., et al., *The fabrication of full color P(St-MAA) photonic crystal structure on polyester fabrics by vertical deposition self-assembly.* Journal of Applied Polymer Science, 2014. **132**(13). DOI: 10.1002/app.41750.

71. Liu, G., et al., *Self-assembly behavior of polystyrene/methacrylic acid (P(St-MAA)) colloidal microspheres on polyester fabrics by gravitational sedimentation.* The Journal of The Textile Institute, 2015. **106**(12): p. 1293–1305. DOI: 10.1080/00405000.2014.998011.

72. Shao, J., et al., *Preparation of monodispersed polystyrene microspheres and self-assembly of photonic crystals for structural colors on polyester fabrics.* The Journal of The Textile Institute, 2014. **105**(9): p. 938–943. DOI: 10.1080/00405000.2013.865864.

73. Zhou, L., et al., *The synthesis of core-shell monodisperse P(St-MAA) microspheres and fabrication of photonic crystals Structure with Tunable Colors on polyester fabrics.* Fibers and Polymers, 2014. **15**(6): p. 1112–1122. DOI: 10.1007/s12221-014-1112-0.

74. Liu, G., et al., *Fabrication of patterned photonic crystals with brilliant structural colors on fabric substrates using ink-jet printing technology.* Materials & Design, 2017. **114**: p. 10–17. DOI: 10.1016/j.matdes.2016.09.102.

75. Liu, G., et al., *The preparation of monodisperse P(St-BA-MAA)@disperse dye microspheres and fabrication of patterned photonic crystals with brilliant structural colors on white substrates.* Optical Materials, 2019. **98**. DOI: 10.1016/j.optmat.2019.109503.

76. Hutchison, P., P. Kingshott, and A. Yu, *Oxide and Hydrogel Inverse Opals and Their Applications as Physical, Chemical and Biological Sensors.* Sensors, 2025. **25**(11). DOI: 10.3390/s25113370.

77. Zhao, Y., et al., *Spherical Colloidal Photonic Crystals.* Accounts of Chemical Research, 2014. **47**(12): p. 3632–3642. DOI: 10.1021/ar500317s.

78. Liu, W., et al., *Ternary non-close-packed photonic crystals with tunable optical properties through varying shell thickness of hollow silica.* Colloids and Surfaces A: Physicochemical and Engineering Aspects, 2025. **719**. DOI: 10.1016/j.colsurfa.2025.136971.

79. Lee, G.H., et al., *Chameleon-Inspired Mechanochromic Photonic Films Composed of Non-Close-Packed Colloidal Arrays.* ACS Nano, 2017. **11**(11): p. 11350–11357. DOI: 10.1021/acsnano.7b05885.

80. Yu, J., *Development of structural-coloured textile materials via self-assembly of photonic crystals*, in *Institute of Textiles and Clothing*. 2021, Hong Kong Polytechnic University. p. 160.

81. Fang, Q., et al., *Fabrication of closed-cell inverse opal photonic crystal pigments with angle-independent and stable structural colors.* Materials Chemistry Frontiers, 2024. **8**(22): p. 3731–3740. DOI: 10.1039/d4qm00608a.

82. Wang, L., et al., *Self-Bonded Hydrogel Inverse Opal Particles as Sprayed Flexible Patch for Wound Healing.* ACS Nano, 2022. **16**(2): p. 2640–2650. DOI: 10.1021/acsnano.1c09388.

83. Liu, Y., et al., *Ethanol-responsive structural colors with multi-level information encryption based on the patterned three-layer inverse opal photonic crystal.* Journal of Colloid and Interface Science, 2025. **677**: p. 99–107. DOI: 10.1016/j.jcis.2024.07.199.

84. Chi, C., et al., *Silica-templated photonic crystal sensors for specific detection of Cu2+.* The Analyst, 2022. **147**(15): p. 3486–3493. DOI: 10.1039/d2an00619g.

85. Armstrong, E. and C. O'Dwyer, *Artificial opal photonic crystals and inverse opal structures – fundamentals and applications from optics to energy storage.* Journal of Materials Chemistry C, 2015. **3**(24): p. 6109–6143. DOI: 10.1039/c5tc01083g.

86. Xiong, Y., et al., *Photonic Crystal Enhanced Fluorescence: A Review on Design Strategies and Applications.* Micromachines, 2023. **14**(3). DOI: 10.3390/mi14030668.

87. Chen, X., et al., *Fabrication of closed-cell polyimide inverse opal photonic crystals with excellent mechanical properties and thermal stability.* Journal of Materials Chemistry, 2008. **18**(19). DOI: 10.1039/b801565a.

88. Wang, W., et al., *Structural color: an emerging nanophotonic strategy for multicolor and functionalized applications.* Opto-Electronic Science, 2025. **4**(4): p. 240030–240030. DOI: 10.29026/oes.2025.240030.

89. Lv, X., et al., *Research Progress in Preparation and Application of Photonic Crystals.* Chinese Journal of Mechanical Engineering, 2023. **36**(1). DOI: 10.1186/s10033-023-00836-2.

90. Zhao, J., et al., *Hazardous Gases-Responsive Photonic Crystals Cryogenic Sensors Based on Antifreezing and Water Retention Hydrogels.* ACS Applied Materials & Interfaces, 2023. **15**(35): p. 42046–42055. DOI: 10.1021/acsami.3c06443.

91. Hoeven, J.E.S.v.d., et al., *Evaporation-Induced Self-Assembly of Metal Oxide Inverse Opals: From Synthesis to Applications.* Accounts of Chemical Research, 2022. **55**(13): p. 1809–1820. DOI: 10.1021/acs.accounts.2c00087.

92. Sakamoto, S., et al., *Scalable and Stable Manufacture of Molecular-Sized Silica Nanoparticles by Evaporation-Induced Self-Assembly.* Chemistry of Materials, 2023. **35**(15): p. 5838–5844. DOI: 10.1021/acs.chemmater.3c00500.

93. Zhang, X., et al., *Structural colored fabrics with hydrophobic and angle-dependent property prepared by one step dip-coating.* Surfaces and Interfaces, 2025. **59**. DOI: 10.1016/j.surfin.2025.105986.

94. Fu, Y., et al., *Construction of amorphous photonic crystal coated fabrics with wash resistance and antifouling performance.* Cellulose, 2023. **30**(6): p. 4057–4070. DOI: 10.1007/s10570-023-05117-8.

95. Martusciello, M., et al., *Dip-Coating Fabrication of All-Polymer Multilayer Photonic Crystals through 3D Printer Conversion.* ACS Applied Polymer Materials, 2025. **7**(8): p. 4779–4786. DOI: 10.1021/acsapm.4c04077.

96. Li, J., et al., *Nanoscale multi-beam lithography of photonic crystals with ultrafast laser.* Light: Science & Applications, 2023. **12**(1). DOI: 10.1038/s41377-023-01178-3.

97. Wu, Y., K. Zhang, and B. Yang, *Ordered Hybrid Micro/Nanostructures and Their Optical Applications.* Advanced Optical Materials, 2019. **7**(7). DOI: 10.1002/adom.201800980.

98. Wang, H., et al., *Enhancing optical transparency of photonic crystals for high-performance electromagnetic interference shielding.* Optics and Lasers in Engineering, 2025. **195**. DOI: 10.1016/j.optlaseng.2025.109293.

99. Gao, W., M. Rigout, and H. Owens, *The structural coloration of textile materials using self-assembled silica nanoparticles.* Journal of Nanoparticle Research, 2017. **19**(9). DOI: 10.1007/s11051-017-3991-7.

100. Tan, P.F., et al., *Highly Crystallized Brilliant Polymeric Photonic Crystals via Repulsion-Induced Precipitation Assembly toward Multiresponsive Colorimetric Films.* Macromolecular Materials and Engineering, 2016. **301**(11): p. 1363–1373. DOI: 10.1002/mame.201600278.

101. Chen, Q., et al., *Preparation and properties of porous P(St-MMA-AA) microsphere anti-glare film.* Progress in Organic Coatings, 2019. **137**. DOI: 10.1016/j.porgcoat.2019.105287.

102. Liu, Y., J. Hu, and Z. Wu, *Fabrication of Coatings with Structural Color on a Wood Surface.* Coatings, 2020. **10**(1). DOI: 10.3390/coatings10010032.

103. Ifijen, I.H., et al., *Ordered Colloidal Crystals Fabrication and Studies on the Properties of Poly (Styrene–Butyl Acrylate–Acrylic Acid) and Polystyrene Latexes*, in *Nanocomposites VI: Nanoscience and Nanotechnology in Advanced Composites*. 2019. p. 125–135. DOI: 10.1007/978-3-030-35790-0_11.

104. Lai, C.-F. and J.-S. Li, *Self-assembly of colloidal Poly(St-MMA-AA) core/shell photonic crystals with tunable structural colors of the full visible spectrum.* Optical Materials, 2019. **88**: p. 128–133. DOI: 10.1016/j.optmat.2018.11.020.

105. Lu, Z. and H. Owens, *Optimum processing parameters for coating polyester with silica nanoparticles using gravity sedimentation.* Journal of Nanoparticle Research, 2019. **21**(10). DOI: 10.1007/s11051-019-4635-x.

106. Bian, F., et al., *Colloidal Crystals from Microfluidics.* Small, 2019. **16**(9). DOI: 10.1002/smll.201903931.

107. Xu, J.-P. and J.-T. Zhu, *Block Copolymer Colloidal Particles with Unique Structures through Three-dimensional Confined Assembly and Disassembly.* Chinese Journal of Polymer Science, 2019. **37**(8): p. 744–759. DOI: 10.1007/s10118-019-2294-0.

108. Song, D.-P., et al., *Hierarchical Photonic Pigments via the Confined Self-Assembly of Bottlebrush Block Copolymers.* ACS Nano, 2019. DOI: 10.1021/acsnano.8b07845.

109. Ikhuoria, E.U., et al., *Raspberry-like and other hexagonal close-packed morphologies of P(St-MMA-AA) particles obtained from different emulsifiers for photonic applications.* Journal of Modern Optics, 2018. **65**(15): p. 1817–1826. DOI: 10.1080/09500340.2018.1461940.

110. Takise, H., et al., *Thin film formation of PEDOT conductive polymer and PVDF piezoelectric polymer by dip-coating method assuming application to flexible power generation element.* Electronics and Communications in Japan, 2020. **103**(8): p. 46–52. DOI: 10.1002/ecj.12238.

111. Fu, Y., et al., *Thermo-oxidative stabilization for natural rubber nanocomposites by polydopamine interfacial tailored clay.* RSC Advances, 2016. **6**(88): p. 84906–84913. DOI: 10.1039/c6ra18269k.

112. Khanadeev, V.A., et al., *Large-scale high-quality 2D silica crystals: dip-drawing formation and decoration with gold nanorods and nanospheres for SERS analysis.* Nanotechnology, 2014. **25**(40). DOI: 10.1088/0957-4484/25/40/405602.

113. Shieh, J.-Y., et al., *Preparation and Evaluation of the Bioinspired PS/PDMS Photochromic Films by the Self-Assembly Dip–Drawing Method.* Langmuir, 2013. **29**(2): p. 667–672. DOI: 10.1021/la303491c.

114. Jones, C., et al., *Textile materials inspired by structural colour in nature.* RSC Advances, 2020. **10**(41): p. 24362–24367. DOI: 10.1039/d0ra01326a.

115. Al-Douri, Y., et al., *Effect of stirring time on the structural parameters of nanophotonic LiNbO3 deposited by spin-coating technique.* Optik, 2018. **156**: p. 886–890. DOI: 10.1016/j.ijleo.2017.12.059.

116. Hung, P.-S., et al., *High throughput fabrication of large-area colloidal crystals via a two-stage electrophoretic deposition method.* Electrochimica Acta, 2019. **317**: p. 52–60. DOI: 10.1016/j.electacta.2019.05.114.

117. Wu, Y., et al., *Rapid preparation of TiO2-SiO2 heterostructure photonic crystal in the near-infrared region via a modified electrophoresis-assisted self-assembly process.* Materials Research Bulletin, 2018. **100**: p. 353–356. DOI: 10.1016/j.materresbull.2017.12.048.

118. Li, M. and Y. Song, *Polymer Photonic Crystals*, in *Encyclopedia of Polymer Science and Technology*. 2014. p. 1–46. DOI: 10.1002/0471440264.pst629.

119. Roemling, L.J., et al., *Quantitative Optical and Structural Comparison of 3D and (2+1)D Colloidal Photonic Crystals.* Langmuir, 2023. **39**(14): p. 5211–5221. DOI: 10.1021/acs.langmuir.3c00293.

120. Yajima, K., et al., *Experimental demonstration of polarization beam splitter based on auto-cloning photonic crystal*, in *2017 22nd Microoptics Conference (MOC)*. 2017. p. 94–95.

121. Chen, H., et al., *Advances in Photonic Crystal Research for Structural Color.* Advanced Materials Technologies, 2024. **10**(4). DOI: 10.1002/admt.202400865.

122. Cai, Z., et al., *From colloidal particles to photonic crystals: advances in self-assembly and their emerging applications.* Chemical Society Reviews, 2021. **50**(10): p. 5898–5951. DOI: 10.1039/d0cs00706d.

123. Shahrokhabadi, H., et al., *A compact sharp-edge wide bandpass near-infrared filter based on graded-index sinusoidally corrugated photonic crystal.* Physics Letters A, 2020. **384**(11). DOI: 10.1016/j.physleta.2020.126235.

124. Appold, M. and M. Gallei, *Bio-Inspired Structural Colors Based on Linear Ultrahigh Molecular Weight Block Copolymers.* ACS Applied Polymer Materials, 2019. **1**(2): p. 239–250. DOI: 10.1021/acsapm.8b00169.

125. Li, H., et al., *Rainbow Photonic Crystals: Self-Assembly of Carbohydrate Bottlebrushes Block Copolymers.* Advanced Materials, 2025. DOI: 10.1002/adma.202514152.

126. Guo, J., et al., *Recent Progress in Block Copolymer Self-Assembly for the Fabrication of Structural Color Pigments.* Macromolecular Rapid Communications, 2024. **46**(5). DOI: 10.1002/marc.202400839.

127. Martín-Palma, R.J. and M. Kolle, *Biomimetic photonic structures for optical sensing.* Optics & Laser Technology, 2019. **109**: p. 270–277. DOI: 10.1016/j.optlastec.2018.07.079.

128. Yue, Y. and T. Kurokawa, *Designing Responsive Photonic Crystal Patterns by Using Laser Engraving.* ACS Applied Materials & Interfaces, 2019. **11**(11): p. 10841–10847. DOI: 10.1021/acsami.8b22498.

129. Wang, K., et al., *Design of photonic crystals for light-emitting diodes.* Journal of the American Ceramic Society, 2023. **106**(12): p. 7146–7188. DOI: 10.1111/jace.19388.

130. Molina, J., et al., *Plasma treatment of polyester fabrics to increase the adhesion of reduced graphene oxide.* Synthetic Metals, 2015. **202**: p. 110–122. DOI: 10.1016/j.synthmet.2015.01.023.

131. Nascimento do Carmo, S., A. Zille, and A.P. Souto, *Plasma-assisted deposition of microcapsule containingAloe veraextract for cosmeto-textiles.* IOP Conference Series: Materials Science and Engineering, 2017. **254**. DOI: 10.1088/1757-899x/254/12/122007.

132. Oliveira, F.R., et al., *Surface Modification on Polyamide 6.6 with Double Barrier Discharge (DBD) Plasma to Optimise Dyeing Process by Direct Dyes.* Materials Science Forum, 2010. **636-637**: p. 846–852. DOI: 10.4028/www.scientific.net/MSF.636-637.846.

133. Zille, A., F.R. Oliveira, and A.P. Souto, *Plasma Treatment in Textile Industry.* Plasma Processes and Polymers, 2015. **12**(2): p. 98–131. DOI: 10.1002/ppap.201400052.

134. Oliveira, F.R., et al., *Physical, Chemical and Morphological Characterization of Polyamide Fabrics Treated with Plasma Discharge.* Materials Research, 2017. **20**(suppl 2): p. 60–68. DOI: 10.1590/1980-5373-mr-2016-1032.

135. Alves, C., et al., *Plasma-treated bacterial nanocellulose-lignin composites for biomedical applications.* International Journal of Biological Macromolecules, 2026. **338**. DOI: 10.1016/j.ijbiomac.2025.149544.

136. Magalhães, C., et al., *DBD plasma-treated polyester fabric coated with doped PEDOT:PSS for thermoregulation.* Applied Surface Science, 2025. **686**. DOI: 10.1016/j.apsusc.2024.162152.

137. Mehravani, B., et al., *In Situ Synthesis of Copper Nanoparticles on Dielectric Barrier Discharge Plasma-Treated Polyester Fabrics at Different Reaction pHs.* ACS Applied Polymer Materials, 2022. **4**(5): p. 3908–3918. DOI: 10.1021/acsapm.2c00375.

138. Oliveira, F.R., et al., *Reuse of effluent from dyeing process of polyamide fibers modified by double barrier discharge (DBD) plasma.* Desalination and Water Treatment, 2016. **57**(6): p. 2649–2656. DOI: 10.1080/19443994.2015.1018334.

139. Mehmood, T., et al., *Study of oxygen plasma pre-treatment of polyester fabric for improved polypyrrole adhesion.* Materials Chemistry and Physics, 2014. **143**(2): p. 668–675. DOI: 10.1016/j.matchemphys.2013.09.052.

140. Mehdizadeh, M., *Plasma applicators at RF and microwave frequencies*, in *Microwave/RF Applicators and Probes*. 2015. p. 335–363. DOI: 10.1016/b978-0-323-32256-0.00010-5.

141. Kusano, R. and Y. Kusano, *Applications of Plasma Technologies in Recycling Processes.* Materials, 2024. **17**(7). DOI: 10.3390/ma17071687.

142. Litter, M.I., *Thermal and Non-Thermal Plasma for Destruction of Pollutants.* Journal of Plasma Chemistry and Plasma Processing Research, 2021. **2**(1): p. 1–6.

143. Wróblewska-Krepsztul, J., et al., *Biopolymers for Biomedical and Pharmaceutical Applications: Recent Advances and Overview of Alginate Electrospinning.* Nanomaterials, 2019. **9**(3). DOI: 10.3390/nano9030404.

144. Aneesa Padinjakkara, A.T., Fernando Gomes Souza, Jr., Sabu Thomas, *Biopolymers and Biomaterials*. 1st Edition ed. 2019.

145. Younes, B., *Classification, characterization, and the production processes of biopolymers used in the textiles industry.* The Journal of The Textile Institute, 2016. **108**(5): p. 674–682. DOI: 10.1080/00405000.2016.1180731.

146. Mowafi, S., H. El-Sayed, and M. Abou Taleb, *Utilization of Proteinic Biopolymers: Current Status and Future Prospects.* Journal of Textiles, Coloration and Polymer Science, 2018. **0**(0): p. 0–0. DOI: 10.21608/jtcps.2018.5007.1002.

147. Montano, V., A. Smits, and S.J. Garcia, *The bio-touch: Increasing coating functionalities via biomass-derived components.* Surface and Coatings Technology, 2018. **341**: p. 2–14. DOI: 10.1016/j.surfcoat.2017.10.073.

148. Reddy, N., et al., *Reducing environmental pollution of the textile industry using keratin as alternative sizing agent to poly(vinyl alcohol).* Journal of Cleaner Production, 2014. **65**: p. 561–567. DOI: 10.1016/j.jclepro.2013.09.046.

149. Shahid ul, I., M. Shahid, and F. Mohammad, *Green Chemistry Approaches to Develop Antimicrobial Textiles Based on Sustainable Biopolymers—A Review.* Industrial & Engineering Chemistry Research, 2013. **52**(15): p. 5245–5260. DOI: 10.1021/ie303627x.

150. Hamed, I., F. Özogul, and J.M. Regenstein, *Industrial applications of crustacean by-products (chitin, chitosan, and chitooligosaccharides): A review.* Trends in Food Science & Technology, 2016. **48**: p. 40–50. DOI: 10.1016/j.tifs.2015.11.007.

151. Fernandes, M., et al., *Polysaccharides and Metal Nanoparticles for Functional Textiles: A Review.* Nanomaterials, 2022. **12**(6). DOI: 10.3390/nano12061006.

152. Yavuz, G., et al., *Structural coloration of chitosan coated cellulose fabrics by electrostatic self-assembled poly (styrene-methyl methacrylate-acrylic acid) photonic crystals.* Carbohydrate Polymers, 2018. **193**: p. 343–352. DOI: 10.1016/j.carbpol.2018.03.084.

153. Shi, X., et al., *Photonic crystals with vivid structure color and robust mechanical strength.* Dyes and Pigments, 2019. **165**: p. 137–143. DOI: 10.1016/j.dyepig.2019.02.023.

154. Gouveia, S., et al., *Polymerisation of Kraft lignin from black liquors by laccase from Myceliophthora thermophila: Effect of operational conditions and black liquor origin.* Bioresource Technology, 2013. **131**: p. 288–294. DOI: 10.1016/j.biortech.2012.12.155.

155. Stöber, W., A. Fink, and E. Bohn, *Controlled growth of monodisperse silica spheres in the micron size range.* Journal of Colloid and Interface Science, 1968. **26**(1): p. 62–69. DOI: 10.1016/0021-9797(68)90272-5.

156. l'Eclairage, C.I.d., *CIE Colorimetry*, in *Official Recommendations of the International Commission on Illumination, 2nd edition*. 1986: Vienna, Austria.

157. Kang, K., et al., *Morphology control of soap-free seeded P(St–EA–AA) latex particles.* European Polymer Journal, 2005. **41**(7): p. 1510–1518. DOI: 10.1016/j.eurpolymj.2005.01.027.

158. Zhang, S., J. Chen, and M. Taha, *Synthesis of monodisperse styrene/methyl methacrylate/acrylic acid latex using surfactant-free emulsion copolymerization in air.* Journal of Applied Polymer Science, 2009. **114**(3): p. 1598–1605. DOI: 10.1002/app.30744.

159. Marinho, R., L. Horiuchi, and C.A. Pires, *Effect of Stirring Speed on Conversion and Time to Particle Stabilization of Poly (Vinyl Chloride) Produced by Suspension Polymerization Process at the Beginning of Reaction.* Brazilian Journal of Chemical Engineering, 2018. **35**(2): p. 631–640. DOI: 10.1590/0104-6632.20180352s20160453.

160. Ifijen, I.H., et al., *Synthesis of Polydispersed P(St-MMA-AA) Microspheres and Fabrication of Colloidal Crystals with Non-Compact Morphology.* Tanzania Journal of Science, 2022. **48**(1): p. 140–147. DOI: 10.4314/tjs.v48i1.13.

161. Ifijen, H.I., E.U. Ikhuoria, and S.O. Omorogbe, *Correlative studies on the fabrication of poly(styrene-methyl-methacrylate-acrylic acid) colloidal crystal films.* Journal of Dispersion Science and Technology, 2019. **40**(7): p. 1023–1030. DOI: 10.1080/01932691.2018.1494605.

162. Chen, Q., et al., *Synthesis of fullerene-modified P(St-MMA-AA) colloids and optical performance in colloidal crystals.* Integrated Ferroelectrics, 2019. **197**(1): p. 43–48. DOI: 10.1080/10584587.2019.1592078.

163. Topçu, G., T. Güner, and M.M. Demir, *Non-iridescent structural colors from uniform-sized SiO 2 colloids.* Photonics and Nanostructures - Fundamentals and Applications, 2018. **29**: p. 22–29. DOI: 10.1016/j.photonics.2018.01.002.

164. Yan, Y., et al., *Controllable synthesis of SiO2 nanoparticles: effects of ammonia and tetraethyl orthosilicate concentration.* Micro & Nano Letters, 2016. **11**(12): p. 885–889. DOI: 10.1049/mnl.2016.0434.

165. Raabe, J., et al., *Evaluation of reaction factors for deposition of silica (SiO2) nanoparticles on cellulose fibers.* Carbohydrate Polymers, 2014. **114**: p. 424–431. DOI: 10.1016/j.carbpol.2014.08.042.

166. Yang, H., et al., *Structural coloration of white cotton fabrics via self-assembly of SiO2/carbon composite microspheres.* Materials Science and Engineering: B, 2024. **303**. DOI: 10.1016/j.mseb.2024.117308.

167. Zhao, X. and Y. Fang, *Structural colored fabric with superhydrophobicity by assembly SiO2@PPy composite microspheres and spraying PDMS on white fabric.* Optical Materials, 2025. **161**. DOI: 10.1016/j.optmat.2025.116826.

168. Ong H.R., I.W.M.E., Chong J., Khan M.M.R., Ong T.K., Chua B.K., *Investigation on Silane Concentration of SiO2 Nanoparticle: FTIR Analysis.* Chemical Engineering Transactions, 2023. **106**. DOI: 10.3303/CET23106225.

169. Madathingal, R.R. and S.L. Wunder, *Thermal degradation of poly(methyl methacrylate) on SiO2 nanoparticles as a function of SiO2 size and silanol density.* Thermochimica Acta, 2011. **526**(1-2): p. 83–89. DOI: 10.1016/j.tca.2011.08.026.

170. Zhu, C., Y. Lin, and G. Fang, *Preparation and thermal properties of microencapsulated stearyl alcohol with silicon dioxide shell as thermal energy storage materials.* Applied Thermal Engineering, 2020. **169**. DOI: 10.1016/j.applthermaleng.2020.114943.

171. Sun, S., et al., *Effects of two-step sintering on sintering-neck growth behavior and densification mechanism of SiO2 nanoparticles.* Ceramics International, 2026. **52**(6): p. 7482–7489. DOI: 10.1016/j.ceramint.2025.12.489.

172. Ju, W.-L., et al., *Controllable Synthesis of a Well-defined Polypropylene grafted Silica Nanoparticles and Its Effect on Crystallization Behavior of Polypropylene.* Chinese Journal of Polymer Science, 2022. **40**(11): p. 1411–1421. DOI: 10.1007/s10118-022-2756-7.

173. Zhang, H., et al., *Color reduction of sulfonated eucalyptus kraft lignin.* International Journal of Biological Macromolecules, 2017. **97**: p. 201–208. DOI: 10.1016/j.ijbiomac.2017.01.031.

174. Ibarra, D., et al., *Chemical characterization of residual lignins from eucalypt paper pulps.* Journal of Analytical and Applied Pyrolysis, 2005. **74**(1-2): p. 116–122. DOI: 10.1016/j.jaap.2004.12.009.

175. Souza, L., et al., *Lignin-incorporated bacterial nanocellulose for proton exchange membranes in microbial fuel cells.* Materials Chemistry and Physics, 2023. **293**. DOI: 10.1016/j.matchemphys.2022.126963.

176. Rashid, T., C.F. Kait, and T. Murugesan, *A "Fourier Transformed Infrared" Compound Study of Lignin Recovered from a Formic Acid Process.* Procedia Engineering, 2016. **148**: p. 1312–1319. DOI: 10.1016/j.proeng.2016.06.547.

177. Fritz, C., et al., *Self-association and aggregation of kraft lignins via electrolyte and nonionic surfactant regulation: stabilization of lignin particles and effects on filtration - OPEN ACCESS.* Nordic Pulp and Paper Research Journal, 2017. **32**(04): p. 572–585. DOI: 10.3183/NPPRJ-2017-32-04-p572-585.

178. de S. M. de Freitas, A., et al., *Improvements in thermal and mechanical properties of composites based on thermoplastic starch and Kraft Lignin.* International Journal of Biological Macromolecules, 2021. **184**: p. 863–873. DOI: 10.1016/j.ijbiomac.2021.06.153.

179. Parit, M. and Z. Jiang, *Towards lignin derived thermoplastic polymers.* International Journal of Biological Macromolecules, 2020. **165**: p. 3180–3197. DOI: 10.1016/j.ijbiomac.2020.09.173.

180. Wei, X., et al., *Effect of organosolv extraction on the structure and antioxidant activity of eucalyptus kraft lignin.* International Journal of Biological Macromolecules, 2021. **187**: p. 462–470. DOI: 10.1016/j.ijbiomac.2021.07.082.

181. Lievonen, M., et al., *A simple process for lignin nanoparticle preparation.* Green Chemistry, 2016. **18**(5): p. 1416–1422. DOI: 10.1039/c5gc01436k.

182. Awal, A. and M. Sain, *Spectroscopic studies and evaluation of thermorheological properties of softwood and hardwood lignin.* Journal of Applied Polymer Science, 2011. **122**(2): p. 956–963. DOI: 10.1002/app.34211.

183. Pe Iii, J.A., J.S. Mun, and S.P. Mun, *Thermal characterization of kraft lignin prepared from mixed hardwoods.* BioResources, 2022. **18**(1): p. 926–936. DOI: 10.15376/biores.18.1.926-936.

184. Nordström, Y., et al., *A new softening agent for melt spinning of softwood kraft lignin.* Journal of Applied Polymer Science, 2012. **129**(3): p. 1274–1279. DOI: 10.1002/app.38795.

185. Fodil Cherif, M., et al., *Comparison of the Physicochemical Properties and Thermal Stability of Organosolv and Kraft Lignins from Hardwood and Softwood Biomass for Their Potential Valorization.* Waste and Biomass Valorization, 2020. **11**(12): p. 6541–6553. DOI: 10.1007/s12649-020-00955-0.

186. Gao, W., M. Rigout, and H. Owens, *Optical properties of cotton and nylon fabrics coated with silica photonic crystals.* Optical Materials Express, 2017. **7**(2). DOI: 10.1364/ome.7.000341.

187. Zeng, Q., et al., *Rapid fabrication of robust, washable, self-healing superhydrophobic fabrics with non-iridescent structural color by facile spray coating.* RSC Advances, 2017. **7**(14): p. 8443–8452. DOI: 10.1039/c6ra26526j.

188. Himel, M.H., et al., *Biomimicry in nanotechnology: a comprehensive review.* Nanoscale Advances, 2023. **5**(3): p. 596–614. DOI: 10.1039/d2na00571a.

189. Subash, M.C. and M. Perumalsamy, *Biomimicry for Sustainable Structural Mimicking in Textile Industries*, in *Biomimicry Materials and Applications*. 2023. p. 215–233. DOI: 10.1002/9781394167043.ch10.

190. Yang, S., et al., *Preparation of Natural Plant Polyphenol Catechin Film for Structural Coloration of Silk Fabrics.* Biomimetics, 2024. **9**(1). DOI: 10.3390/biomimetics9010015.

191. Kohri, M., *Progress in polydopamine-based melanin mimetic materials for structural color generation.* Science and Technology of Advanced Materials, 2021. **21**(1): p. 833–848. DOI: 10.1080/14686996.2020.1852057.

192. Zhou, J., et al., *Preparation of structural colors on cotton fabrics with hydrophobicity and high color fastness through chemical bonds between polyphenolic hydroxyl groups and polysiloxanes.* Cellulose, 2023. **30**(10): p. 6639–6653. DOI: 10.1007/s10570-023-05243-3.

193. Fernandes, R.D.V., *Nano coloração – revestimento de substratos têxteis com cristais fotónicos*, in *Repositorium*. 2019, University of Minho: Guimarães, Portugal.

194. Cheng, X., et al., *Preparation of high color fastness structural colored cotton fabric via SiO2@PDA photonic crystal.* Dyes and Pigments, 2024. **226**. DOI: 10.1016/j.dyepig.2024.112151.

195. Li, S., et al., *Construction of photonic crystal structural colors on white polyester fabrics.* Optical Materials, 2021. **116**. DOI: 10.1016/j.optmat.2021.111115.

196. Yang, D., et al., *Facile Synthesis of Monodispersed SiO2@Fe3O4 Core–Shell Colloids for Printing and Three-Dimensional Coating with Noniridescent Structural Colors.* ACS Omega, 2019. **4**(1): p. 528–534. DOI: 10.1021/acsomega.8b02987.

197. Zhou, X., et al., *Production of Full Biomass Photonic Materials from Lignin Extracted from Wood with High-Purity and Rich-Hydroxyl in Molten Salt Hydrate.* ACS Sustainable Chemistry & Engineering, 2025. **13**(13): p. 4926–4936. DOI: 10.1021/acssuschemeng.4c08084.

198. Shang, G., M. Eich, and A. Petrov, *Photonic glass based structural color.* APL Photonics, 2020. **5**(6). DOI: 10.1063/5.0006203.

199. Lu, Y., et al., *Fabrication of Prussian Blue Dye/SiO2 Composite Microspheres and Their Structurally Coloration on White Fabrics.* Fibers and Polymers, 2025. **26**(9): p. 3941–3950. DOI: 10.1007/s12221-025-01044-6.

200. Hu, J., et al., *Structural color layers constructed from colored disperse-dye-dyed microspheres and their iridescent effect.* Dyes and Pigments, 2026. **247**. DOI: 10.1016/j.dyepig.2025.113497.

201. Lu, Y., et al., *Full-Spectrum Low-Angle-Dependent Structural Color Coatings Based on Silica Nanospheres for Fabrics.* ACS Applied Nano Materials, 2026. **9**(11): p. 5084–5093. DOI: 10.1021/acsanm.5c05827.

202. Wu, S., et al., *Different Structural Colors or Patterns on the Front and Back Sides of a Multilayer Photonic Structure.* ACS Applied Materials & Interfaces, 2019. **11**(30): p. 27210–27215. DOI: 10.1021/acsami.9b07823.

203. Yu, X., W. Ma, and S. Zhang, *Hydrophobic polymer-incorporated hybrid 1D photonic crystals with brilliant structural colors via aqueous-based layer-by-layer dip-coating.* Dyes and Pigments, 2021. **186**. DOI: 10.1016/j.dyepig.2020.108961.

Annexes

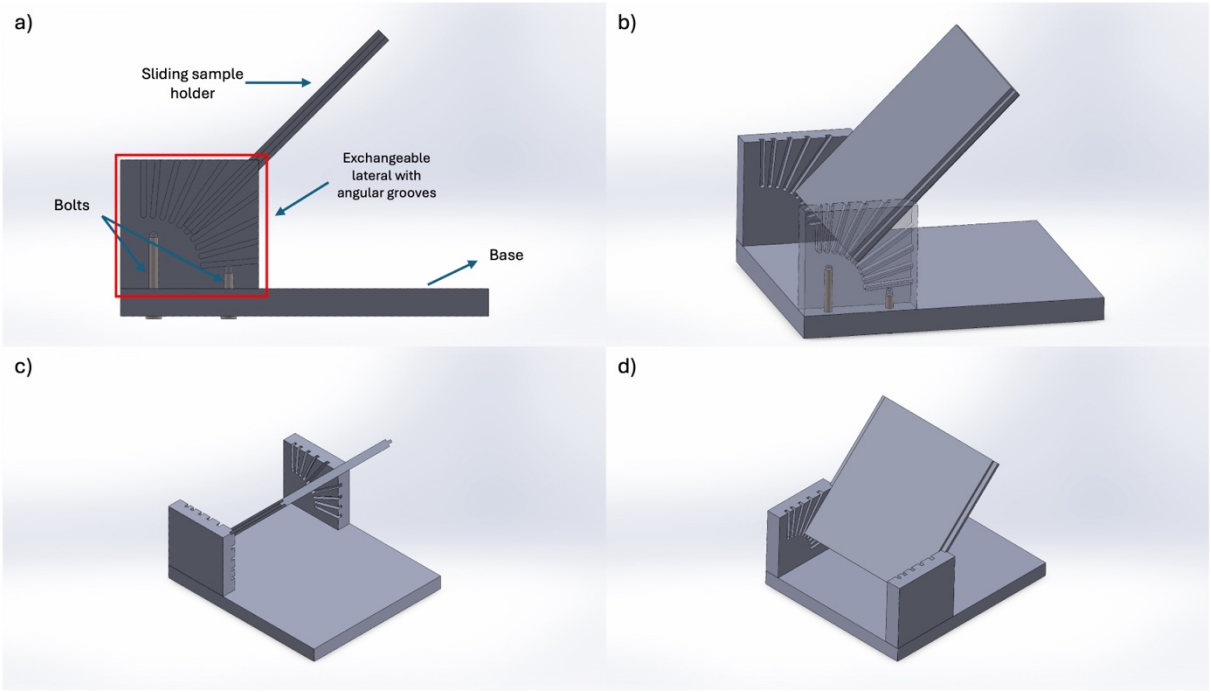


Figure A 1 The design of a sample holder for structurally colored fabrics. Schematics in a) side view, b) overall view, c) back view and d) front view.

Two different and exchangeable types of laterals were designed, one with angular grooves from 0 to 90 degrees with a 10-degree increment (0, 10, 20,..., 80, 90°), other with intermediary angular grooves, from 5 to 85 degrees, also with a 10-degree increment (5, 15, 25,..., 75, 85°). With this sample holder, photographs of structurally colored fabrics can be obtained with high reproducibility, choosing a determined angle (from 19 possible angles), minimizing human error.

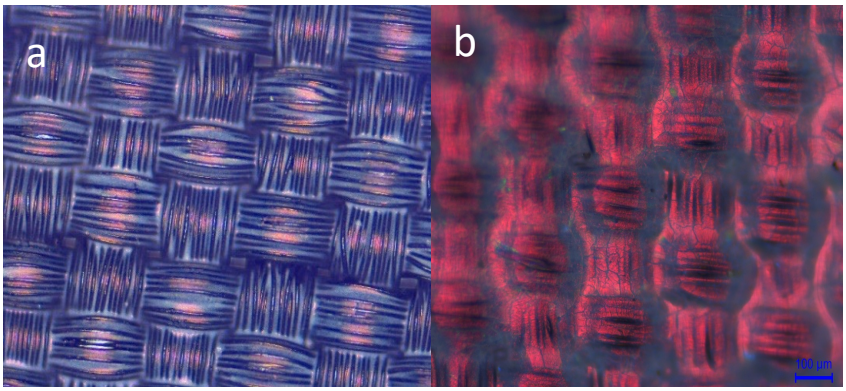


Figure A 2 Size optimization of 250 nm P(St-MMA-AA) PCs. Red structural color on PA fabric, a) synthetized at 60°C and 300 rpm reactional conditions and b) synthetized varying monomers proportions, at 70°C and 300 rpm reactional conditions.

Table A 1 CIEL*a*b* color coordinates of violet, blue, green and red photonic crystals applied onto black polyester substrate, with 1 and 2 dippings.

Black PES	CIELab Color coordinates (1 dipping)			CIELab Color coordinates (2 dippings)		
PC Color	L*	a*	b*	L*	a*	b*
Violet	29.45	5.68	-19.44	48.15	3.15	-23.25
Blue	32.48	-3.94	-10.61	42.13	-5.07	-14.16
Green	49.55	-18.59	-2.61	61.12	-18.29	-5.19
Red	44.44	10.41	-6.31	55.25	10.45	-7.49

Table A 2 CIEL*a*b* color coordinates of violet, blue, green and red photonic crystals applied onto different colored PES substrates (1 dippping).

Pristine PCs	Violet PCs			Blue PCs			Green PCs			Red PCs		
PES Color	L*	a*	b*	L*	a*	b*	L*	a*	b*	L*	a*	b*
Violet	39.17	48.68	-37.73	41.00	41.39	-34.41	53.77	17.70	-21.86	48.94	43.53	-27.90
Blue	38.66	14.21	-46.47	42.48	6.79	-40.87	48.28	-3.98	-33.88	51.91	13.34	-33.54
Petrol	44.88	-16.55	-25.51	43.53	-19.65	-22.24	53.31	-29.04	-15.89	57.30	-9.66	-15.90
Green	44.9	-19.62	0.01	47.04	-28.09	8.49	55.73	-34.13	13.72	58.92	-10.65	11.88
Yellow	77.97	-6.70	66.64	78.56	-9.30	73.29	81.59	-13.02	66.58	82.13	-6.03	60.99
Orange	53.06	38.59	26.47	55.73	32.92	29.31	59.76	24.34	33.87	60.67	35.10	31.97
Pink	45.28	54.62	-8.97	47.11	50.13	-5.88	50.60	42.15	0.37	52.82	51.15	-2.47
Red	41.65	51.43	4.81	45.77	41.62	6.45	50.12	34.70	16.72	49.69	48.47	14.06

Table A 3 CIEL*a*b* color coordinates of violet, blue, green and red photonic crystals applied onto different colored PES substrates (2 dipppings).

Pristine PCs	Violet PCs			Blue PCs			Green PCs			Red PCs		
PES Color	L*	a*	b*	L*	a*	b*	L*	a*	b*	L*	a*	b*
Violet	49.71	34.72	-36.09	50.26	27.31	-31.06	63.36	5.19	-17.31	56.94	33.73	-22.48
Blue	50.18	6.51	-40.99	46.95	1.76	-36.96	56.75	-10.78	-26.99	59.83	10.47	-26.5
Petrol	51.72	-14.44	-27.15	51.6	-18.86	-22.39	58.51	-27.72	-15.04	61.41	-7.79	-14.39
Green	55.46	-13.87	-9.17	54.22	-23.18	0.20	61.45	-29.51	7.71	68.88	-3.19	3.45
Yellow	77.56	-4.86	47.54	78.18	-8.71	54.5	81.89	-12.11	50.78	83.77	-2.42	39.71
Orange	57.93	32.73	8.42	61.21	25.30	13.64	63.46	18.76	24.10	66.97	29.89	18.21
Pink	53.48	42.82	-16.76	51.85	41.07	-10.67	58.12	27.62	-2.47	60.05	41.78	-4.75
Red	47.93	41.82	-7.24	54.68	30.73	-4.03	59.61	20.29	6.94	57.74	39.90	4.76

Table A 4 CIEL*a*b* color coordinates of 210 nm PCs@DBV-R (2 wt%) applied onto dyed polyester samples with one and five dippings.

210 nm PCs @Violet Dye	CIELab Color coordinates (1 dipping)			CIELab Color coordinates (5 dippings)		
PES Color	L*	a*	b*	L*	a*	b*
White	58,91	22,92	-19,72	59,42	20,33	-16,57
Black	31,48	-6,72	-6,14	51,85	5,77	-16,99
Violet	43,04	24,18	-23,52	55,57	19,18	-17,34
Blue	40,25	0,40	-32,72	53,66	7,63	-20,49
Petrol	42,83	-11,52	-21,06	54,96	10,97	-19,4
Green	42,21	-19,46	7,82	54,59	6,76	-13,49
Yellow	53,96	11,17	32,29	56,82	15,94	-7,87
Orange	47,03	27,91	16,65	56,35	19,45	-9,16
Pink	44,49	36,40	-7,33	56,49	17,95	-13,51
Red	42,05	36,22	9,44	56,10	15,35	-12,24

Table A 5 CIEL*a*b* color coordinates of 210 nm PCs@ SRB-ADS (2 wt%) applied onto dyed polyester samples with one and five dippings.

210 nm PCs @Blue Dye	CIELab Color coordinates (1 dipping)			CIELab Color coordinates (5 dippings)		
PES Color	L*	a*	b*	L*	a*	b*
White	58,17	-10,75	-23,43	60,03	-14,50	-21,17
Black	34,84	-14,62	-7,21	53,99	-17,23	-15,58
Violet	38,56	9,31	-31,13	55,61	-15,06	-20,04
Blue	42,71	-10,58	-30,73	55,43	-15,68	-19,92
Petrol	45,99	-24,16	-18,92	56,38	-18,19	-18,25
Green	44,69	-31,53	7,40	55,09	-20,18	-12,81
Yellow	52,90	-25,54	28,72	57,45	-23,06	-10,73
Orange	42,87	-0,09	8,58	56,08	-20,52	-13,14
Pink	36,25	8,12	-0,15	55,17	-16,61	-13,71
Red	39,56	10,84	-17,25	54,83	-13,39	-17,10

Table A 6 CIEL*a*b* color coordinates of 210 nm PCs@GD11 (2 wt%) applied onto dyed polyester samples with one and five dippings.

210 nm PCs @Green Dye	CIELab Color coordinates (1 dipping)			CIELab Color coordinates (5 dippings)		
PES Color	L*	a*	b*	L*	a*	b*
White	61,80	-29,08	20,54	64,14	-33,08	25,17
Black	34,36	-20,63	8,68	57,77	-31,80	23,67
Violet	39,29	-2,86	-3,71	59,33	-32,43	22,87
Blue	43,42	-28,63	-3,80	60,63	-37,89	24,65
Petrol	48,28	-38,98	6,36	60,74	-39,88	26,54
Green	47,52	-36,20	23,24	61,31	-35,62	27,19
Yellow	58,61	-24,09	44,87	61,51	-35,70	30,13
Orange	46,65	3,28	27,64	60,85	-30,43	28,12
Pink	41,20	10,81	6,36	59,24	-29,13	24,64
Red	39,09	11,13	15,60	58,48	-27,12	22,83

Table A 7 CIEL*a*b* color coordinates of 210 nm PCs@ YS-ADS (2 wt%) applied onto dyed polyester samples with one and five dippings.

210 nm PCs @Yellow Dye	CIELab Color coordinates (1 dipping)			CIELab Color coordinates (5 dippings)		
PES Color	L*	a*	b*	L*	a*	b*
White	81,17	-11,55	58,73	84,27	-10,71	66,97
Black	41,02	-22,80	21,50	66,36	-21,99	47,78
Violet	45,76	6,73	13,69	72,31	-14,99	54,12
Blue	44,51	-30,34	4,21	69,73	-31,50	46,47
Petrol	53,14	-43,02	22,44	74,90	-24,01	56,51
Green	50,81	-33,98	31,47	74,16	-26,23	56,70
Yellow	77,08	-2,85	76,22	81,03	-7,74	71,20
Orange	57,38	27,11	50,07	73,84	-1,61	58,61
Pink	50,02	31,39	26,67	74,35	-6,33	57,82
Red	47,52	30,20	33,04	72,28	-6,28	55,80

Table A 8 CIEL*a*b* color coordinates of 210 nm PCs@ RD-K3G (2 wt%) applied onto dyed polyester samples with one and five dippings.

210 nm PCs @Red Dye	CIELab Color coordinates (1 dipping)			CIELab Color coordinates (5 dippings)		
PES Color	L*	a*	b*	L*	a*	b*
White	56,11	29,10	11,59	57,28	27,11	15,99
Black	29,76	-5,21	0,91	50,75	15,34	13,16
Violet	39,66	23,80	-5,09	53,31	22,81	14,90
Blue	36,50	-4,36	-14,12	50,99	7,71	6,70
Petrol	39,49	-12,82	-6,04	51,65	6,64	10,67
Green	40,19	-12,15	15,94	52,91	13,70	12,91
Yellow	54,76	27,03	44,52	55,65	23,79	22,41
Orange	47,65	36,96	30,61	54,77	25,47	19,74
Pink	44,61	40,26	9,86	55,20	25,53	16,14
Red	40,96	41,75	21,01	53,52	23,63	20,50

Table A 9 CIEL*a*b* color coordinates of 210 nm PCs@ RD-K3G (0.5 wt%) applied onto dyed polyester samples with 1, 3 and 5 dippings.

210 nm PCs @Red Dye	CIELab Color coordinates (0.5%, 1 dipping)			CIELab Color coordinates (0.5%, 3 dippings)			CIELab Color coordinates (0.5%, 5 dippings)		
PES Color	L*	a*	b*	L*	a*	b*	L*	a*	b*
White	69,25	23,37	6,65	64,82	26,08	6,91	66,25	25,94	9,08
Black	31,22	-8,15	-2,20	43,71	-5,58	-3,03	50,81	-3,70	-1,00
Violet	40,56	29,09	-20,86	47,43	18,64	-13,46	54,99	11,68	-5,59
Blue	42,21	-6,92	-22,67	47,45	-10,08	-17,44	54,14	-7,89	-8,78
Petrol	45,37	-18,23	-12,40	49,19	-16,72	-11,45	57,43	-9,76	-2,15
Green	44,58	-17,46	13,76	49,39	-13,96	7,53	55,37	-5,64	4,15
Yellow	64,31	20,22	51,27	62,69	21,71	33,30	64,70	22,14	23,71
Orange	52,73	36,05	31,86	56,46	28,15	20,10	61,75	24,24	15,09
Pink	47,20	43,85	2,64	53,22	32,04	2,52	57,26	26,83	3,83
Red	45,25	36,90	15,13	49,99	28,23	9,70	55,82	22,21	8,23

Table A 10 CIEL*a*b* color coordinates of 210 nm PCs@ RD-K3G (1 wt%) applied onto dyed polyester samples with 1, 3 and 5 dippings.

210 nm PCs @Red Dye	CIELab Color coordinates (1%, 1 dipping)			CIELab Color coordinates (1%, 3 dippings)			CIELab Color coordinates (1%, 5 dippings)		
PES Color	L*	a*	b*	L*	a*	b*	L*	a*	b*
White	62,57	27,06	8,22	57,93	29,40	10,09	58,65	30,31	11,30
Black	31,51	-6,61	-1,28	40,08	-6,33	-1,46	47,29	-0,89	3,52
Violet	40,29	26,61	-12,54	44,41	18,32	-6,96	49,43	15,8	-1,80
Blue	38,43	-5,38	-20,18	45,26	-5,67	-8,48	53,38	-0,38	3,71
Petrol	42,88	-12,08	-8,86	47,33	-10,04	-4,38	51,86	-1,22	4,94
Green	41,83	-13,39	14,36	45,97	-8,23	8,06	50,99	0,98	7,45
Yellow	58,41	24,82	46,22	56,69	24,18	31,98	58,72	24,57	22,53
Orange	50,45	36,06	30,54	52,41	29,44	20,60	55,55	27,78	18,25
Pink	45,56	42,74	6,23	50,35	32,72	7,07	53,89	28,00	8,80
Red	42,46	41,05	18,25	48,30	29,54	12,87	52,17	25,80	11,45